LARGE-SCALE FORECASTING OF LARGE FLUCTUATIONS USING WAVELET COHERENCE AND MULTIFRACTAL BEHAVIOR AND DEVELOPING WAVELET COHERENCE FOR MULTIPLE TIME SERIES

TUNÇ OYGUR

JUNE,

2022

LARGE-SCALE FORECASTING OF LARGE FLUCTUATIONS USING WAVELET COHERENCE AND MULTIFRACTAL BEHAVIOR AND DEVELOPING WAVELET COHERENCE FOR MULTIPLE TIME SERIES

BY

TUNÇ OYGUR

SUPERVISOR

PROF. DR. YAMAN ÖMER ERZURUMLU

PH.D. THESIS

INSTITUTE OF SOCIAL SCIENCES

DEPARTMENT OF FINANCIAL ECONOMICS

YEDİTEPE UNIVERSITY

JUNE, 2022

PLAGIARISM

I hereby declare that all information in this document has been obtained and presented in accordance with academic rules and ethical conduct. I also declare that, as required by these rules and conduct, I have fully cited and referenced all material and results that are not original to this work.

Date: 10.06.2022

Name/Surname: Tunç OYGUR

ABSTRACT

Shocks, jumps, booms, and busts are typical large fluctuation markers that appear in crisis. Identifying financial crises and estimating leading indicators with strong relations during crisis periods have an essential role in the literature. This thesis examines the dynamic co-movements of leading indicators' multifractal features to identify financial crises due to large fluctuations. The detected dynamic relationships predict leading indicators with scale-by-scale analysis and make large-scale predictions better than challenger models. As a natural result of these studies, the n-dimensional wavelet coherence method is examined, and the vectorwavelet package is transferred to the R program. This thesis consists of three independent parts, and the contents of the studies are summarized below. In the first part, stock returns' co-movements with other leading indicators in crisis periods are analyzed with multiple and quadruple wavelet coherence using interest rate, exchange rate, and trade balance differences. The scale-by-scale wavelet transformation was used to predict large-scale relationships, and stock return estimation was performed. In the second part, the multifractal characteristics of sectoral default probabilities of the real sector in Turkey and Turkey sovereign CDS rates were examined by detrended fluctuation analysis. Significant dynamic connections between the Hölder exponents of the default rates and CDS during financial crisis periods have been examined. During the periods of financial crises, among the Hölder exponents, severely correlated large scales show multifractal features. Scale-by-scale wavelet transform has been used to predict large-scale relationships, and hence vector fractionally autoregressive integrated moving average forecasting provides better results than scalar models. The final part of the thesis introduces a new wavelet methodology to handle multivariate time series

dynamic co-movements by extending multiple quadruple wavelet coherence methodologies. The primary motivation of our works is to measure wavelet coherence analytically for the specific dimension.

Keywords: Financial crises; large fluctuations, large-scale forecast, multiscale analysis, vector wavelet coherence

ÖZET

Şoklar, sıçramalar, patlamalar ve düşüşler, krizde görülen tipik büyük dalgalanma belirteçleridir. Kriz dönemlerinde finansal krizlerin belirlenmesi ve güçlü ilişkilerle öncü göstergelerin tahmin edilmesi literatürde önemli bir yere sahiptir. Bu tez, büyük dalgalanmalardan kaynaklanan finansal krizleri belirlemek için öncü göstergelerin çoklu fraktal özelliklerinin dinamik ilişki hareketlerini incelemektedir. Tespit edilen dinamik ilişkiler, ölçek-ölçek analizi ile öncü göstergeleri öngörmekte ve büyük ölçekli tahminleri alternatif modellerden daha tahminlemektedir. Bu çalışmaların doğal bir sonucu olarak n-boyutlu dalgacık korelasyon yöntemi incelenmiştir ve vectorwavelet R paketi oluşturulmuştur. Bu tez üç bağımsız bölümden oluşmaktadır ve çalışmaların içerikleri aşağıda özetlenmiştir. Birinci bölümde, hisse senedi getirilerinin kriz dönemlerinde diğer öncü göstergelerle birlikte hareketleri, faiz oranı, döviz kuru ve ticaret dengesi farkları kullanılarak üçlü ve dörtlü dalgacık korelasyon metodu ile analiz edilmiştir. Büyük ölçekli ilişkileri tahmin etmek için ölçek-ölçek bazında dalgacık dönüşümü kullanılmış ve stok getiri tahminleri gerçekleştirilmiştir. İkinci bölümde, Türkiye'de reel sektörün sektörel temerrüt olasılıkları ve Türkiye devlet CDS oranlarının çoklu fraktal özellikleri meyilden arındırılmış dalgalanma analizleri ile incelenmiştir. Finansal kriz dönemlerinde temerrüt oranları ile CDS oranlarının Hölder üstelleri arasındaki önemli dinamik bağlantılar incelenmiştir. Finansal kriz dönemlerinde, büyük ölçeklerde Hölder üstelleri arasında tespit edilen anlamlı ilişkiler, çoklu fraktal özellikler göstermektedir. Ölçek-ölçek dalgacık dönüşümü, büyük ölçekli ilişkileri tahmin etmek için kullanılmıştır ve bu nedenle VFARIMA tahminleri skaler modellerden daha iyi sonuçlar sağlamaktadır. Tezin son bölümünde üçlü ve dörtlü dalgacık korelasyon metodolojileri genişletilerek çok

boyutlu zaman serileri için dinamik ilişkileri ele alacak yeni bir dalgacık metodolojisi sunar. Çalışmalarımızın temel motivasyonu, çok boyutlu dalgacık korelasyonunu belirli bir boyut için analitik olarak ölçmektir.

To Nesli

ACKNOWLEDGMENTS

First and foremost, I am astonishingly thankful to my advisor, Prof. Dr. Gazanfer Unal, for their precious advice, ongoing assistance, and endurance during my Ph.D. Their tremendous expertise and remarkable experience have encouraged me in all the time of my academic research. His guidance helped me in all the time of research and writing of this thesis. He is forever living in my memories.

Also, I appreciate my advisor, Prof. Dr. Yaman Ömer Erzurumlu, for not leaving me unattended and for his great guidance.

Just as importantly, I would like to manifest my gratitude to my wife and parents. Without their enormous understanding and support, it would be impossible to achieve my study.

TABLE OF CONTENTS

PLAGIARISM ..... **i**
ABSTRACT ..... **ii**
ÖZET ..... **iv**
ACKNOWLEDGMENTS ..... **vii**
LIST OF SYMBOLS ..... **xi**
LIST OF ABBREVIATIONS ..... **xii**
LIST OF TABLES ..... **xiv**
LIST OF FIGURES ..... **xv**
1. The Large Fluctuations of the Stock Return and Financial Crises Evidence from Turkey: Using Wavelet Coherency and VARMA Modelling to Forecast Stock Return **1**
1.1. Introduction 2
1.2. Methodology 5
1.2.1. Wavelet Analysis 5
1.2.2. Multiple wavelet coherence 7
1.2.3. Quadruple wavelet coherence 8
1.3. Empirical Analysis 11
1.3.1. Preliminary analysis 11
1.3.2. The wavelet transform 15
1.3.3. The cross-wavelet transform 16
1.3.4. Wavelet coherence 19
1.3.5. Multiple wavelet coherence 22
1.3.6. Quadruple wavelet coherence 24
1.4. Forecast 26
1.4.1. Panel A 27
1.4.2. Panel B 29
1.5. Conclusion 32

2. Traces of the Multifractal Nature of the Financial Crises in Turkey: Co-Movement of the Hölder Exponents and Large-Scale Forecast 35
2.1. Introduction 36
2.2. Methodology 38
2.2.1. Moody's KVM expected default frequency 38
2.2.2. Multifractal analysis 39
2.2.2.1. Multifractal detrended fluctuation analysis 39
2.2.2.2. Multifractal detrended cross-correlation analysis 41
2.2.2.3. Multifractal detrended moving average cross-correlation analysis 43
2.2.2.4. Pointwise and local Hölder exponents 43
2.3. Empirical Analysis 44
2.3.1. Preliminary analysis 45
2.3.2. Multifractal analysis 51
2.3.2.1. Multifractal detrended fluctuation analysis 51
2.3.2.2. Multifractal detrended cross-correlation analysis 62
2.3.2.3. Multifractal detrended moving average cross-correlation analysis 67
2.3.2.4. The Hölder exponent analysis 71
2.3.3. Wavelet analysis 78
2.3.3.1. Wavelet coherence 79
2.4. Large-Scale Forecast 86
2.4.1. Consumer cyclical 88
2.4.2. Basic materials 91
2.4.3. Utilities 94
2.5. Conclusion 97
2.6. Wavelet Power Spectra 99
2.7. The Cross-Wavelet Transforms 105
3. Vector Wavelet Coherence for Multiple Time Series 110

3.1. Introduction 111
3.2. Methodology 112
3.2.1. Vector Wavelet Coherence 112
3.3. Examples 113
3.3.1. Co-movement of VIX and stock indices 113
3.3.2. Simulations 116
3.4. Conclusion 120
3.5. Supplemental material 121
4. References 122
5. Appendix A: R programming codes for VWC 129

LIST OF SYMBOLS

ω	Dimensionless frequency
η	Dimensionless time
ψ	Wavelet function
W_n^X	Wavelet transform
$\|W_n^X\|^2$	Wavelet power
R_n^2	Wavelet coherence
S	Smoothing operator
M	Hermitian matrix
$*$	Complex conjugate
C	Smoothed complex wavelet coherencies
det	Determinant of a matrix
$\|x\|$	Absolute value
$\|\|x - y\|\|$	Euclidean distance
t	Time
P_t	Price at time = t
R_t	Return at time = t
A	Firm value
μ	Mean
σ	Volatility
E	Firm market value
D	Total dept of the firm
$\mathcal{N}$	Normal distribution
dW	Standard Weiner process
F_q	qth-order fluctuation function
H	Hurst exponent
H_q	Generalized (local) Hurst exponent
τ_q	Renyi exponents
α	Hölder exponent
$\lfloor x \rfloor$	The largest integer smaller than x
$\lceil x \rceil$	The smallest integer larger than x

LIST OF ABBREVIATIONS

A-D	Anderson-Darling
ADF	Augment Dickey-Fuller
AE	Absolute Error
AR	Autoregressive
ARCH LM	Autoregressive Conditional Heteroscedasticity-Lagrange Multiplier
ARMA	Autoregressive Moving Average
BIST	Borsa Istanbul
B-P	Box-Pierce
BVSP	Sao Paulo Bovespa Index, IBovespa
CAC	Cotation Assistée En Continu, FCHI
CDS	Credit Default Swap
COI	Cone of Influence
CWT / WT	The Continuous Wavelet Transform
DD	Distance-to-Default
DFA	Detrended Fluctuation Analysis
Dh	Multifractal Spectrum
DJI	Dow Jones Industrial Average
DOG	Derivative of Gaussian
DP	Default Point
FARIMA	Fractionally Autoregressive Moving Average
FTSE	Financial Times Stock Exchange
GSPC / S&P	Standard and Poor's
IMF	International Monetary Fund
IXIC	Nasdaq Composite
J-B	Jarque-Bera
KPSS	Kwiatkowski–Phillips–Schmidt–Shin
KVM	Kealhover, Mcquown, and Vasicek
L-B	Ljung-Box
MAE	Mean Absolute Error
MAPE	Mean Absolute Percentage Error
MCS	Model Confidence Set

ME	Mean Error
MF-DCCA	Multifractal Detrended Cross-Correlation Analysis
MF-DFA	Multifractal Detrended Fluctuation Analysis
MF-X-DMA	Multifractal Detrended Moving Average Cross-Correlation Analysis
MPE	Mean Percentage Error
MWC	Multiple Wavelet Coherence
MXX	IPC Mexico
N225	Nikkei 225
OECD	Organization for Economic Co-Operation and Development
PD	Probability of Default
Ph	Probability Distributions
PP	Phillips-Perron
PSR	Priestley-Subba Rao
QLIKE	Quasi-Likelihood
QWC	Quadruple Wavelet Coherence
R/S	Rescaled Range Analysis
RMS	Root-Mean-Square
RMSE	Root-Mean-Square Error
RUT	Russell 2000
SE	Standard Error
VARMA	Vector Autoregressive Moving Average
VFARMA	Vector Fractionally Autoregressive Moving Average
VIX	Volatility Index
VMC	Vector Wavelet Coherence
WTC	Wavelet Coherence
XTC	The Cross-Wavelet Transform

LIST OF TABLES

Table 1-1. Phase difference.....7

Table 1-1. Fundamental statistics. 13

Table 1-2. Correlation results of all the return series.....14

Table 1-3. Panel A and Panel B correlation matrix. 29

Table 1-4. Panel A Forecast results. 29

Table 1-5. Panel A and Panel B forecast performance comparison. 30

Table 1-6. Panel B Forecast results.....31

Table 1-7. Phase difference results. 34

Table 2-1. Sectoral distributions of firms. 44

Table 2-2. Descriptive statistics. 48

Table 2-3. Hurst exponents. 49

Table 2-4. Correlation results of all PD series against the CDSs. 50

Table 2-5. Local Hurst exponent results. 61

Table 2-6. Window definitions. 87

Table 2-7. Forecast performance comparison: CDS versus Consumer Cyclicals. 90

Table 2-8. Model confidence set: Consumer Cyclicals. 90

Table 2-9. Forecast performance comparison: CDS versus Basic Materials.....93

Table 2-10. Model confidence set: Basic Materials.....93

Table 2-11. Forecast performance comparison: CDS versus Utilities.....95

Table 2-12. Model confidence set: Utilities.....95

Table 3-1. Stationarity tests 114

Table 3-2. Correlation results of VIX against stock indices.....115

LIST OF FIGURES

Figure 1-1. Return series. 12

Figure 1-2. Power spectrums. 15

Figure 1-3. The cross wavelet transforms of return series. 17

Figure 1-4. The wavelet coherence of the return series. 20

Figure 1-5. Multiple wavelet coherence. 23

Figure 1-6. Quadruple wavelet coherence. 25

Figure 1-7. Panel A: Return series. 28

Figure 1-8. Stock returns the out-of-sample forecast for Panel A. 28

Figure 1-9. Panel B: Return series. 30

Figure 1-10. Stock returns the out-of-sample forecast for Panel B. 31

Figure 2-1. Sectoral PDs (red) and CDSs plot (blue) 46

Figure 2-2. Cross-correlation tests. 51

Figure 2-3. The q-order RMSs and the corresponding regression lines. 52

Figure 2-4. The q-order Hurst (Hq) and Renyi (tq) exponents. 53

Figure 2-5. Multifractal spectrum. 54

Figure 2-6. Multifractal spectrum. 54

Figure 2-7. Hölder exponents, probability distributions (Ph), multifractal spectrum (Dh). 55

Figure 2-8. Fxy(s) versus s. 62

Figure 2-9. Cross-correlation Hurst exponents, Hxy(q). 63

Figure 2-10. Scaling exponents with q varying from -10 to 10. 64

Figure 2-11. The relationship between τxy(q) and q. 65

Figure 2-12. The relationships between τxy(q) and q. 65

Figure 2-13. The multifractal spectrum, fxy(α). 66

Figure 2-14. The multifractal spectra both in the long term and short term. 67

Figure 2-15. Fxy(q, s) versus s. 68

Figure 2-16. Cross-correlation Hurst exponents, Hxy(q).....69

Figure 2-17. The multifractal spectrum, fxy(α). 70

Figure 2-18. Local and Pointwise Hölder exponents. 72

Figure 2-19. The wavelet coherences of all series. 80

Figure 2-20. Selected window and forecast plot: CDS versus Consumer Cyclicals. ..89

Figure 2-21. Forecast accuracy: CDS versus Consumer Cyclicals.....91

Figure 2-22. Selected window and forecast plot: CDS versus Basic Materials.....92

Figure 2-23. Forecast accuracy: CDS versus Basic Materials. 94

Figure 2-24. Selected window and forecast plot: CDS versus Utilities.....96

Figure 2-25. Forecast accuracy: CDS versus Utilities. 97

Figure 2-26. Wavelet power spectra of all series.....99

Figure 2-27. The cross-wavelet transforms of all series. 105

Figure 3-1. Vector wavelet coherence. 115

Figure 3-2. Simulations.....117

Figure 3-3. Multiple wavelet coherence. 120

Figure 3-4. vectorwavelet R package.....121

1. The Large Fluctuations of the Stock Return and Financial Crises Evidence from Turkey: Using Wavelet Coherency and VARMA Modelling to Forecast Stock Return

Summary

Shocks, jumps, booms, and busts are typical large fluctuation markers that appear in crisis. Models and leading indicators vary according to crisis type despite the fact that there are many different models and leading indicators in the literature to determine the crisis structure. This chapter investigates the structure of dynamic correlation of stock return, interest rate, exchange rate, and trade balance differences in Turkey's crisis periods over the period between October 1990 and March 2015 by applying wavelet coherency methodologies to determine the nature of crises. The time period includes Turkey's currency and banking crises, the US sub-prime mortgage crisis, and the European sovereign debt crisis in 1994, 2001, 2008, and 2009. Empirical results showed that stock return, interest rate, exchange rate, and trade balance differences were significantly linked during Turkey's financial crises. The cross-wavelet power, the wavelet coherency, the multiple wavelet coherency, and the quadruple wavelet coherency methodologies have been used to examine the dynamic correlation structure. Moreover, due to quadruple and multiple wavelet coherence, at strongly correlated large scales indicate linear behavior and, hence VARMA (vector autoregressive moving average) gives better fitting and forecasting performance. Besides, increasing the model's dimensions for strongly correlated scales leads to more accurate results compared to scalar counterparts.

1.1. Introduction

Nowadays, all financial markets have become integrated with each other due to globalization and technological innovations in financial markets. It is known as financial liberalization. While financial liberalization usually increases financial openness, it makes developing and emerging market economies transform domestic markets, as well. Likewise, it provides shocks, jumps, booms, and busts merger and capital allocation enhancement, it increases contagious macroeconomic fluctuations. Due to financial liberalization, a piece of new information transferred to any precursor market spreads rapidly to all financial markets with the domino effect. This situation makes macroeconomic fluctuations more substantial. Shocks, jumps, booms, and busts are typical large fluctuation markers that appear in crisis. The stock indexes, exchange rates, interest rates, and trade balance associated with each other react sharply, and consequently, the country's leading economic indicators fluctuated. In this chapter, the dynamic alteration between stock indexes, exchange rates, interest rates, and trade balance is investigated by the wavelet analysis framework.

Financial crises cannot often be explained by one factor; they have common elements and arise in various forms. Ordinarily, financial crises deal with one or more chasing events related to asset prices and credits. Financial crises are distinguished two types of crises, which are determined using qualitative methods (currency and sudden stop crises) and judgmental analysis (foreign and domestic debt and banking crises) by Reinhart and Rogoff [1]. Many empirical models exist in the literature, and explanatory variables exist to predict crises and have evolved over time. One of these methods is analyzing equity return, foreign exchange, and interest rate movements. Following researchers found that exchange rates and stock price are potent relationships based on co-movement analysis, expressly in crises ([2], [3], [4], [5]). Analyzing the long-term association among variables, the unstableness or lack of association can be offered ([6], [7], [8], [9], [10]) demonstrates that it stabilized high interest rates during

the currency crises. For this reason, the cross-currency rate and/or interest rate movements impress the equity returns ([11], [12], [13]). Few researchers consider the joint movement of equity prices, foreign exchanges, and interest rates, unlike others ([14], [15], [16], [17]).

This study's main objective is to investigate the structure of dynamic association of the most crucial macroeconomic indicators in crisis periods using wavelet coherency analysis. The most important reason for choosing wavelet analysis in this study is to allow time series to be extracted to the time-frequency domain and examine the non-linear correlation at scales. The wavelet toolbox consists of the continuous transform, the cross transform, cross-phase angle, bivariate, and multiple and quadruple coherence methodologies. Multiple wavelet coherence and quadruple wavelet coherence indicate how to determine equity return by the cross-currency, interest, and trade balance returns despite other studies. This research promotes empirical literature in the field as the first study investigating the structure of equity return, interest, foreign currency, and trade balance deviations in Turkey using wavelet analysis, especially multiple wavelet coherence and quadruple wavelet coherence.

After the mid-1980s, wavelet theory quickly spread to several fields, such as physics, epidemiology, electrical engineering, and mathematical analysis. Although wavelet analysis can disintegrate the series into a time-frequency domain and work non-stationary series, this methodology has not become a favorite economics application, unlike the other disciplines. After the introduction to cross transform (Maraun & Kurths presented the evaluation [18]), bivariate (Maraun & Kurths developed a statistical test [18]. Torrence & Compo [19] and Grinsted et al. [20] implemented a software package) and multiple coherence (Mihanović et al. introduced [21], [22]), wavelet analysis can cope with multivariate analysis. For this reason, by separating the financial time series into its time components using wavelet analysis, more perceptiveness can be gained about the co-movement of the series.

In this chapter, we have two main reasons to choose Turkey: a) According to the IMF and World Bank lists, Turkey is a developing country, and according to the majority of rating firms, Turkey is rated at the lowest investment grade. In light of this information, the financial market in Turkey is more important for investors. b) Turkey has experienced all kinds of crises in the last two decades. Thus, the results of wavelet analysis can be observed in various types of crises.

The chapter structure is presented. Sec. 1.2, background knowledge of the wavelet analysis is discussed, and quadruple wavelet coherence is introduced. In Sec. 1.3, equity, foreign exchange, interest rate, and trade gap returns are represented and analyzed by the wavelet toolbox presented in Sec. 1.2. Furthermore, multivariate and univariate time series techniques are VARMA and ARMA models presented in Sec. 1.4. Candidate models are determined and predicted. Conclusion and remarks will also be discussed.

1.2. Methodology

1.2.1. Wavelet Analysis

In this division, we describe both univariate and multivariate continuous wavelet transform methods. “When using wavelets for feature extraction purposes, the Morlet wavelet (with $\omega_0 = 6$) is the right choice since it provides a good balance between time and frequency localization. We, therefore, restrict our further treatment to this wavelet.” [20] For this reason, we start to define one of the remarkable wavelets, which is Morlet,

$$\psi_0(\eta) = \pi^{-1/4} e^{i\omega_0\eta} e^{-\frac{1}{2}\eta^2}. \tag{1-1}$$

where ω_0 and η denote non-dimensional frequency and time, respectively.

The CWT is defined by scaled plus normalized wavelet as follows;

$$W_n^X(s) = \sqrt{\frac{\delta t}{s}} \sum_{m=1}^{N} x_n, \psi_0[(m-n)\frac{\delta t}{s}]. \quad n = 1, \ldots, N \tag{1-2}$$

where x_n is a time series, δt indicates uniform time step. Consequently, wavelet power is represented as $|W_n^X(s)|^2$.

“The standard procedure is to calculate this convolution as a simple product in the Fourier domain, using the Fast Fourier Transform algorithm to go forth and back from time to the spectral domain. As with other types of transforms, the CWT applied to a finite length time series inevitably suffers from border distortions, which increase with s. The region where the transform suffers from these edge effects is called the Cone of Influence (COI). In this area, the results are unreliable and must be interpreted carefully. Here we take the COI as the area in which the wavelet power caused by a discontinuity at the edge has dropped to e^{-2} of the value at the edge.” [20], [23]

Torrence and Compo have introduced statistical significance via Monte-Carlo methods for wavelet power. [19] “Distribution for the local wavelet power spectrum at each time n and scale s as follows;

$$D\left(\frac{|W_n^X(s)|^2}{\sigma_X^2} < p\right) = \frac{1}{2} P_k \chi_v^2(p), \tag{1-3}$$

where P_k is AR(0) and AR(1) stationary process with certain background power spectrum, v is equal to 1 for real and 2 for complex wavelets." [20]

"The cross-wavelet transform (XWT) provides theoretical distribution of the cross-wavelet power of two-time series. Torrence and Compo defined as:

$$D\left(\frac{|W_n^X(s) W_n^{Y*}(s)|}{\sigma_X \sigma_Y} < p\right) = \frac{Z_v(p)}{v} \sqrt{P_k^X P_k^Y}, \tag{1-4}$$

where $Z_v(p)$ is the confidence level associated with the probability p for a pdf defined by the square root of the product of two χ^2 distributions." [19], [20]

According to Aguiar- Conraria et al., wavelet coherence described "the ratio of the cross-spectrum to the product of the spectrum of each series and can be thought of as the local (both in time and frequency) correlation between two time-series." [24]

Torrence and Webster [25] illustrate wavelet coherence as:

$$R_n^2(s) = \frac{|S(s^{-1} W_n^{XY}(s))|^2}{S(s^{-1}|W_n^X(s)|^2) \cdot S(s^{-1}|W_n^Y(s)|^2)} \tag{1-5}$$

where S denotes the smoothing operator. The sense of the formula is a similar standard correlation measure. Hence, we can easily illustrate that wavelet coherence is a localized correlation measure in the time-frequency domain. In addition, Monte-Carlo-based methods are hired to figure wavelet coherence's statistical significance because of a lack of knowledge about theoretical distribution. Nevertheless, Aguiar-Conraria mentions remarkable reasons why it will concentrate on wavelet coherence rather than the cross-wavelet. "(1) the wavelet coherency has the advantage of being normalized by the power spectrum of the two time-series, and (2) that the wavelets cross-spectrum can show strong peaks even for the realization of independent processes suggesting the possibility of spurious significance tests". [23]

The phase difference in two-time series is established by calculating the phase difference's mean and confidence level. The arrows give the phase difference as following rules:

Table 1-1. Phase difference.

	Up	Down	
Right	Lagging	Leading	In phase
Left	Leading	Lagging	Out of phase

Note. The table is designed for the second element. Hence, right and up means that variables in-phase and second-time series are lagging.

1.2.2. Multiple wavelet coherence

Extension from doublet to triplet wavelet coherence was introduced by Mihanović et al. (2009 [21]. "MWC works like multiple correlation that is capable of seeking the resulting coherence, which gives the resulting wavelet coherence squared that computes the proportion of wavelet power of the dependent time series y that is explainable by the two independents x_1 and x_2 at a given time and frequencies. The significant levels are again calculated with the Monte Carlo method." [22]

The multiple (triplet) wavelet coherence (y versus x_1 and x_2) is represented as follows:

$$R^2_{y(x_1x_2)} = R^2_{y(q)} = 1 - \frac{M^d}{S_{yy}M^d_{yy}}, \tag{1-6}$$

where $R^2_{y(x_1x_2)}$(or $R^2_{y(q)}$) exhibits the squared multiple wavelet coherence. The Hermitian matrix M $(3x3)$ presentations all the smoothed cross-wavelet spectra SW_{ij} which is the smoothed version of W_{ij}

$$SW_{ij} = S(W_{ij}), \tag{1-7}$$

where SW is a certain smoothing operator.

$$M = \begin{bmatrix} SW_{yy} & SW_{yx_1} & SW_{yx_2} \\ SW_{x_1y} & SW_{x_1x_1} & SW_{x_1x_2} \\ SW_{x_2y} & SW_{x_2x_1} & SW_{x_2x_2} \end{bmatrix}. \tag{1-8}$$

Remember, if the matrix M is a Hermitian, we can express $M = M^*$, where $*$ is a conjugate transpose. Hence,

$$\begin{cases} \forall\, i \neq j, & SW_{ij} = SW_{ji}^* \\ \forall\, i, & SW_{ii} = S(|W_i|^2) \in \Re^+ \end{cases} \tag{1-9}$$

The cofactor of the (i,j) element in matrix M is named as:

$$M_{ij}^d = (-1)^{(i+j)} \det M_i^j, \tag{1-10}$$

where M_i^j shows the sub-matrix, which achieves from M via removing row i and column j. Additionally, $M^d = \det M$.

The matrix C represents the smoothed complex wavelet coherencies (ρ_{ij}) that are derived from the matrix M.

$$C = \begin{bmatrix} 1 & \rho_{yx_1} & \rho_{yx_2} \\ \rho_{x_1y} & 1 & \rho_{x_1x_2} \\ \rho_{x_2y} & \rho_{x_2x_1} & 1 \end{bmatrix}. \tag{1-11}$$

Note that $\rho_{jj} = \frac{S(W_{jj})}{\sqrt{(S(|W_j|^2)S(|W_j|^2))}} = \frac{S(|W_j|^2)}{S(|W_j|^2)} = 1$. The matrix C, like the M matrix, reveals the Hermitian feature ($\rho_{ij} = \rho_{ji}^*$).

Then, we can define the multiple coherence by the following formulas:

$$R_{y(q)}^2 = 1 - \frac{C^d}{C_{yy}^d}, \tag{1-12}$$

$$\rho_{yj.q_j} = -\frac{C_{j1}^d}{\sqrt{C_{yy}^d C_{jj}^d}}. \tag{1-13}$$

1.2.3. Quadruple wavelet coherence

The squared quadruple wavelet coherency between series y and other series x_1, x_2 and x_3 will be denoted by $R_{y(x_1x_2x_3)}^2$ (or $R_{y(q)}^2$ or $R_{1(234)}^2$) and is given by the formula

$$R^2_{y(q)} = R^2_{1(234)} = 1 - \frac{M^d}{S_{11}M^d_{11}}, \tag{1-14}$$

where M ($4x4$ Hermitian matrix) is the smoothed cross-wavelet spectra SW_{ij} which is the smoothed version of W_{ij}

$$SW_{ij} = S(W_{ij}), \tag{1-15}$$

where S is a certain smoothing operator.

$$M = \begin{bmatrix} SW_{11} & SW_{12} & SW_{13} & SW_{14} \\ SW_{21} & SW_{22} & SW_{23} & SW_{24} \\ SW_{31} & SW_{32} & SW_{33} & SW_{34} \\ SW_{41} & SW_{42} & SW_{43} & SW_{44} \end{bmatrix}. \tag{1-16}$$

Remember, if the matrix M is a Hermitian, we can express $M = M^*$, where $*$ is a conjugate transpose. Hence,

$$\begin{cases} \forall\, i \neq j, & SW_{ij} = SW^*_{ji} \\ \forall\, i, & SW_{ii} = S(|W_i|^2) \in \Re^+ \end{cases} \tag{1-17}$$

The cofactor of the (i, j) element in matrix M is named as:

$$M^d_{ij} = (-1)^{(i+j)}\det M^j_i, \tag{1-18}$$

where M^j_i shows the sub-matrix, which achieves from M via removing row i and column j. Additionally, $M^d = \det M$.

The matrix C represents the smoothed complex wavelet coherencies (ρ_{ij}) that are derived from the matrix M.

$$C = \begin{bmatrix} 1 & \rho_{12} & \rho_{13} & \rho_{14} \\ \rho_{21} & 1 & \rho_{23} & \rho_{24} \\ \rho_{31} & \rho_{32} & 1 & \rho_{34} \\ \rho_{41} & \rho_{42} & \rho_{43} & 1 \end{bmatrix}, \tag{1-19}$$

Note that $\rho_{jj} = \frac{S(W_{jj})}{\sqrt{(S(|W_j|^2)S(|W_j|^2))}} = \frac{S(|W_j|^2)}{S(|W_j|^2)} = 1$. The matrix C, like the M matrix, reveals the Hermitian feature ($\rho_{ij} = \rho^*_{ji}$).

Then, we can define the quadruple wavelet coherence by the following formulas:

$$R^2_{1(q)} = 1 - \frac{C^d}{C^d_{11}}. \tag{1-20}$$

In order to calculate the squared quadruple wavelet coherence, the C^d_{11} is needed to be calculated from coherence matrix C as follows:

$$C = \begin{bmatrix} 1 & \rho_{23} & \rho_{24} \\ \rho_{32} & 1 & \rho_{34} \\ \rho_{42} & \rho_{43} & 1 \end{bmatrix}, \tag{1-21}$$

After solving the above matrix, the result comes up as

$$\begin{aligned} C^d_{11} &= 1 - \rho_{23}\rho_{32} - \rho_{24}\rho_{42} - \rho_{34}\rho_{43} + \rho_{23}\rho_{34}\rho_{42} + \rho_{24}\rho_{32}\rho_{43} \\ &= 1 - R^2_{23} - R^2_{24} - R^2_{34} - 2\Re(\rho_{23}\rho_{34}\rho^*_{24}). \end{aligned} \tag{1-22}$$

We evaluated C^d from Eq. (1-22) as

$$C^d = C^d_{11} - \rho_{12}C^d_{12} + \rho_{13}C^d_{13} - \rho_{14}C^d_{14}, \tag{1-23}$$

After having the above equation, we inserted all the relevant terms into it and got the following formula;

$$\begin{aligned} C^d = \; & 1 - \rho_{12}\rho_{21} - \rho_{13}\rho_{31} - \rho_{24}\rho_{42} - \rho_{23}\rho_{32} \\ & -\rho_{14}\rho_{41} - \rho_{34}\rho_{43} + \rho_{12}\rho_{23}\rho_{31} + \rho_{13}\rho_{21}\rho_{32} \\ & +\rho_{12}\rho_{24}\rho_{41} + \rho_{14}\rho_{23}\rho_{32}\rho_{41} - \rho_{13}\rho_{24}\rho_{32}\rho_{41} \\ & +\rho_{13}\rho_{34}\rho_{41} - \rho_{12}\rho_{23}\rho_{34}\rho_{41} + \rho_{14}\rho_{21}\rho_{42} \\ & -\rho_{14}\rho_{23}\rho_{31}\rho_{42} + \rho_{13}\rho_{24}\rho_{31}\rho_{42} - \rho_{13}\rho_{21}\rho_{34}\rho_{42} \\ & +\rho_{23}\rho_{34}\rho_{42} + \rho_{14}\rho_{31}\rho_{43} - \rho_{12}\rho_{24}\rho_{31}\rho_{43} \\ & -\rho_{14}\rho_{21}\rho_{32}\rho_{43} + \rho_{24}\rho_{32}\rho_{43} + \rho_{12}\rho_{21}\rho_{34}\rho_{43}, \end{aligned} \tag{1-24}$$

To simplify Eq. (1-27) in terms of R-squared, it is as follows:

$$\begin{aligned} C^d = \; & 1 - R^2_{12} - R^2_{13} - R^2_{14} - R^2_{23} - R^2_{24} - R^2_{34} \\ & +R^2_{14}R^2_{23} + R^2_{12}R^2_{34} + R^2_{13}R^2_{24} \\ & +2\Re(\rho_{12}\rho_{24}\rho^*_{14}) + 2\Re(\rho_{13}\rho_{34}\rho^*_{14}) \\ & +2\Re(\rho_{12}\rho_{23}\rho^*_{13}) + +2\Re(\rho_{23}\rho_{34}\rho^*_{24}) \\ & -2\Re(\rho_{12}\rho_{23}\rho_{34}\rho^*_{14}) \\ & -2\Re(\rho_{13}\rho^*_{12}\rho_{34}\rho^*_{24}) \\ & -2\Re(\rho_{13}\rho^*_{14}\rho^*_{23}\rho_{24}). \end{aligned} \tag{1-25}$$

After placing Eq. (1-25) and Eq. (1-28) to the Eq. (1-23), we can write the detailed squared multiple wavelet coherency formulae, which is then used in the numerical calculations.

1.3. Empirical Analysis

To investigate the association among equity return, interest rate, cross-currency rate, and trade deficit differences, we used monthly frequency data between October 1990 and March 2015. In total, 294 observations are used. The stock price is measured as the closing price of the BIST 100 index collected from the CBRT. Interest rate (IRSTCI) is the interbank money rate from the CRBT. The real exchange rate is calculated via the foreign exchange rate. Interest and exchange rates are built by OECD and sourced from its official website. The trade balance is collected from the Bloomberg data services. In the study, we employed logarithmic returns for the series to express. The logarithmic returns are evaluated as: $R_t = \ln(P_t/P_{t-1}) \times 100$. Note that R_t is the percent return and P_t and P_{t-1} denote the closing price on time t and $t-1$, respectively. *Figure 1-1* shows all the return series and *Table 1-1* provides fundamental statistics of the time series used in the investigation.

1.3.1. Preliminary analysis

Table 1-1 displays preliminary basic statistics of all analyzed series. The mean of stock, real exchange rate, and trade balance returns are positive, unlike the mean of interest rate return. The standard deviation of interest rate and trade balance returns are greater than other variables in terms of volatility. *Figure 1-1* supports these findings. Trade balance and interest rate returns are more volatile with respect to stock and real exchange rate returns, especially during the financial crisis periods. S, E, I, and T denote stock, foreign exchange, interest rate, and trade deficit, respectively.

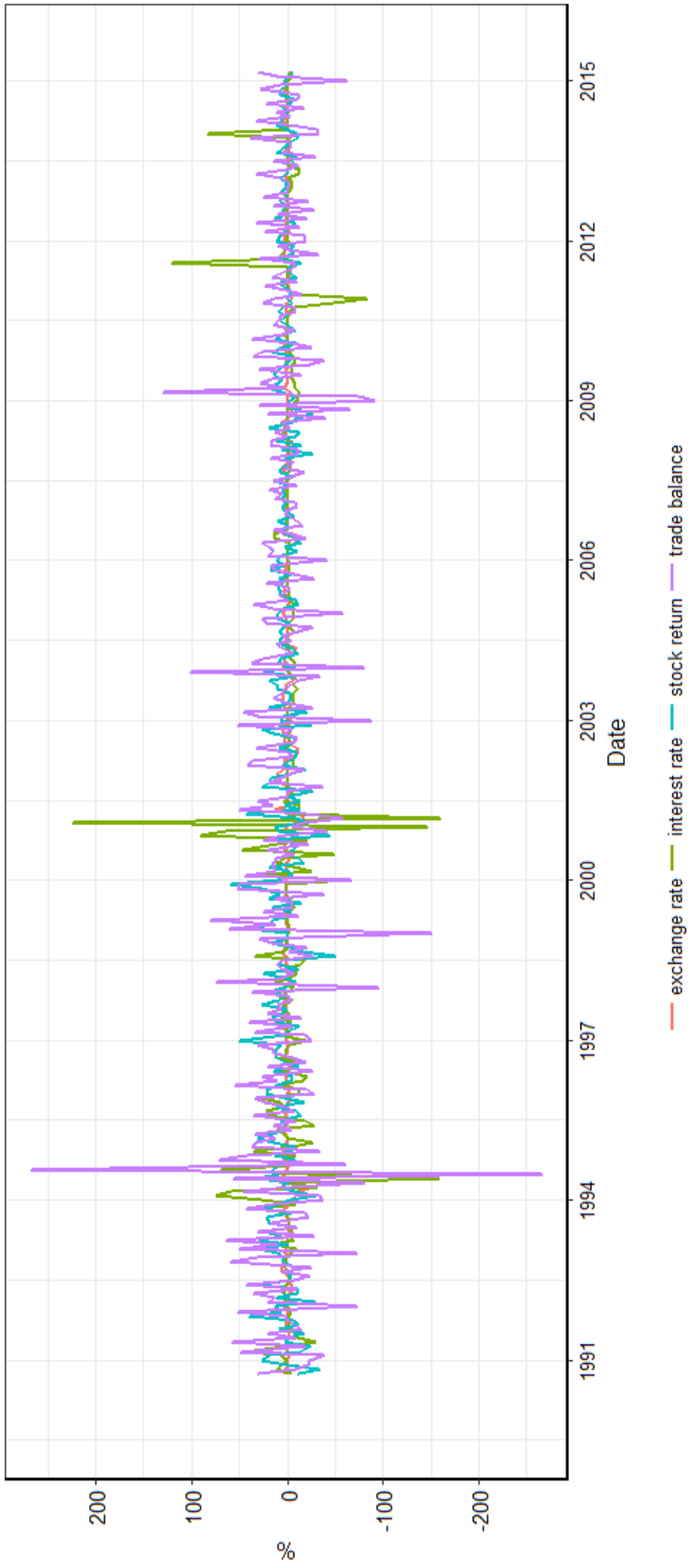


Figure 1-1. Return series.

Table 1-2. Fundamental statistics.

	S	E	I	T
Mean	2.5072	0.0737	-0.6891	3.0150
Median	2.4345	0.4310	0.0000	2.2043
Maximum	58.6585	12.0580	223.794	267.057
Minimum	-49.4856	-27.6243	-159.534	-266.419
Std. Dev.	13.4570	3.8063	26.6980	38.3698
Skewness	0.2103 [0.1440]	-1.9963 [0.000]	0.7097[0.0000]	-0.3321 [0.0213]
Kurtosis	2.2642 [0.0000]	11.5309 [0.0000]	29.0230 [0.0000]	15.7199 [0.0000]
J-B	64.97 [0.0000]	1824.09 [0.0000]	10343.4 [0.0000]	3032.58 [0.0000]
A-D	1.8224 [0.0001]	10.3395 [0.0000]	49.5731 [0.0000]	7.3674 [0.0000]
T-test	3.1946 [0.0015]	0.3324 [0.7397]	-0.4426 [0.6583]	1.3473 [0.1739]
Ljung-Box	9.4025 [0.4943]	48.7961 [0.0000]	49.7935 [0.0000]	77.0106 [0.0000]
Box-Pierce	9.0849 [0.5240]	48.0953 [0.0000]	49.0551 [0.0000]	76.0338 [0.0000]
ARCH LM	27.4674 [0.0066]	29.2767 [0.0035]	80.7697 [0.0000]	86.3995 [0.0000]
ADF	-5.0600 [0.0100]	-6.0597 [0.0100]	-7.1105 [0.0100]	-7.8203 [0.0111]

Note. J–B and A–D indicate Jarque–Bera and Anderson–Darling normality tests, respectively. Ljung–Box and Box–Pierce denote serial correlation tests. ARCH LM checks heteroscedasticity. ADF shows Augmented Dickey-Fuller, [.] indicates probability value.

A measure of skewness indicates that the distribution of stock return is symmetric. The distribution of exchange rate, interest rate, and trade balance returns are negative, positively, and negatively skewed, respectively. The measure for kurtosis shows the distributions of all the return series have fat tails. According to Jarque-Bera and Anderson-Darling, test statistics reject normality to a 5% significance level for all indicators. T-test results are statistically significant for all the return series, unlike S. The mean of E, I, and T are statistically zero at a 95% confidence level.

Table 1-3. Correlation results of all the return series.

	S	E	I	T
(a) Pearson Correlation				
S	1			
E	0.0864	1		
I	-0.2380	-0.0483	1	
T	0.0980	-0.0204	0.0607	1
(b) Kendall Correlation				
S	1			
E	0.0865	1		
I	-0.1456	0.0149	1	
T	0.0526	-0.0600	-0.0039	1
(c) Spearman Correlation				
S	1			
E	0.1300	1		
I	-0.2112	0.0216	1	
T	0.0755	-0.0876	-0.0054	1

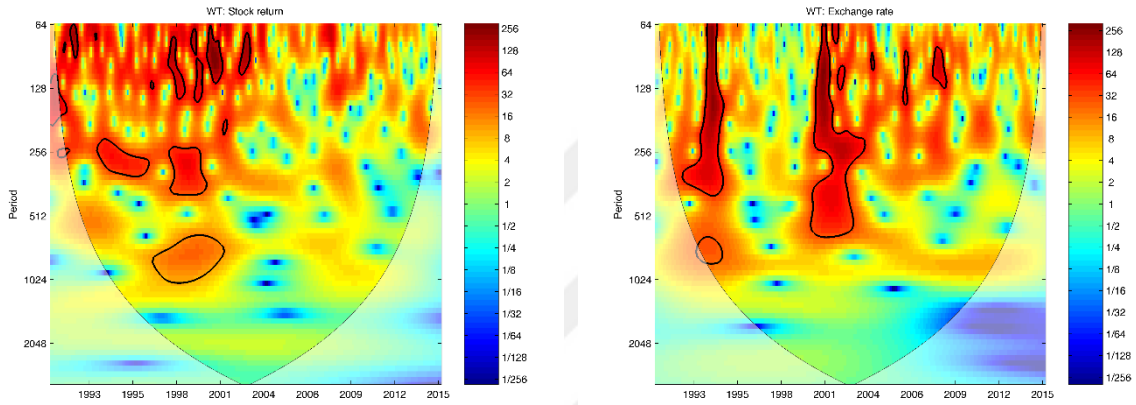
Note. S denotes stock, E shows exchange rate, I indicates interest rate, and T shows trade balance returns.

According to Ljung-Box and Box-Pierce serial correlation tests, the stock return test statistic shows no autocorrelation. Otherwise, autocorrelation occurs in exchange rate, interest rate, and trade balance returns. Besides, ARCH LM heteroscedasticity tests show that the return series exhibit time-varying volatility clustering. The next step is to perform the unit root tests of the return series. According to the Augment Dickey-Fuller (ADF) test, all the return series are stationary.

Table 1-2 indicates Pearson, Kendall, and Spearman correlations, respectively. According to the correlation matrices, the historical relationship between all the return pairs is weak. In other respects, the correlation between E and I is negative regarding Pearson correlation, unlike Kendall and Spearman correlations.

1.3.2. The wavelet transform

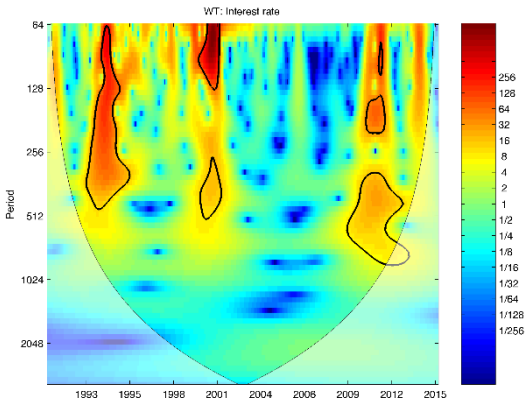
Figure 1-2 confers the power spectrum plots of all variables. The stock return plot (*Figure 1-2*(a)) has only a small number of significant regions: from 1999 to 2003, the wavelet power spectrum of stock return detects high common power in high frequency for 2.1 - 4.2 months periods (cycle). In addition, from 1994 to 1996 and 1998 to 2001, there are two significant regions over eight months to 1.4 years periods. From 1997 to 2001, it reveals significant power for 1.6 months to 2.8 years periods.



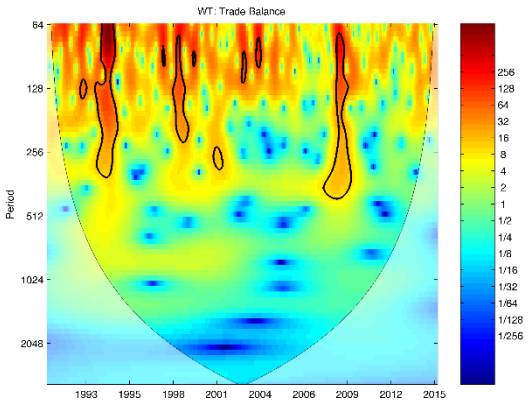
(a) WT: S (b) WT: E

Figure 1-2. Power spectrums.

In *Figure 1-2*, unlike stock return, the exchange rate (b) plus interest rate (c) wavelet power spectra exhibit the same common islands. These periods are clear for only Turkey's currency and banking crises in 1994 and 2001, respectively. There are significant regions from 2009 to 2012 in the wavelet power spectrum of interest rate return apart from exchange rate return.



(c) WT: I



(d) WT: T

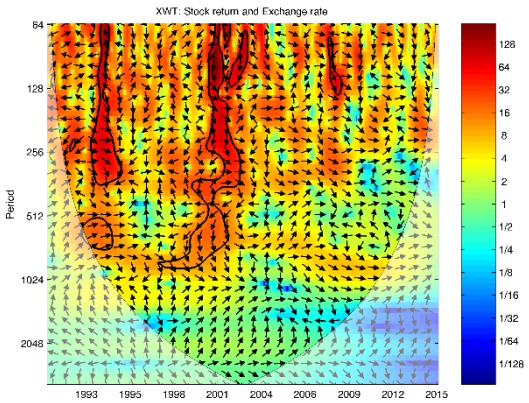
Fig. 1-2. (Continued)

The trade balance spectrum in *Figure 1-2*(d) determines high common power in high frequencies for two months to 1 year in 1994, 1999, and 2007 to 2009.

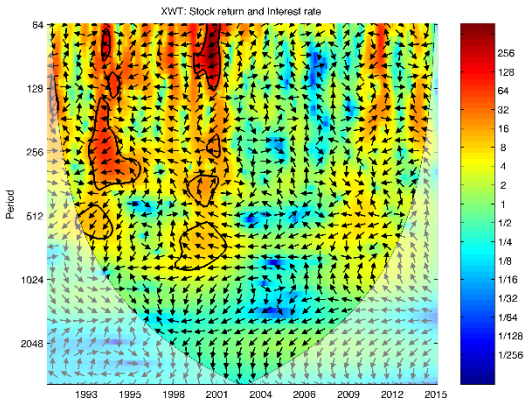
1.3.3. The cross-wavelet transform

Figure 1-3 displays all pairs, which are XWT results, captured the same meaningful regions denoted via a black outline in 1994 and 2001.

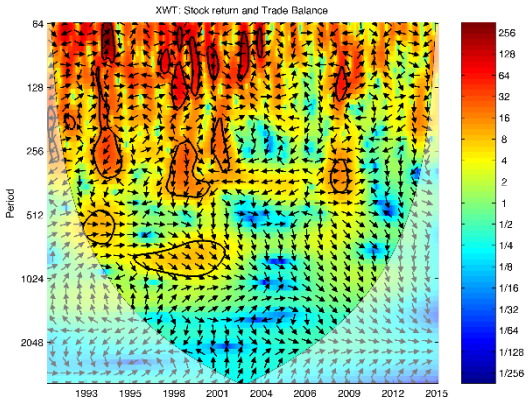
For stock and exchange rate returns doublet, (*Figure 1-3*(a)), there are significant regions for the 1994 Turkey's currency crisis period the two months - 1-year; variables positively are related, and the exchange rate is leading. In a 1.4 - 2 years span, variables are still positively correlated, and the exchange rate is lagging. About 2001, during the banking crisis, over two months - 2.8 years and about 2008 and about 2008, over less than four months cycle, series exhibit positive relationship and exchange rate is leading.



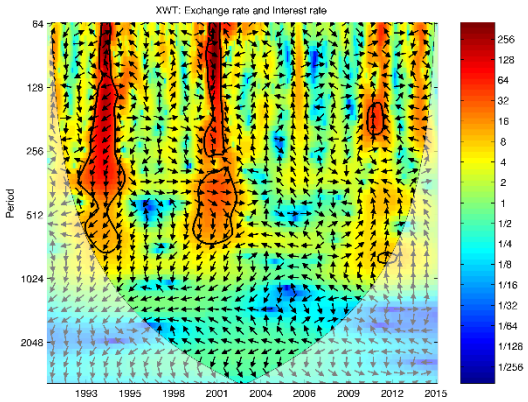
(a) XWT: S–E



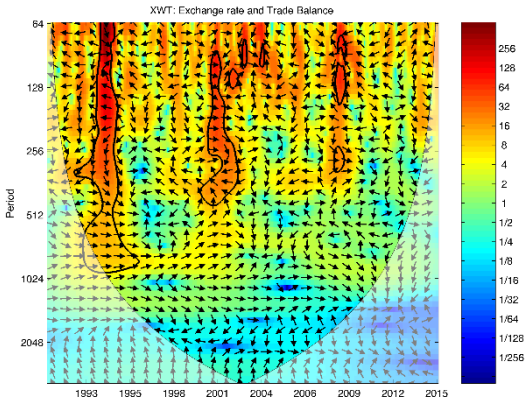
(b) XWT: S–I



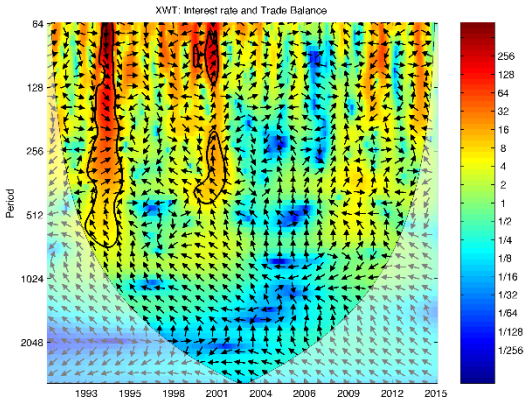
(c) XWT: S–T



(d) XWT: E–I



(e) XWT: E–T



(f) XWT: I–T

Figure 1-3. The cross wavelet transforms of return series.

In *Figure 1-3*(b), for stock and interest rate doublet, there are significant periods about 1994 over two months - 1.5 years and about 2001 over 2-months span; series are negatively correlated, and interest rate is lagging. In addition, about 2001 over 1.6-2.8 years, variables are still negatively correlated, and interest rate return leads.

Figure 1-3(c) presents the exchange rate and trade balance returns' cross wavelet transform. It indicates significant dependence in 1994, between 1998 - 2001 and 2009 over high frequencies for two months - 1-year cycle. Besides, about 1994, over 1.4 - 2 years cycle series have a positive relationship. From 1995 to 2001, over 2.2 and 2.8 years, results indicate that series exhibit positive correlation and trade balance return leads.

For exchange rate and interest rate returns doublet (*Figure 1-3*(d)), there are significant periods about 1994 across two months - 2.3 years, series designate reverse connection and interest rate return is lagging. Around 2001 across two months - 2 years, direction and lead-lag relation change, variable exhibit positive correlation and interest rate return leads.

For the pair of exchange rate and trade balance returns (*Figure 1-3*(e)), there are significant periods about 1994 across 2 - 8.5 months sequence, series are negatively correlated, and trade balance is lagging. At the same time horizon in 8.5 months - 2.8 years, the sign of the relationship turns into positive and trade balance leads. Around 2001 in three months - 1.3 years, series still positive correlation and trade balance continue to lead.

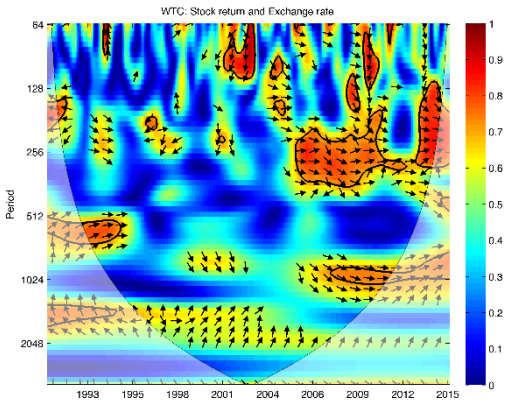
Finally, in *Figure 1-3*(f), for interest rate and trade balance doublet, there are significant periods around 1994 in 2 - 8.5 months, series exhibit positive correlation and trade balance leads. On the other hand, the relationship is still positive over 8.5 months - 1.4 years, but the trade balance is not leading anymore. About 2001 in 2.3 - 4 months cycle, variables are positively correlated, and trade balance return is lagging. At the same time horizon over

8.3 months - 1.3 years period relationship turns opposite, which means that series are negatively correlated, and trade balance leads.

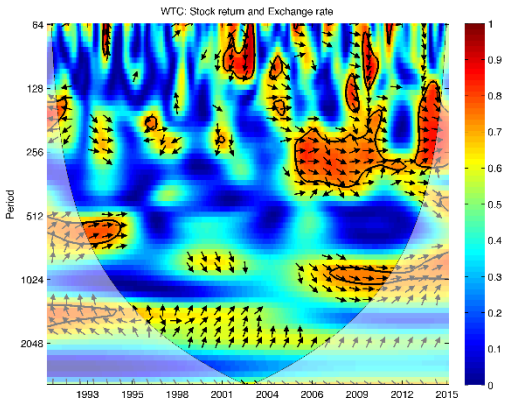
1.3.4. Wavelet coherence

For stock and exchange rate returns doublet (*Figure 1-4*(a)), there are significant periods around 1994 in high frequency for two and mode than two months cycle, series are negatively correlated, and exchange rate return leads. Across 1.4 - 1.9 years, the relationship turns in the opposite direction, series exhibit positive correlation, and exchange rate return is lagging. About 2001 in high frequency for 2 - 4 months cycle, they are negatively correlated, and exchange rate return is lagging. Around 2006 - 2012 over eight months - 1.2 years, series are the same direction, and exchange rate return leads. Between 2008 - 2010 in low frequency for 2.8 years, series exhibit positive relationship and exchange rate leads.

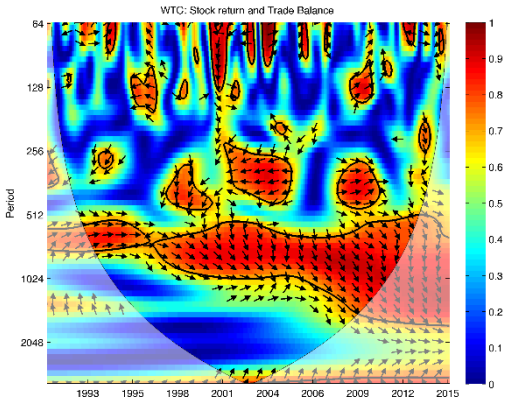
In *Figure 1-4*(b), for stock and interest rate returns doublet, there are significant periods around 1994 in high frequency for two months cycle, over eight months and 1.4-2 years, variables exhibit negative association. In terms of the lead-lag relationship, in high-frequency interest rate return leads, unlike other cycles. Around 1998 across 2.6 - 8 months cycle, series are negatively correlated, and interest rate return leads. Roughly 2001 in low frequency for 1.4 - 2.8 years, series still show same information which is negatively correlated and interest rate return leads. Around 2011, in high frequency for two and more than two months, variables display opposite relation, and interest rate return is lagging. Nearby 2014 across 4.5 - 8.5 months, series exhibit contrary co-movement and interest rate return leads.



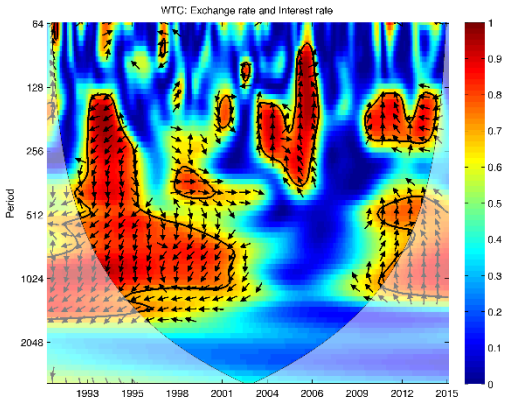
(a) WTC: S–E



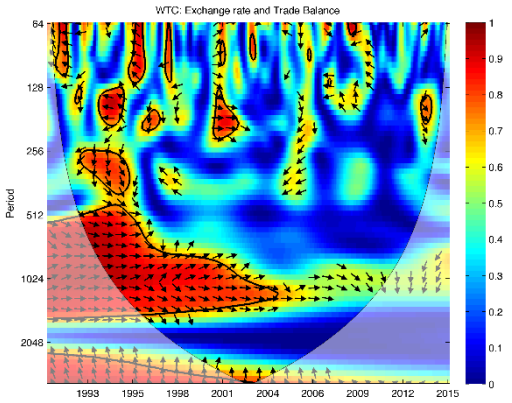
(b) WTC: S–I



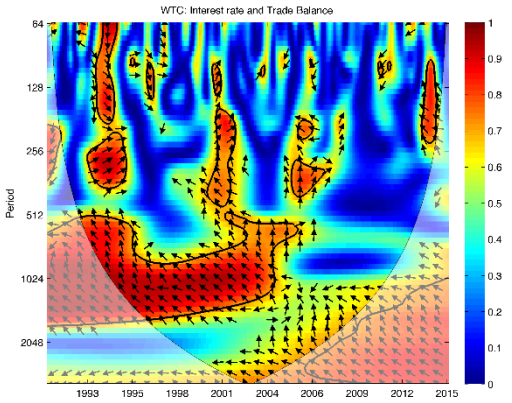
(c) WTC: S–T



(d) WTC: E–I



(e) WTC: E–T



(f) WTC: I–T

Figure 1-4. The wavelet coherence of the return series.

There are significant regions for the pair of stock and trade balance returns (*Figure 1-4*(c)); in all the time domain over 1.4 - 4 years, series exhibit positive relation and trade balance leads. Besides, wavelet coherence indicates significant dependence between stock and trade balance returns in high frequency for 2 - 4 months from 1994 up to 2015. Around 1994, between 1998 - 2000, 2001 - 2005, and 2009 over eight months - 1.4 years, variables negatively correlate all time horizons except 2009. On the other hand, trade balance returns are lagging all the time slots.

In *Figure 1-4*(d), for exchange rate and interest rate returns doublet, there are significant periods around 1994 - 2001 over four months - 2.8 years, series are negatively correlated, and interest rate return is lagging. Around 1999 across 10 - 15 months, the relationship and directions turn opposite, which means they exhibit positive association and interest rate return leads. Between 2004- 2006 over 2 - 11 months and about 2010 - 2014 over 4 - 6 months cycles, pairs are negatively correlated and interest rate return leads.

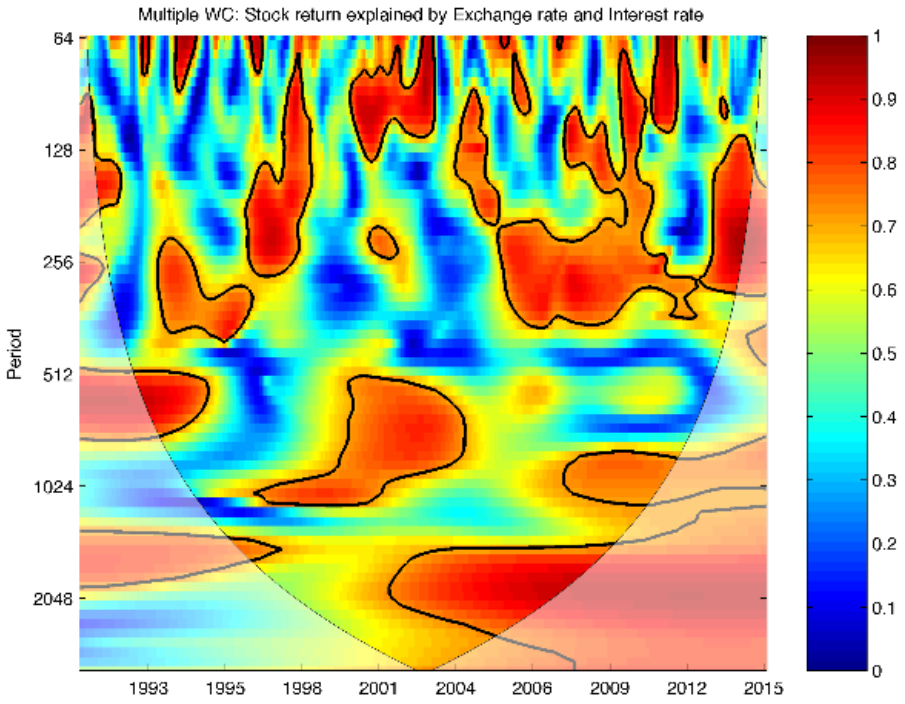
For exchange rate and trade, balance returns doublet (*Figure 1-4*(e)), there are significant periods between 1994 - 1995 in high frequency for 2 - 6 months cycle, series indicates negative relationship and trade balance return leads. Across 1 - 1.4 years, co-movement changes the direction of the relation sign, and trade balance return still leads. In addition, *Figure 1-4*(e) shows a significant positive relationship among exchange rate and trade balance returns in low frequency for 1.4 - 5 years cycle from 1994 up to 2004. Around 2001, across 4.5 - 6.5 months period, variables exhibited positive correlation and trade balance return leads.

Finally, for the pair of interest rate and trade balance returns (*Figure 1-4*(f)), there are significant periods around 1994 in high frequency for 2 - 6 months, and six months - 1 year period, series indicates positive relationship. Regarding the lead-lag analysis, trade balance leads in the first region, and in the second, it is lagging. Around 2001 across 2.5 - 8.5 months,

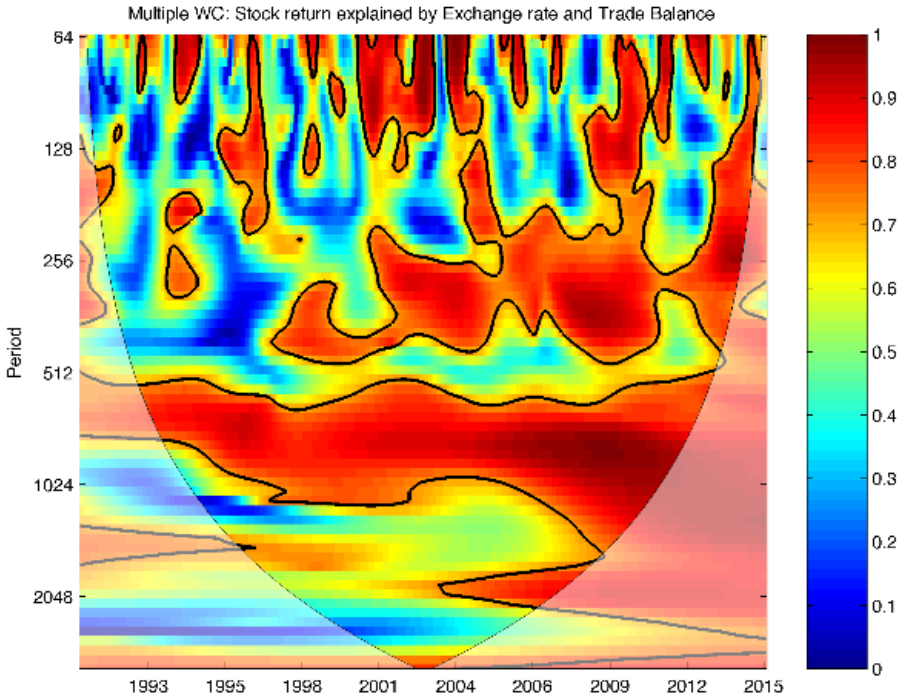
series are positively correlated. On the contrary, 8.5 months - 1.4 years, the direction of the association turns negative. In both cases, trade balance return is leading. About 2006 across 6.5 months - 1.2 years and about 2014 over 2.5 - 8 months cycles, variables exhibit negative association and trade balance return leads. In addition, *Figure 1-4*(f) demonstrates a significant negative relationship between interest rate and trade balance returns in low frequency for 1.4 - 5 years from 1993 up to 2005.

1.3.5. Multiple wavelet coherence

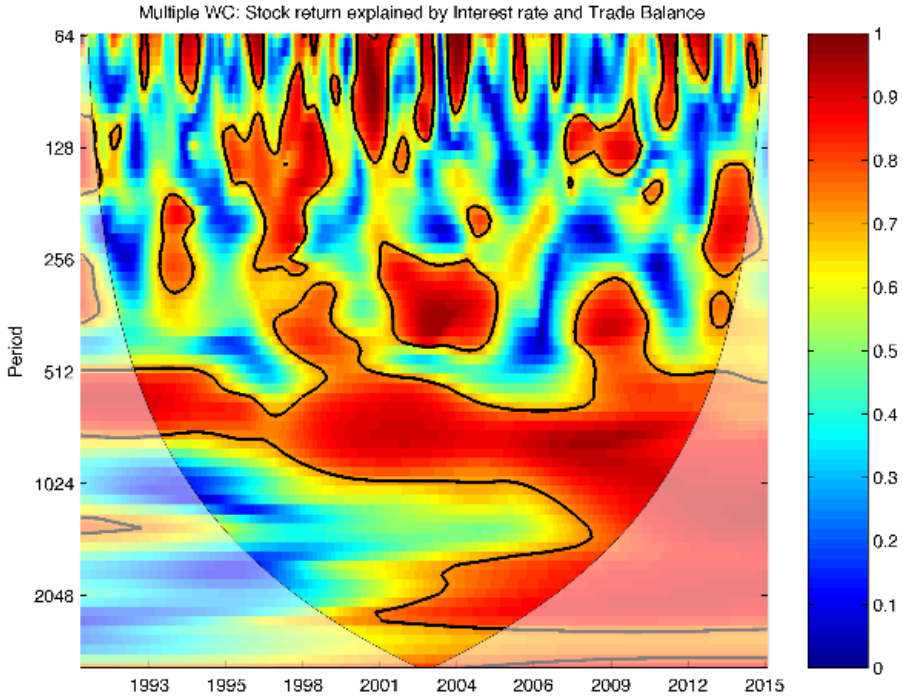
Figure 1-5 demonstrates the results of multiple wavelet coherence for all possible triplets. MWC indicates that stock return is lagging other variables. According to the results of *Figure 1-5*(a), all-time domains in high frequency up to a 1-year, the exchange rate interprets the stock and interest rate returns.



(a) S, E, and I



(b) S, E, and T



(c) S, I, and T

Figure 1-5. Multiple wavelet coherence.

Figure 1-5 (b)-(c) present the results of multiple wavelet coherence of stock-exchange rate-trade balance and stock-interest rate-trade balance returns, respectively. The results can be discussed in two parts as high and low frequency. First, in high frequency for two months up to 1-year cycle, the stock return is explained by explanatory variables in all the time domains. Second, in low frequency for 1.4 - 4 years cycle, the stock return is significantly determined by the others in all the time domain. As a result, the stock return is significantly described by exchange rate-trade balance and interest rate-trade balance doublets in the entire time horizon (October 1990 - March 2015).

1.3.6. Quadruple wavelet coherence

Multiple wavelet coherence has been discussed in the last section (Sec. 1.3.5). *Figure 1-6* illustrates quadruple wavelet coherence, which investigates the disclosure of stock returns (S) by all other indicator series (E, I, T) together.

Stock return is exactly explained by explanatory variables in all time and frequency domains. It means that multivariate time series models might be used to explain stock returns. For this reason, the stock return was fitted to both $VARMA(1,1)$ (vector autoregressive moving average) and $ARMA(1,1)$ (autoregressive moving average) processes, and forecasting performances of these models were compared with each other in the last section.

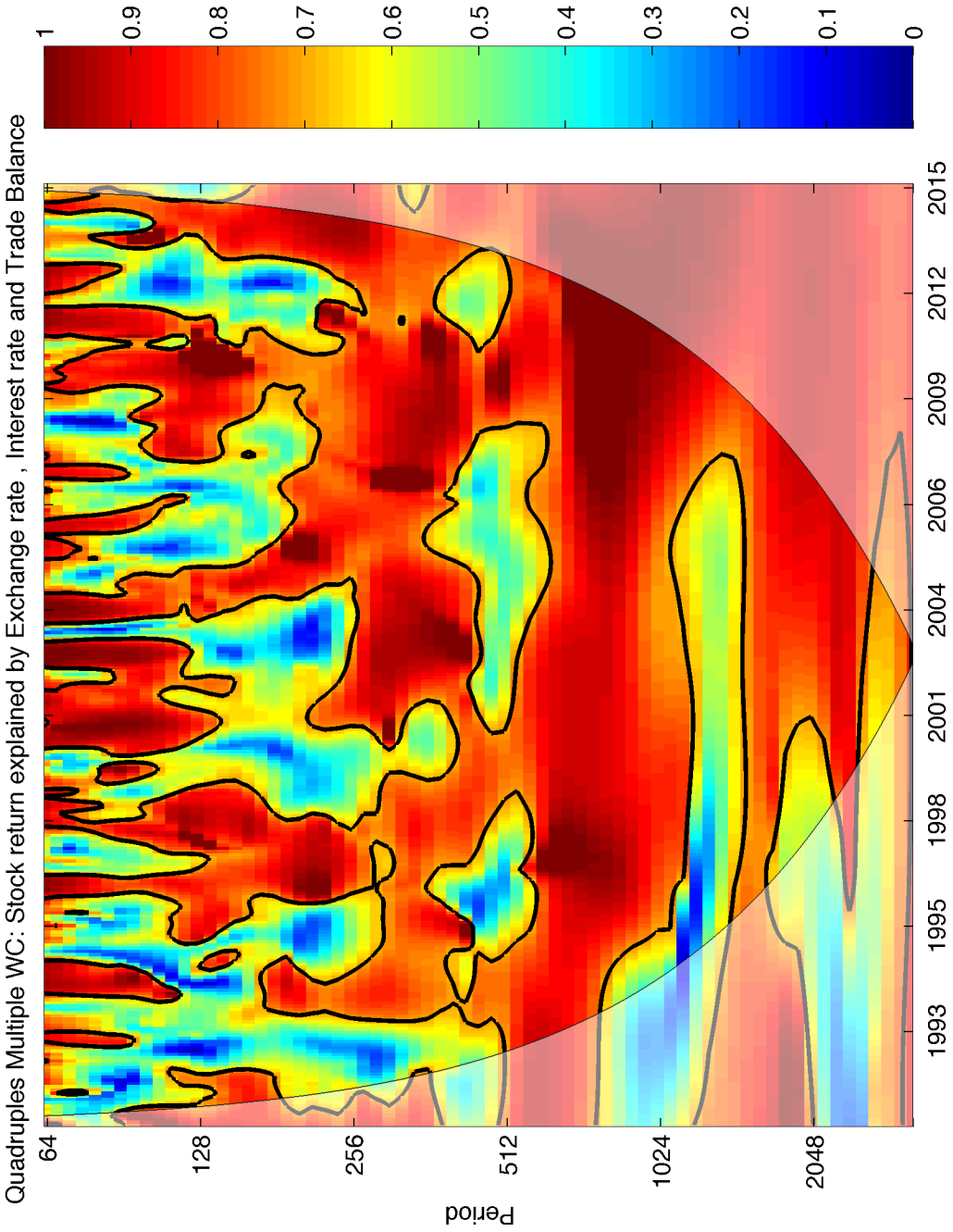


Figure 1-6. Quadruple wavelet coherence.

1.4. Forecast

Our QWC analysis showed that stock return is highly correlated with explanatory variables returns in the most time-frequency domains. Two significant regions are examined deeply. The first region denoted by Panel A is between January 1995 and August 2003 in low frequency for 1.4 - 2.8 years cycle in *Figure 1-6*. The second region (Panel B) arises from January 2002 to September 2009 for 8.5 months - the 1-year cycle in *Figure 1-6*. The time series which correspond to an interested region should be extracted to make scale by scale analyzing. Primarily, whole return series are extracted into the time and frequency domain by continuous wavelet transform. Scale and octave-voice were matched with each other by using a wavelet scalogram. After that, the time series representing the interested regions is obtained by inverse wavelet transform for only related octave-voice. Thus, the linear relation of the time series that corresponds to time-frequency space is determined using the non-linear link deciding by QWC.

Multivariate time series models allow us to verify the high relation between the variables using wavelet analysis and express numerically. Multivariate time series analysis considers synchronically various time series. In particular, Vector autoregressive moving-average models are suitable to recognize dynamic associations among analyzed time series [26]. These models make linear forecasts not only to use the history of the related data but also to consider other related variables. For this reason, it provides quietly good results in economic data forecasting than similar models [27]. Moreover, Mihaela Simionescu (2014) showed that VARMA models give better results for the short-run forecast of economic variables as against VAR (vector autoregressive) and AR (autoregressive) models [28]. Therefore, we employ univariate and vector-based autoregressive moving-average models to examine stock returns in Panel A and Panel B. In this section, stock return was fitted and forecast five-step ahead for Panel A and three-step ahead for Panel B by using both VARMA

and ARMA models ([29], [30]). The best model was selected by comparing the forecast performances.

The general form of the vector autoregressive moving average VARMA(p,q) is as follows:

$$\phi(B)z_t = \phi_0 + \theta(B)a_t. \tag{1-26}$$

z_t denotes time series with dimension k, ϕ_0 is invariable and $a_t \in \text{I. I. D}$

$$\phi(B) = I_k - \sum_{i=1}^{p} \phi_i B^i$$

$$\theta(B) = I_k - \sum_{i=1}^{q} \theta_i B^i$$

1.4.1. Panel A

The Panel A consists of stock, exchange rate, interest rate, and trade balance returns from January 1995 to August 2003 in low frequency for 1.4 - 2.8 years cycle in Quadruple wavelet coherence (*Figure 1-6*). In total, 104 observations were used. *Figure 1-7* indicates all the return series in Panel A, and *Table 1-3*(a) provides a correlation matrix for the Panel A. According to the Panel A's correlation matrix, all return series are highly correlated in a selected time and frequency domain, unlike *Table 1-2*(a, b, c).

Stock, exchange rate, interest rate, and trade balance returns are fitted, and stock return is predicted five steps ahead by VARMA(1,1) and ARMA(1,1) models. Five-step ahead prediction results of VARMA(1,1) and ARMA(1,1) models are shown in Figure 1-8. Actual stock returns, forecast values, and standard errors are listed for all models from September 2003 to January 2004 in *Table 1-4*.

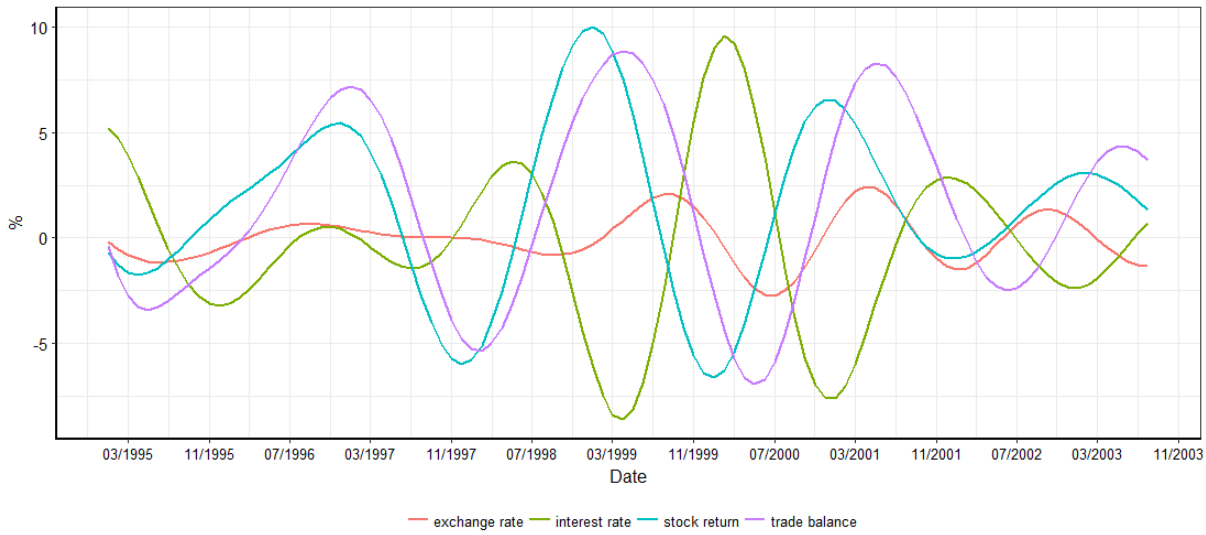
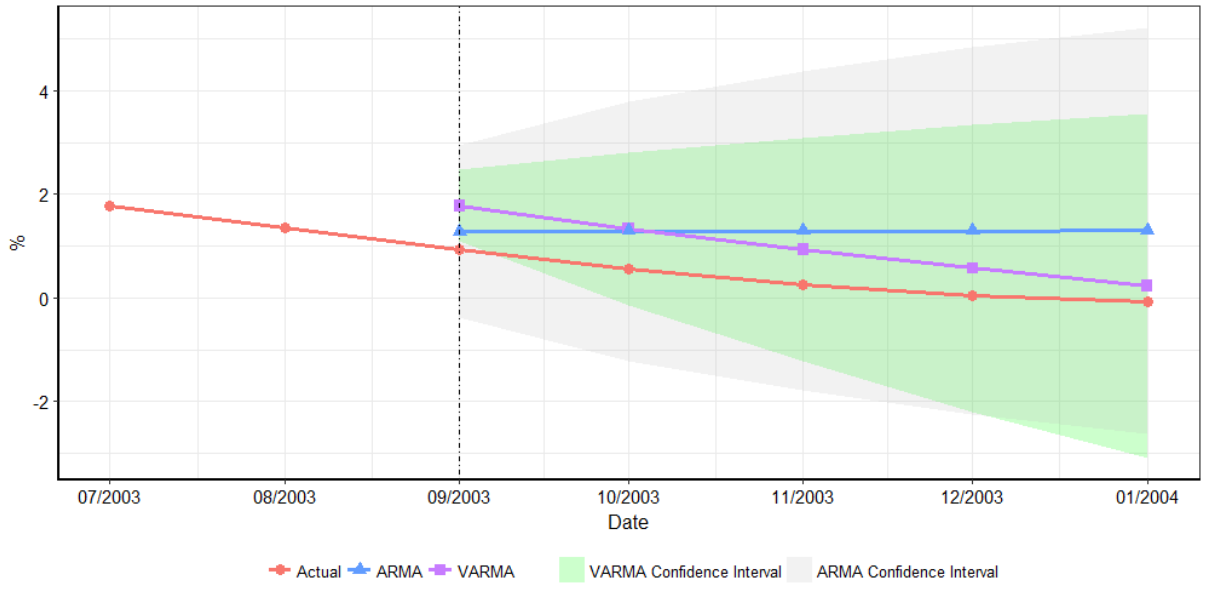


Figure 1-7. Panel A: Return series.

We utilize several performance metrics (RMSE and MAE) to compare the out-of-sample forecast performance in alternative models. It is shown in *Table 1-5*(a) and indicates that the VARMA(1,1) model has the best performance according to the results of both criteria.



Note. Yellow and gray colored areas represent 95% confidence bands for VARMA and ARMA models, respectively.

Figure 1-8. Stock returns the out-of-sample forecast for Panel A.

Table 1-4. Panel A and Panel B correlation matrix.

	S	E	I	T
(a) Panel A				
S	1			
E	0.1621	1		
I	-0.7189	-0.3458	1	
T	0.6718	0.5917	0.5533	1
(b) Panel B				
S	1			
E	0.6481	1		
I	-0.0693	-0.2251	1	
T	0.3138	0.1873	-0.1033	1

Note. S denotes stock, E shows exchange rate, I indicates interest rate, and T shows trade balance returns.

Table 1-5. Panel A Forecast results.

		VARMA(1,1)		ARMA(1,1)	
Date	Actual	Forecast	SE	Forecast	SE
2003-09	0.9339	1.7776	0.3531	1.2851	0.8437
2003-10	0.5637	1.3327	0.7490	1.2885	1.2744
2003-11	0.2575	0.9351	1.0981	1.2917	1.5718
2003-12	0.0370	0.5703	1.4147	1.2948	1.8044
2004-01	-0.0800	0.2268	1.6983	1.2977	1.9961

Note. SE denotes standard errors of the forecast.

1.4.2. Panel B

The Panel B consists of stock, exchange rate, interest rate, and trade balance returns from January 2002 to September 2009 for 8.5 months - the 1-year cycle in Quadruple wavelet coherence (*Figure 1-6*). In total, 93 observations were used. *Figure 1-9* indicates all the return series in Panel B, and *Table 1-3*(b) provides a correlation matrix for Panel B.

Table 1-6. Panel A and Panel B forecast performance comparison.

	RMSE	MAE
(a) Panel A		
VARMA(1,1)	0.6543	0.6261
ARMA(1,1)	1.0196	0.9491
(b) Panel B		
VARMA(1,1)	0.3228	0.3184
ARMA(1,1)	0.6130	0.5716

Note. RMSE stands for root mean square error. MAE denotes mean absolute error.

According to the correlation matrix Panel B, all return series are highly correlated in a selected time and frequency domain, unlike *Table 1-2*(a, b, c) except for the correlation between stock and interest rate returns.

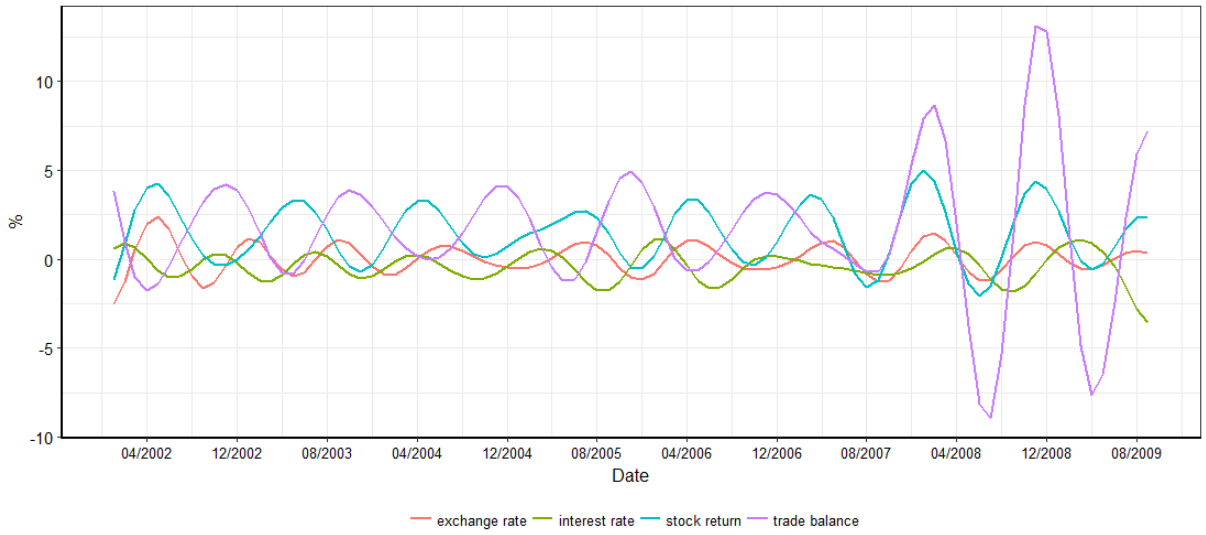
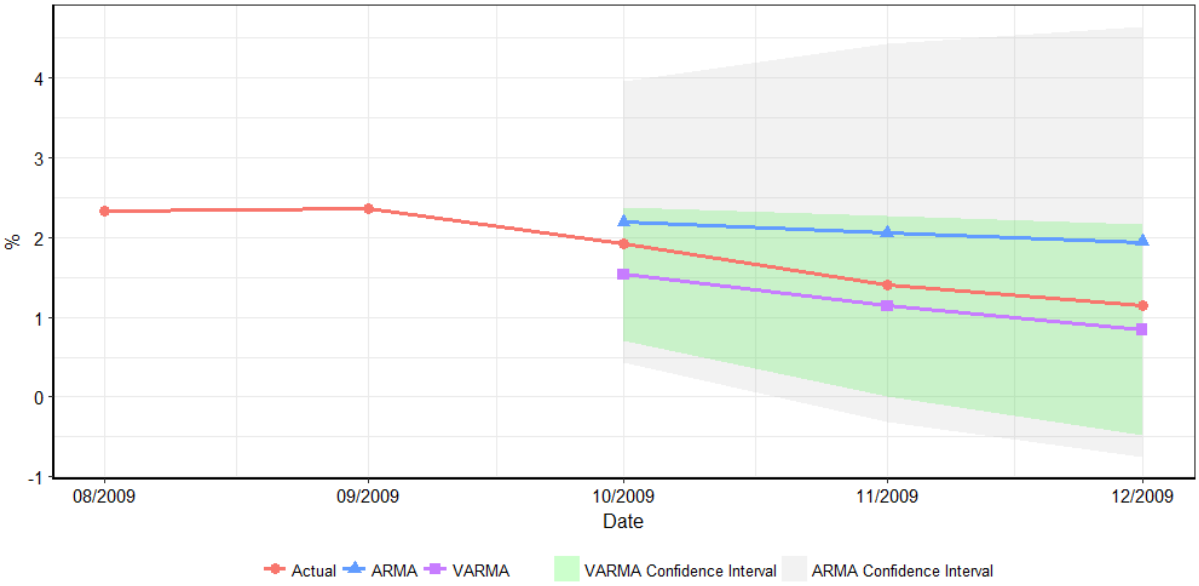


Figure 1-9. Panel B: Return series.

Stock, exchange rate, interest rate, and trade balance returns are fitted, and stock return is predicted three-step ahead by VARMA(1,1) and ARMA(1,1) models. Three-step ahead prediction results of VARMA(1,1) and ARMA(1,1) models are shown in Figure 1-10.



Note. Yellow and gray colored areas represent 95% confidence bands for VARMA and ARMA models, respectively.

Figure 1-10. Stock returns the out-of-sample forecast for Panel B.

Actual stock returns, forecast values, and standard errors are listed for all models from October 2009 to December 2009 in *Table 1-6*. We utilize several performance metrics (RMSE and MAE) to compare the out-of-sample forecast performance in alternative models. It is shown in *Table 1-5*(b) and indicates that the VARMA(1,1) model has the best performance according to the results of both criteria.

Table 1-7. Panel B Forecast results.

		VARMA(1,1)		ARMA(1,1)	
Date	Actual	Forecast	SE	Forecast	SE
2009-10	1.9277	1.5369	0.1816	2.1974	0.8973
2009-11	1.4057	1.1397	0.3356	2.0552	1.2112
2009-12	1.1449	0.8462	0.4536	1.9406	1.3773

Note. SE denotes standard errors of the forecast.

1.5. Conclusion

We investigate and determine the structure of the dynamic association of the most critical indicators from October 1990 to March 2015. The period covers Turkey's currency and banking crises; the US sub-prime mortgage crisis and the European sovereign debt crisis occurred in 1994, 2001, 2008, and 2009. The traditional wavelet analysis and quadruple wavelet coherency approaches have been employed.

The cross-wavelet results (XWT) capture Turkey's currency and banking crises in 1994 and 2001, respectively. About 1994, in terms of stock and exchange rate returns doublet, series are exhibit positive relation and exchange rate leads. For stock and interest rate returns doublet, series are negatively correlated, and interest rate is lagging. In terms of stock and trade balance returns, series are negatively correlated, and trade balance is lagging like stock and interest rate doublet. For exchange rate and interest rate doublets, variables are also exhibited negative relation, and interest rate return is lagging. As a result of this, stock fluctuations may be affected significantly by exchange rate (in-phase), interest rate (out of phase), and trade balance (out of phase) returns during the 1994 currency crisis. There is almost the same picture in 2001 regarding stock and exchange rate and stock, and interest rate doublets. However, in terms of exchange rate and interest rate returns doublets, the arrows show that the series is positively correlated, and interest rate returns lead.

The wavelet coherence results (WTC) demonstrate both financial crises (1994 currency, 2001 banking, 2008 sub-prime mortgage, and 2009 European debt crises) and shocks. On the other hand, the cross-wavelet results (XWT) capture only the 1994 currency and 2001 banking crises. About 1994, for stock and exchange rate returns doublet, series are negatively correlated over two and more than two months, and exchange rate leads. In terms of stock and interest rate returns, series are shown a negative relationship, and interest rate is lagging. For stock and trade balance returns doublet, in high frequency, the arrows indicate

series are opposite direction and trade balance is lagging. In terms of exchange rate and interest rate, series exhibit negative relation, and interest rate return is lagging. Around 2001, the series of stock and exchange rate returns are negatively correlated, and exchange rate return is lagging. For stock and interest rate returns doublet, variables exhibit opposite relation, and interest rate leads. In terms of stock and trade balance returns, in high frequency, series have negative connection and trade balance is lagging. The relationship direction is negative for exchange rate and interest rate doublet, which is lagging.

According to the lead-lag relationship, the results of XWT and WTC support together for the 1994 currency crisis. Nevertheless, for the 2001 banking crisis, phase difference results are different. According to Andries et al. (2014) [14], "cross wavelet describes the common power of two processes without normalization to the single wavelet power spectrum. This can produce misleading results because one essentially multiplies the continuous wavelet transform of two time series." Because of this, we consider wavelet coherence results.

Table 1-7 demonstrates that these two crises have structural differences. In the 1994 currency crisis, fluctuations of currency may affect stock, interest rate, and trade balance returns. Unlike the 1994 currency crisis, the 2001 banking crisis was based on interest rate fluctuations and affected Turkey’s whole banking system. Phase difference results confirm this information. These results indicate that macroeconomic fluctuations often appear in crisis periods as stock and interest rate return fluctuations occurred in Turkey’s crises and provide us information about the reasons for the occurrence of crises.

Table 1-8. Phase difference results.

	1994		2001	
	XTC	WCT	XTC	WTC
S & E	Lead	Lead	Lead	Lag
S & I	Lag	Lag	Lag	Lead
S & T	Lag	Lag	Lag	Lag
E & I	Lag	Lag	Lead	Lag

Note. S indicates stock return, E denotes exchange rate return, I stands for interest rate return, and T denotes trade balance return. The table is designed for the second element. (XTC: 1994, exchange rate returns are leading)

In addition, wavelet coherence and multiple wavelet coherence capture financial crises and whole shocks in the time-frequency domain. Consequently, all findings revealed that the most crucial indicators are significantly associated with Turkey's financial crises.

In other respects, multiple and quadruple wavelet coherences demonstrate that stock returns are explained by the exchange rate, interest rate, and trade balance returns in the most time-frequency domain. This finding allows us to analyze stock returns scale by scale and strongly correlated large scales indicating linear behavior. For this reason, we applied multivariate and univariate time series methodologies for predicting stock returns in selected regions. According to Panel A and Panel B forecast performances, the VARMA(1,1) model appears to be the most appropriate model.

2. Traces of the Multifractal Nature of the Financial Crises in Turkey: Co-Movement of the Hölder Exponents and Large-Scale Forecast

Summary

This chapter investigates the multifractal behavior of the probability of default of real sector firms and Turkey sovereign CDS. Moreover, we emphasize the co-movements of Hölder exponents during financial crisis periods. For this reason, first, it is necessary to figure out the default probabilities of real sector firms. The default probability is evaluated weekly by the methodology of Moody's Analytics, a commonly used approach in which the market value of a firm is a call option written on its total assets. Following techniques are applied to recognize the multifractal behavior of the large-scale fluctuations of PDs and CDS: Multifractal detrended fluctuation analysis, cross-correlation analysis, and moving average cross-correlation analysis. This way, we can evaluate local Hurst exponents. Besides, the oscillation method employs to estimate the pointwise and local Hölder exponents. Between January 2001 and March 2018, the structure of dynamic co-movements of Hölder exponents determined by applying wavelet coherency methodology, and the relations in the crisis period are revealed. The selected period covers crises with structural differences: the Turkey banking crisis, the mortgage crisis[1], and the debt crisis[2] in 2001, 2008, and 2009, respectively. Besides, during periods of financial crises, among the local Hölder exponents, severely correlated large scales show multifractal features, and hence VARFIMA (vector autoregressive fractionally integrated moving average) forecasting provides better results than scalar models.

[1] US sub-prime mortgage crisis
[2] European sovereign debt crisis

2.1. Introduction

The real sector is crucial for countries' stability and healthy growth. At the same time, global influences affect faster and more severe countries that depend on imports to export, like Turkey. This fact appears as a result of globalization and financial openness. Hence, shocks, jumps, booms, busts, and the consequences of these effects, financial crises contagion as a rapid epidemic. This situation can summarize large-scale macroeconomic fluctuations resulting from financial liberalization, particularly import-dependent countries' real sectors. Along with many components in the real sector, it suits a leading indicator of financial crises. It generally consists of five main sub-sectors: Consumer Cyclical, Industrials, Basic Materials, Consumer Non-Cyclical, and Utility.

Various studies in the literature explore the derivative financial instrument called credit default swap (CDS) and stock exchange relations during crisis periods. CDS is one of the successful financial invitations of the last few years due to its use as a risk perception indicator by analysts, governments, and decision-makers [31]. From local or regional events to global events, they can influence by many various factors. Therefore, sovereign CDS is used to establish a connection between financial crises and sectoral default probabilities.

Fractal theory, one of the most significant achievements of recent times, was developed by Mandelbrot [32]. Edgar E. Peters [33] is the first to practice fractal theory in the economic aspect. Then, various researches have been conducted that examine the non-linear features of the financial time series. Among all models, multifractal ones are considered reliable models representing complexity in economic systems [34]. Many studies have applied the multifractal approach to financial time series to discover financial crises. Agaev et al. [35] discovered local Hölder exponents to determine crashes in stock markets. Tang et al. [34] identified the foreign exchange market's multifractal features and inspected the mortgage crisis evidence. According to the extensive literature, the local Hölder exponent can capture

crashes better. The local Hölder exponents can be used to investigate the relationship between CDSs and sectoral default rates, especially during financial crises with severe crashes. For this reason, this study concentrates on revealing that the relation of dynamic co-movement between the sectoral default probabilities and CDS is an important leading indicator in determining the financial crises through the multifractality and both pointwise and local Hölder exponents.

In this research, we have three principal purposes of choosing Turkey [36]: (a) It is dependent on export and import due to the structural shortage in Turkey. Import-depending causes the problem of chronic current account deficit. Hence, Turkey can be affected by more influence from macroeconomic fluctuations. (b) According to the IMF and World Bank records, Turkey is a developing market. According to the majority of rating firms, Turkey's rating is at the lowest investment class. (c) Turkey has encountered all species of crises in the last two decades. Therefore, the results of wavelet analysis can recognize various types of financial crises.

The chapter is mapped as follows: Section 2.2 provides a refresher on the following background knowledge. Section 2.2.1 highlights Moody's KVM expected default frequency. The multifractal detrended analysis presents in Section 2.2.2. Wavelet analysis is introduced in Section 1.2.1 and similarly employed in this chapter. In Section 2.3, first, sectoral default probabilities are evaluated. Then, the multifractal toolbox analyzes CDS and PDs and determines multifractal spectrums and q-order Hurst, pointwise, and local Hölder exponents, which are present in Section 2.2.2.4. In the last part of Section 2.3, we implement the wavelet toolbox to discover dynamic co-movements of CDS and PDs for both levels and all multifractal exponents. Moreover, multivariate and univariate time series techniques, VFARIMA, VARMA, FARIMA, and ARMA models, are presented in Section 2.4. Candidate models are measured and predicted.

2.2. Methodology

2.2.1. Moody's KVM expected default frequency

The Mood's KMV[3] expected default frequency model calculates a default probability for each firm at any given time and depends on its capital structure, asset value, and volatility [37]. The KMV-Merton model predicts debt's market value by implementing the Merton (1974) model, and it essentially has two critical assumptions.

1. The firm's total value mimics a geometric Brownian motion.

$$dA = \mu A dt + \sigma_A A dW \tag{2-1}$$

   where A is the total value of the firm, μ is the expected log-return on A, σ_A is the volatility of firm value, and dW is a standard Weiner process.

2. The firm has issued only one discount bond maturing in T periods.

In light of these assumptions, the firm's equity is a call option, drawing from the Black-Scholes-Merton formula. Subsequently, we estimate probability at default in the following steps:

Step 1:

$$E_0 = A_0 \mathcal{N}(d_1) - D e^{-rT} \mathcal{N}(d_2). \tag{2-2}$$

$$d_1 = \frac{\ln(\frac{A_0}{D}) + (r + 0.5\sigma_A^2)}{\sigma_A \sqrt{T}}; d_2 = d_1 - \sigma_A \sqrt{T}.$$

Step 2:

$$\sigma_E = \frac{A_0}{E_0} \mathcal{N}(d_1) \sigma_A. \tag{2-3}$$

[3] Kealhover, McQuown, and Vasicek, cofounders of the KMV Corporation

where E is a total market value, σ_E is stock log-return volatility, A is a market value of a firm's asset, and σ_A the volatility of the firm's asset, and D indicates total dept. Equations (2-2) and (2-3) are solved together and found the firm's asset's volatility.

Step 3:

$$DP = STD + \frac{1}{2}LTD. \tag{2-4}$$

Step 4:

$$DD = \frac{A_T - DP}{\sigma_A A_T}. \tag{2-5}$$

Step 5:

$$PD = \mathcal{N}(-DD). \tag{2-6}$$

where STD and LTD denote short and long term debts, respectively. DP is the default point, and DD denotes distance-to-default, and PD is the probability of default.

2.2.2. Multifractal analysis

2.2.2.1. Multifractal detrended fluctuation analysis

By employing DFA analysis, local Hurst exponents for fluctuations are evaluated; hence the multifractal properties of the series can be determined. We can quantify and compare the multifractality of the financial time series via deriving the singularity spectra. We examine multifractality in the MF-DFA procedure, consisting of five marks proposed by Kantelhardt et al. [38].

(1) First, the series average subtracts from the cumulative sum for each point of the time series.

$$Y_i = \sum_{k=1}^{i} (x_k - \overline{x}), \tag{2-7}$$

where x_k represents the value of the series at the time k and $\overline{x}$ denotes the average of x_i.

(2) Second, the time series of length N divides into N_s segments. s denotes the length of an individual division, $N_s \equiv int(N/s)$. On the other hand, a similar procedure applies from $2N_s$ so that the end of the series ignores. Hence $2N_s$ segments are obtained.

(3) Third, the series local trend $\widetilde{Y}_v\,(i)$ is determined for each segment v,

$$\widetilde{Y}_v\,(i) = \widetilde{a}_k\, i^m + \ldots + \widetilde{a}_1\, i + \widetilde{a}_0 \tag{2-8}$$

where $i = 1, \ldots, s$ and $v = 1,2, \ldots, N_s$ and $m = 1,2, \ldots$ .Then, the least-squares fit is employed to calculate the variance of the local trends in each of the $2N_s$ members.

$$F^2(s, v) = \frac{1}{s}\sum_{j=1}^{s}(\,Y_{(v-1)s+j} - \widetilde{Y}_v\,(i))^2, \tag{2-9}$$

for $\forall\ v$ segment, $v = 1, \ldots, N$ and,

$$F^2(s, v) = \frac{1}{s}\sum_{j=1}^{s}(\,Y_{N-(v-N_s)s+j} - \widetilde{Y}_v\,(i))^2, \tag{2-10}$$

for $v = N_s + 1, \ldots, 2N_s$. Here $\widetilde{Y}_v\,(i)$ is the fitting polynomial in segment v.

(4) Next, we take the average over all segments to calculate the qth-order fluctuation function.

$$F_q(s) = \{\frac{1}{2N_s}\sum_{v=1}^{2N_s}[\,F^2(v, s)]^{q/2}\}^{(1/q)}, \tag{2-11}$$

where index variable q can take any real value. $F_q(s)$ expresses the generalized q dependent fluctuation function. We are involved in how $F_q(s)$ depends on the time scale s for various q.

(5) Finally, scaling features of the fluctuation functions define via investigating log-log plots $F_q(s)$ versus s for each value of q.

$$F_q(s) \sim s^{H(q)}. \tag{2-12}$$

where $H(q)$ denotes Generalized (local) Hurst exponent. In stationary time series, $H(2)$ and Hurst exponent (H) are indistinguishable from each other. When $H(q)$ is constant for various q indicates that the time series are monofractal. Positive and negative values of q can use for

expanding the effects of large and small price fluctuations in the scaling analysis, respectively.

2.2.2.2. Multifractal detrended cross-correlation analysis

By employing multifractal detrended cross-correlation analysis, we briefly introduce six marks proposed by Zhou [39].

(1) Consider two nonstationary time series x_i and y_i of the same length N, where $i = 1, \ldots, N$.

$$X_i = \sum_{k=1}^{i} (x_k - \overline{x}), \qquad Y_i = \sum_{k=1}^{i} (y_k - \overline{y}), \qquad i = 1, \ldots, N \tag{2-13}$$

where x_k and y_k represents the value of the series at the time k, $\overline{x}$ and $\overline{y}$ denote the average of x_i and y_i, respectively.

(2) Second, the time series of length N divides into N_s non-overlapping segments. s denotes the length of an individual division, $N_s \equiv int(N/s)$. On the other hand, a similar procedure applies from $2N_s$ so that the end of the series ignores. Hence $2N_s$ segments are obtained. The N_s is set as $10 < N_s < N/4$.

(3) Third, the series local trend $\widetilde{X}_v(i)$ and $\widetilde{Y}_v(i)$ are determined for each segment v,

$$\widetilde{X}_v(i) = \widetilde{a}_k\, i^m + \ldots + \widetilde{a}_1\, i + \widetilde{a}_0\,, \qquad \widetilde{Y}_v(i) = \tilde{b}_k\, i^m + \ldots + \tilde{b}_1\, i + \tilde{b}_0 \tag{2-14}$$

where $i = 1, \ldots, s$ and $v = 1,2, \ldots, N_s$ and $m = 1,2, \ldots$

(4) Then, the least-squares fit is employed to calculate the covariance of the local trends in each of the $2N_s$ members.

$$F^2(s, v) = \frac{1}{s} \sum_{j=1}^{s} [X_{(v-1)s+j} - \widetilde{X}_v(i)][Y_{(v-1)s+j} - \widetilde{Y}_v(i)], \tag{2-15}$$

for $\forall\, v$ segment, $v = 1, \ldots, N$ and,

$$F^2(s, v) = \frac{1}{s} \sum_{j=1}^{s} [X_{N-(v-N_s)s+j} - \widetilde{X}_v(i)][Y_{N-(v-N_s)s+j} - \widetilde{Y}_v(i)], \tag{2-16}$$

for $v = N_s + 1, \ldots, 2N_s$. Here $\widetilde{X}_v\,(i)$ and $\widetilde{Y}_v\,(i)$ are the fitting polynomial in segment v. Next, we take the average over all segments to calculate the qth-order fluctuation function.

$$F_q(s) = \{\frac{1}{2N_s}\sum_{v=1}^{2N_s}[\,F^2(v,s)]^{q/2}\}^{(1/q)}, \tag{2-17}$$

where the index variable q can take any real value $q \neq 0$. $F_q(s)$ expresses the generalized q-dependent fluctuation function. When $q = 0$, the equation is defined by,

$$F_0(s) = \exp\{\frac{1}{4N_s}\sum_{v=1}^{2N_s}\ln\,(F^2(s,v))\}, \tag{2-18}$$

(5) Analyze the scaling behavior of the fluctuation function by observing the log-log plots of $F_q(s)$ versus s. If two series are long-range cross-correlated, we obtain a power-law relationship as follows:

$$F_q(s) \sim s^{H_{xy}(q)}. \tag{2-19}$$

where $H_{xy}(q)$ denotes Generalized (local) Hurst exponent.

(6) The Renyi exponent $\tau_{xy}(q)$ can be used to characterize the multifractal nature,

$$\tau_{xy}(q) = qH_{xy}(q) - 1 \tag{2-20}$$

If the Renyi exponent function is a linear function of q, the cross-correlation of the two correlated series is monofractal; otherwise, it is multifractal. The singularity spectrum $f(\alpha)$ that describes the singularity content of the time series can be obtained through Legendre transform:

$$\alpha_{xy}(q) = H_{xy}(q) + H'_{xy}(q) \tag{2-21}$$

$$f_{xy}(\alpha) = q[\alpha_{xy} - H_{xy}(q)] + 1 \tag{2-22}$$

Here, α is the Hölder exponent that characterizes the singularities in time series.

2.2.2.3. Multifractal detrended moving average cross-correlation analysis

In Section 2.2.2.2, we investigate the local trends $\widetilde{X}_v\,(i)$ and $\widetilde{Y}_v\,(i)$ using least-square regression methods. There are many different approaches to the determination of $\widetilde{X}_v\,(i)$ and $\widetilde{Y}_v\,(i)$. One of these could be the moving average, in which the algorithm is called MF-X-DMA [40]. The extension of the MF-DCCA algorithms to high dimensions is straightforward [39]. The moving average function $\widetilde{Z}\,(t)$ of $Z \in X, y$ in a moving window [41] can be calculated as follows,

$$\widetilde{Z}\,(t) = \frac{1}{n}\sum_{k=-\lfloor (n-1)Q \rfloor}^{\lceil (n-1)(1-Q) \rceil} Z\,(t-k) \tag{2-23}$$

where n is the window size, $\lfloor g \rfloor$ is the largest integer smaller than g, $\lceil g \rceil$ is the smallest integer larger than g, and Q is the position parameter with the value varying in the range $[0,1]$. Hence, the moving average function considers $\lceil (n-1)(1-Q) \rceil$ data points in the past and $\lfloor (n-1)Q \rfloor$ points in the future.

2.2.2.4. Pointwise and local Hölder exponents

Pointwise and local Hölder exponents are defined as the following equations [42]. Let $\alpha \in (0,1)$, and $x_0 \in K \subset \mathbb{R}$. A function $f: K \to \mathbb{R}$ is in $C_{x_0}^{\alpha}$ if, for all x in a neighborhood of x_0,

$$|f(x) - f(x_0)| \leq c|x - x_0|^{\alpha} \tag{2-24}$$

where c is a constant. The pointwise Hölder exponent of f at x_0, denoted $\alpha_p(x_0)$, is the supremum of the α for which the Eq. (2-24) holds.

Let us introduce the local Hölder exponent: let $\alpha \in (0,1)$, $\Omega \subset \mathbb{R}$. We say that $f \in C_l^{\alpha}(\Omega)$ if:

$$\exists C: \forall x, y \in \Omega: \frac{|f(x) - f(y)|}{|x - y|^{\alpha}} \leq C \tag{2-25}$$

Let: $\alpha_l(f, x_0, \rho) = sup\{\alpha: f \in C_l^{\alpha}(B(x_0, p))\}$ and notice that $\alpha_l(f, x_0, \rho)$ is non-increasing as a function of ρ. Hence, we can set the following definition.

Let f be a continuous function. The local Hölder exponent of f at x_0 is the real number:

$$\alpha_l(x_0) = \alpha_l(f, x_0) = \lim_{\rho \to 0} \alpha_l(f, x_0, \rho) \tag{2-26}$$

The general approach to evaluation regularity is to apply the "oscillation" method. A function $f(t)$ is Hölderian with exponent $\alpha \in (0,1)$ at t if there exists α constant c such that for all t' in a neighborhood of t, $|f(t) - f(t')| \leq c|t - t'|^{\alpha}$. In terms of oscillations, this condition may design as $\exists c, \forall \tau \; osc_{\tau}(t) \leq c\tau^{\alpha}$ where $osc_{\tau}(t) = sup_{|t-t\prime|\leq\tau} f(t') - inf_{|t-t\prime|\leq\tau} f(t') = sup_{t\prime,t\prime\prime\in[t-\tau,t+\tau]} |f(t') - f(t'')|$. The estimator is then directly determined as the slope in the least-square linear regression.

2.3. Empirical Analysis

To investigate the dynamic link between the probability of default (called PD) of real sector firms and Turkey's CDS during crisis periods, the real sector firms in BIST 100 gather in 5 main sectors recommended by Thomson Reuters. *Table 2-1* presents sector descriptions and the number of firms included. We used both the market (stock price, interest rate, and CDS) and the firm's balance sheet data, weekly and quarterly, from January 2001 to March 2018. In total, 900 observations are employed.

Table 2-1. Sectoral distributions of firms.

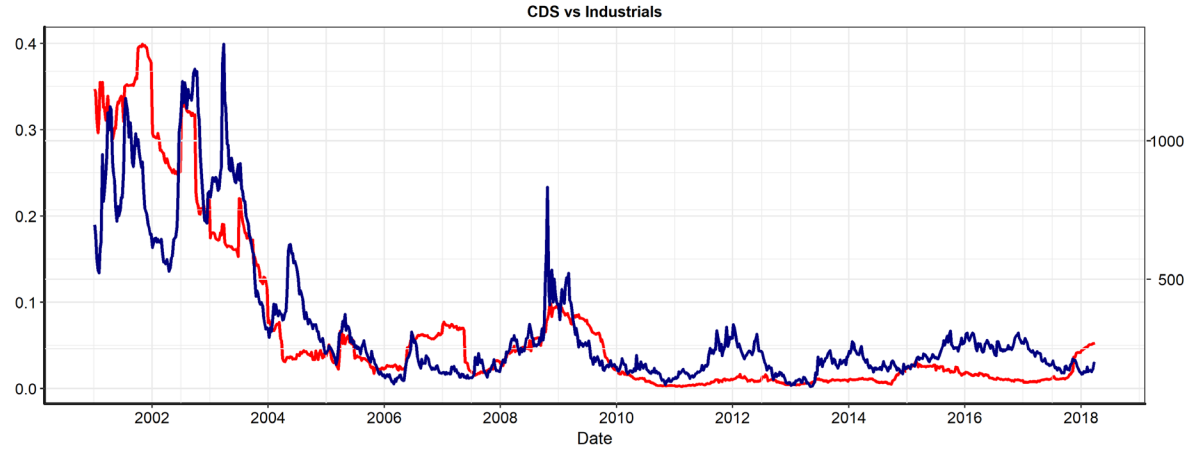
Sector	Number of firms
Consumer Cyclicals	22
Industrials	19
Basic Materials	15
Consumer Non-Cyclicals	9
Utilities	8

The sectoral probabilities of default consist of both financials and stock prices of real sector firms. Financials, stock prices, interest rates, and Turkey's five-year CDS gathered

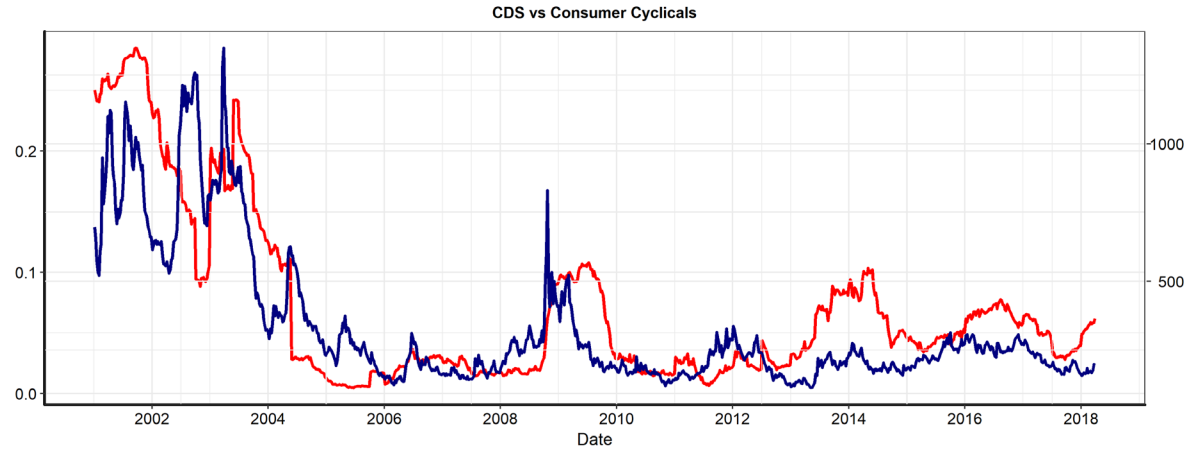
from the Thomson Reuters data service. The firms' default probabilities estimate by the methodology detailed in Section 2.2.1. Next, sectoral default probabilities estimate the PDs are weighted averages according to the market value of firms.

2.3.1. Preliminary analysis

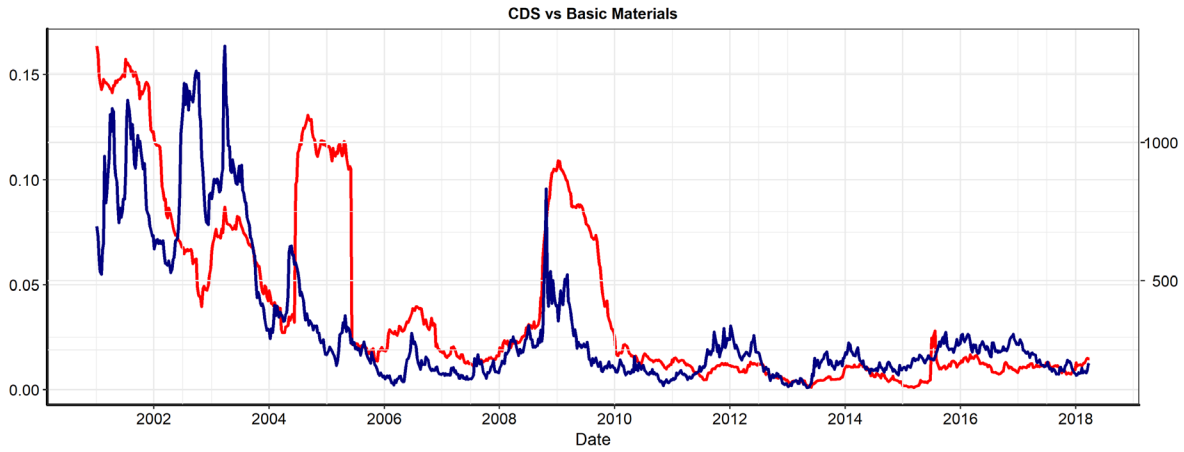
Figure 2-1 displays all sectoral default probabilities vs. CDS (red lines: PD, navy-blue: CDS). The following preliminary findings are available from the graphs of sectoral default rates with CDS. After the 2001 banking crisis, all sectors are returning to normal levels quicker. On the contrary, the pressure on the CDS has slowed back to normal according to sectoral risks.



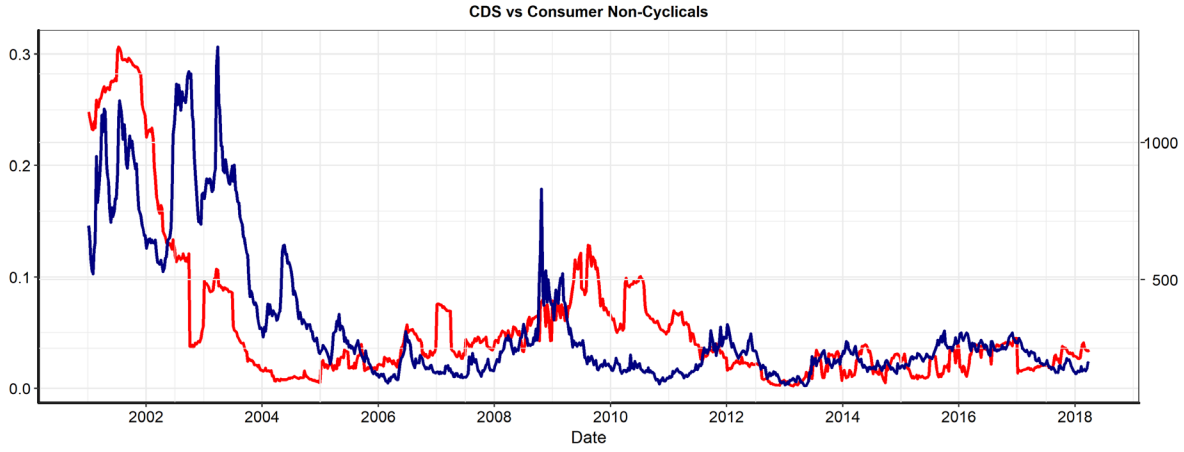
(a) CDS versus PD of Industrials



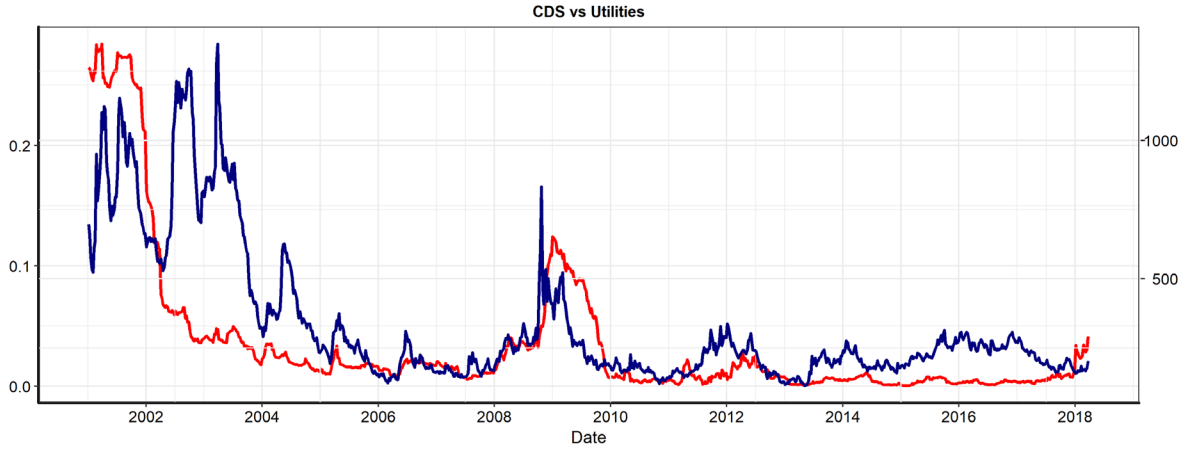
(b) CDS versus PD of Consumer Cyclicals



(c) CDS versus PD of Basic Materials



(d) CDS versus PD of Consumer Non-Cyclicals



(e) CDS versus PD of Utilities

Figure 2-1. Sectoral PDs (red) and CDSs plot (blue)

Between 2004 and 2006, unlike other sectors, there is a stress in the Basic Materials sector not reflected in the CDS. Between 2008 and 2009, all sectoral default probabilities and CDS prove the influences of US sub-prime mortgage and European sovereign debt crises. Sectoral risks experienced a structural breakdown in the post-2010 period. The Consumer Cyclical sector is at the forefront as the sector in which the default probabilities are most volatile. The Basic Materials and the Consumer Non-Cyclical sectors have a similar oscillation with CDS. The Industrials and Utilities sectors are also flat under the CDS.

Table 2-2 provides descriptive statistics for both PDs and CDS. The sample means of the default probabilities of all sectors are in the 3-7% band. Except for the Basic Materials sector, the maximum levels of historical default probabilities are 28-40%. The skewness and kurtosis mean that all series distributions are asymmetric, positively skewed, and have fat tails. According to Jarque–Bera, and Anderson–Darling, test statistics reject normality in all series. According to Ljung–Box and Box–Pierce serial correlation tests statistics, all series have no serial correlation. Also, ARCH LM heteroscedasticity tests prove that all series exhibit time-varying volatility clustering. The next step is to perform the stationarity tests of all series. Both unit root (ADF, PP, and KPSS) and spectrum based (PSR) stationarity tests are applied. The PP, KPSS, and PSR test results indicate that there is clear evidence to reject stationarity. These findings confirm by the ADF test excluding the Basic Materials and Utilities sectors.

The Hurst exponent is referred to as the “index of long-range dependence” or persistent behavior. The Hurst exponent is between 0.5 and 1, showing that the time series has long-term memory. We apply R/S, empirical, spectral, and detrended fluctuation analysis (DFA)-based approaches to estimate the Hurst exponents. The Hurst exponents’ results are

Table 2-2. Descriptive statistics.

	CDS	CC	Industrials	Basic Materials	CNC	Utilities
Mean	334.077	0.070	0.069	0.039	0.056	0.036
Max	1348.333	0.285	0.399	0.164	0.306	0.284
Min	112.887	0.005	0.002	0.001	0.002	0.000
Median	235.411	0.041	0.026	0.016	0.034	0.014
Std. Dev.	255.143	0.070	0.096	0.042	0.064	0.062
Skewness	1.908	1.605	1.981	1.330	2.436	2.902
	[0.0000]	[0.0000]	[0.0000]	[0.0000]	[0.0000]	[0.0000]
Kurtosis	2.766	1.645	2.810	0.519	5.542	7.723
	[0.0000]	[0.0000]	[0.0000]	[0.0000]	[0.0000]	[0.0000]
J-B	832.812	487.692	884.590	275.579	2042.149	3500.045
	[0.0000]	[0.0000]	[0.0000]	[0.0000]	[0.0000]	[0.0000]
A-D	102.775	73.283	120.781	84.589	97.646	149.684
	[0.0000]	[0.0000]	[0.0000]	[0.0000]	[0.0000]	[0.0000]
L-B	9122.195	9732.706	9901.795	9342.007	9516.493	9389.941
	[0.0000]	[0.0000]	[0.0000]	[0.0000]	[0.0000]	[0.0000]
B-P	9039.542	9643.273	9810.359	9257.196	9429.497	9304.626
	[0.0000]	[0.0000]	[0.0000]	[0.0000]	[0.0000]	[0.0000]
ARCH LM	856.064	878.385	876.191	878.867	883.257	883.442
	[0.0000]	[0.0000]	[0.0000]	[0.0000]	[0.0000]	[0.0000]
ADF	-2.808	-2.237	-2.133	-3.583	-2.843	-3.999
	[0.2363]	[0.4145]	[0.5220]	[0.0344]	[0.2215]	[0.0100]
PP	-20.138	-7.482	-7.037	-16.347	-9.613	-8.685
	[0.0700]	[0.6924]	[0.7172]	[0.1979]	[0.5735]	[0.6252]
KPSS	6.029	4.206	6.885	7.010	3.847	4.126
	[0.0100]	[0.0100]	[0.0100]	[0.0100]	[0.0100]	[0.0100]
PSR	636.963	563.663	1232.120	1150.144	221.796	783.463
	[0.0000]	[0.0000]	[0.0000]	[0.0000]	[0.0000]	[0.0000]

Note. J-B and A-D indicate Jarque-Bera and Anderson Darling normality tests, respectively. L-B (Ljung-Box) and B-P (Box-Pierce) denote serial correlation tests. ARCH LM test indicates heteroscedasticity test. ADF denotes Augmented Dickey-Fuller; PP indicates Phillips-Perron, and KPSS shows Kwiatkowski–Phillips–Schmidt–Shin unit root tests. PSR shows Priestley-Subba Rao spectrum-based stationarity test. The test significance level is 95%, [.] indicates p-value.

Table 2-3. Hurst exponents.

	CDS	CC	Industrials	Basic Materials	CNC	Utilities
R/S	0.975	0.977	0.973	0.950	0.935	0.894
Empirical	0.943	0.935	0.890	0.896	0.931	0.862
Whittle	1.010	1.030	0.981	1.020	0.990	1.042
DFA	1.248	1.552	1.647	1.488	1.665	1.656
Spectral	1.539	1.613	1.647	1.640	1.515	1.752
SS	1.556	1.663	1.734	1.658	1.569	1.795
Robinson	1.000	1.000	1.000	1.000	1.000	1.000

Note. R/S and Empirical indicate corrected re-scaled range analysis and empirical methods, respectively. Whittle shows the SDF (spectral density function) for a fractionally differenced (FD) process fitting; Spectral, Smoothed Spectral (SS), and Robinson indicate spectral regression fitting; DFA denotes detrended fluctuation analysis based on Hurst exponent calculations.

presented in *Table 2-3*. The results of Spectral and DFA-based methods are above 1 ($H > 1$), unlike the Hurst exponent definitions ($0 < H < 1$).

Non-stationarities are so complicated that some models fail to accommodate them, resulting in estimates of the Hurst parameter greater than or equal to 1. However, this still does not block self-similarity and long-range dependence. According to R/S and empirical results, all series have long-range memory. In the following section, we explore the fractal features of all series.

Table 2-4 indicates Pearson, Spearman, and Kendall correlations of the default probabilities of sectors against CDS. Historical correlation results are statistically highly significant with respect to 99% confidence level even by parametric or non-parametric models. According to the parametric Pearson's product-moment correlation model, the historical relationship between CDS and all the default probabilities is high. In other respects, historical linear correlations are weaker in non-parametric Spearman's rank and Kendall's rank correlation models. On the other hand, when studying the correlation results, it should be considered that linear correlation is not significant for non-stationary variables. Hence, unlike

linear correlation models, dynamic non-linear methods will be examined to determine the relationship between variables.

Table 2-4. Correlation results of all PD series against the CDSs.

Sector	Pearson	Spearman	Kendall
Consumer Cyclicals	0.808135	0.571717	0.408361
	[0.0000]	[0.0000]	[0.0000]
Industrials	0.867573	0.662841	0.482460
	[0.0000]	[0.0000]	[0.0000]
Basic Materials	0.677604	0.634035	0.435621
	[0.0000]	[0.0000]	[0.0000]
Consumer Non-Cyclicals	0.644248	0.304581	0.195392
	[0.0000]	[0.0000]	[0.0000]
Utilities	0.652134	0.590255	0.407931
	[0.0000]	[0.0000]	[0.0000]

Note. Pearson indicates Pearson's product-moment correlation, Kendall shows Kendall's rank correlation tau, and Spearman presents Spearman's rank correlation rho.

Figure 2-2 represents the cross-correlation tests [43] for all the CDS vs. PDs pairs. For two time series x_i and y_i with the equal length N, the test statistic is defined as

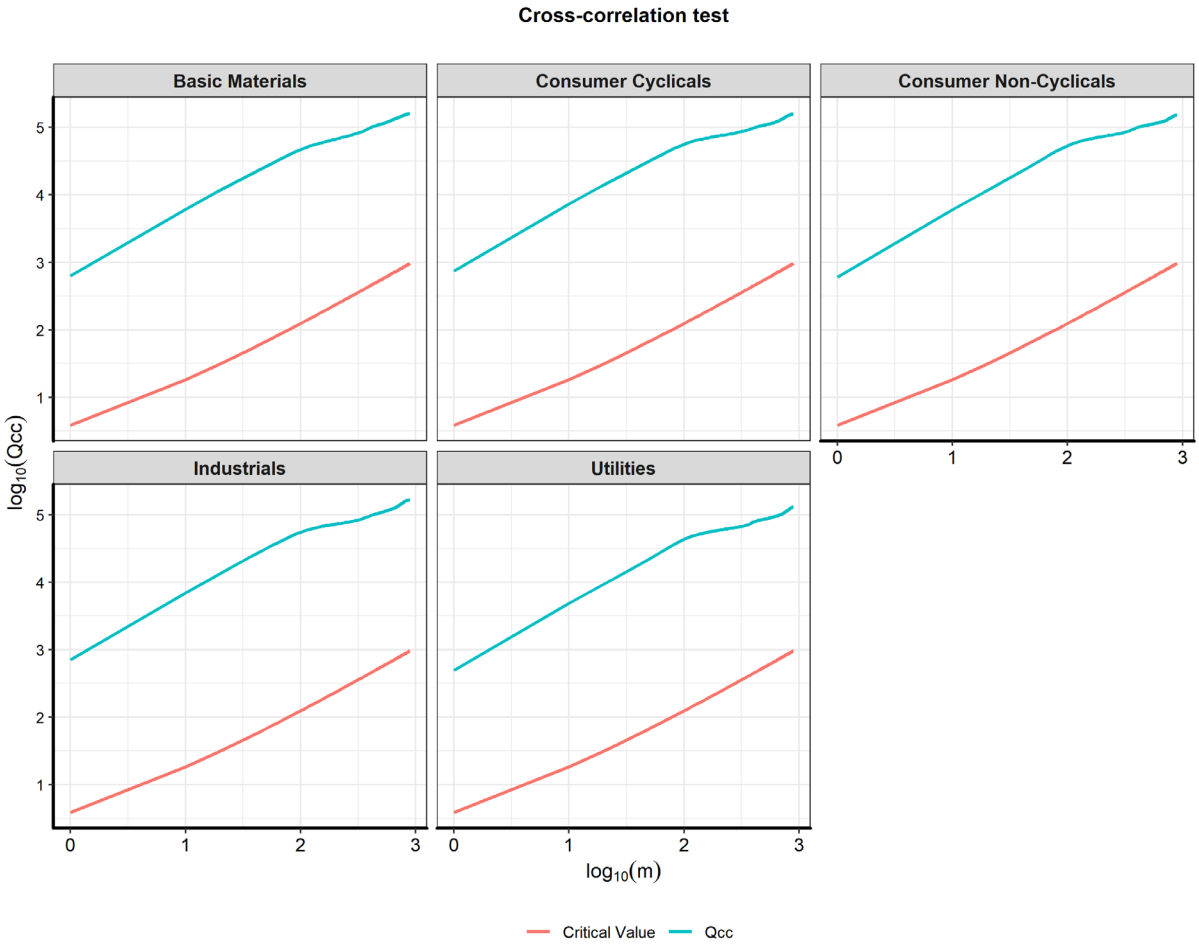
$$Q_{cc}(n) = N^2 \sum_{k=1}^{n} \frac{X_k^2}{N-k} \tag{2-27}$$

where X_i^2 is the cross-correlation function,

$$X_i = \frac{\sum_{k=i+1}^{N} x_k \, y_{k-i}}{\sqrt{\sum_{k=1}^{N} x_k^2 \sum_{k=1}^{N} y_k^2}} \tag{2-28}$$

The test statistic $Q_{cc}(n)$ is approximately $\chi^2(n)$ distributed with n degrees of freedom. The null hypothesis is that none of the first n cross-correlation coefficients is different from zero. Thereby, if the value of $Q_{cc}(n)$ is larger than the critical value of $\chi^2(n)$, the cross-correlation

is significant. According to the results, the degrees of freedom (n) varies from 1 to 10^3. Whereas all the cross-correlation pairs are statistically significant. Regardless of n changes, $Q_{cc}(n)$ of the blue line is always higher than the value of the critical value of $\chi^2(n)$ (red line).



Note. $Q_{cc}(n)$ represents cross-correlation statistics. m denotes the degrees of freedom. Blue and red lines indicate cross-correlation test statistics and critical values, respectively.

Figure 2-2. Cross-correlation tests.

2.3.2. Multifractal analysis

2.3.2.1. Multifractal detrended fluctuation analysis

Within this part, the DFA analysis was hired to examine the multifractal behavior of the series. MF-DFA Matlab codes consist of two algorithms implemented in calculations [44]. We have used three synthetic time series with known properties for comparing the

multifractal characteristics of the PDs and CDS. In addition to PDs and CDS series, multifractal, monofractal, and white noise series results are observed in all graphs.

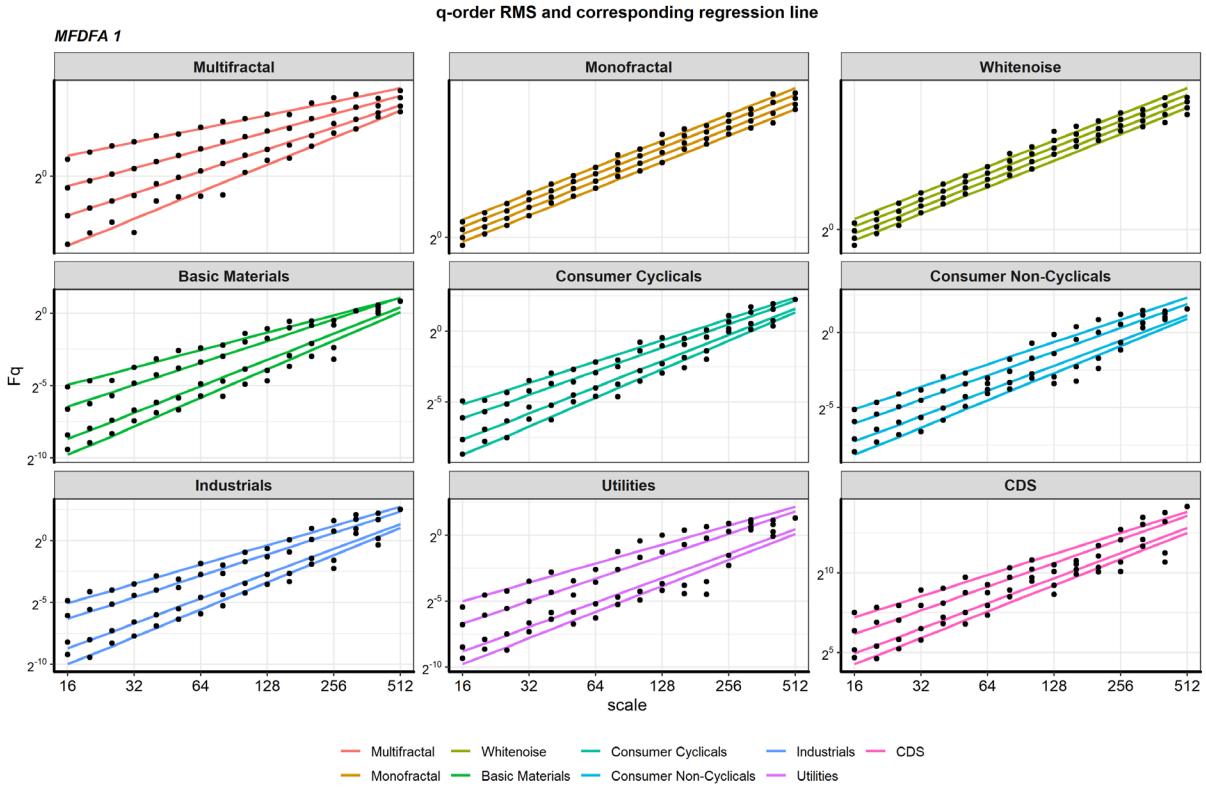


Figure 2-3. The q-order RMSs and the corresponding regression lines.

When discussing their algorithms, the contrast betwixt DFA-1 and DFA-2 is that the MF-DFA-2 multifractal spectrum is calculated directly from the local fluctuations. It gives a less abstract definition of the multifractal spectrum. We hire both methods to uncover the multifractal behavior.

Figure 2-3 - 2-5 designate MF-DFA-1 algorithm results. Figure 2-3 shows that q-order RMSs and corresponding regression lines. According to Ihlen, the following keys are valid for multifractal series: the contrast between the q-order RMSs for positive and negative q's (q moves from -5 to 5) provides a more visual appearance at the small compared to the large scales.

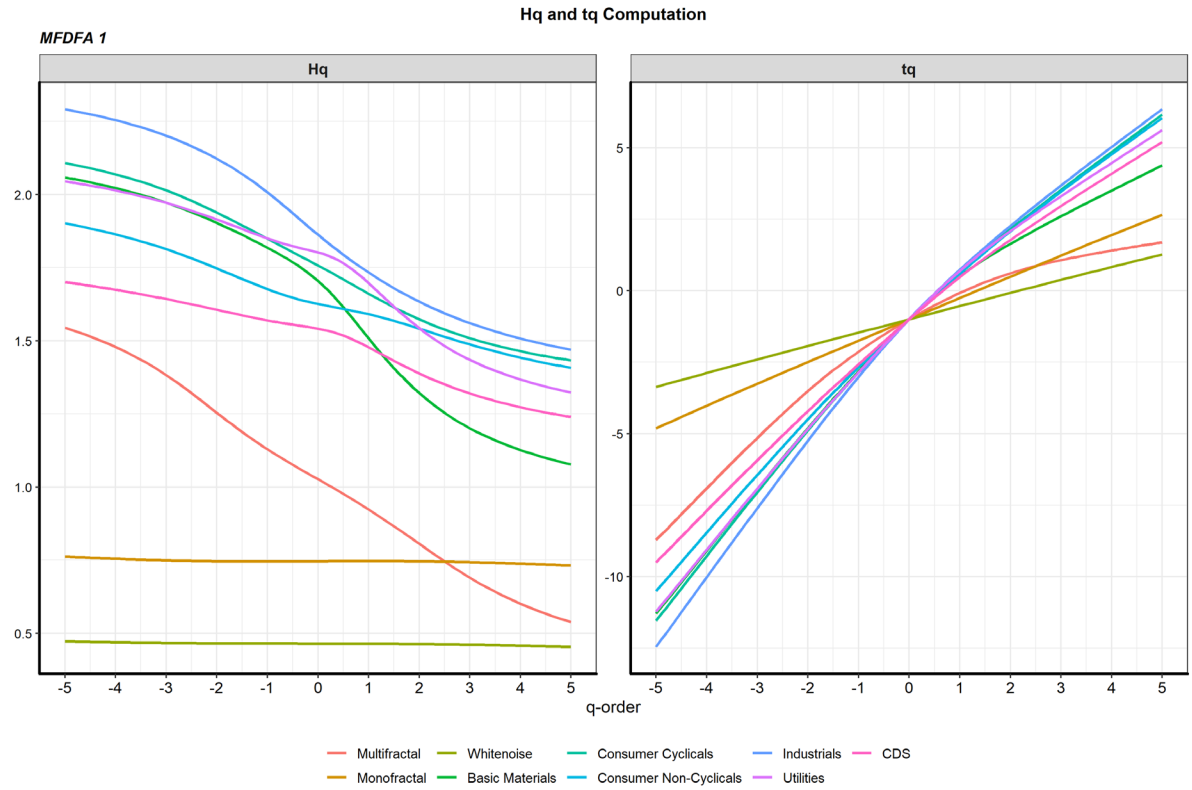


Figure 2-4. The q-order Hurst (Hq) and Renyi (tq) exponents.

Figure 2-4 (left) indicates q-order Hurst exponents. Multifractality points that the slopes Hq of the regression lines are q-dependent for multifractal series, unlike monofractal and white noise series. Figure 2-4 (right) shows q-order Renyi exponents. When the time series is not multifractal, Renyi exponents have a linear q-dependency. To determine the multifractal spectrum, firstly, Renyi exponents (tq) are calculated. Then, the singularity dimension (Dq) can estimate using q-order Hurst (Hq) and Renyi (tq) exponents. Hence, the plot of Hq versus Dq (see Figure 2-5) is referred to as the multifractal spectrum. In terms of MF-DFA-1 findings, PDs and CDS series are similar to the multifractal time series.

Figure 2-6 - 2-7, and Table 2-5 infer MF-DFA-2 algorithm results. q-order Hurst exponents present in Figure 2-6. When q varies from -5 to 5, Hq decreases and not consistent, indicating multifractality. Figure 2-6 verifies multifractality because the q-order Hurst exponents of all PDs and CDS decrease and are not fixed.

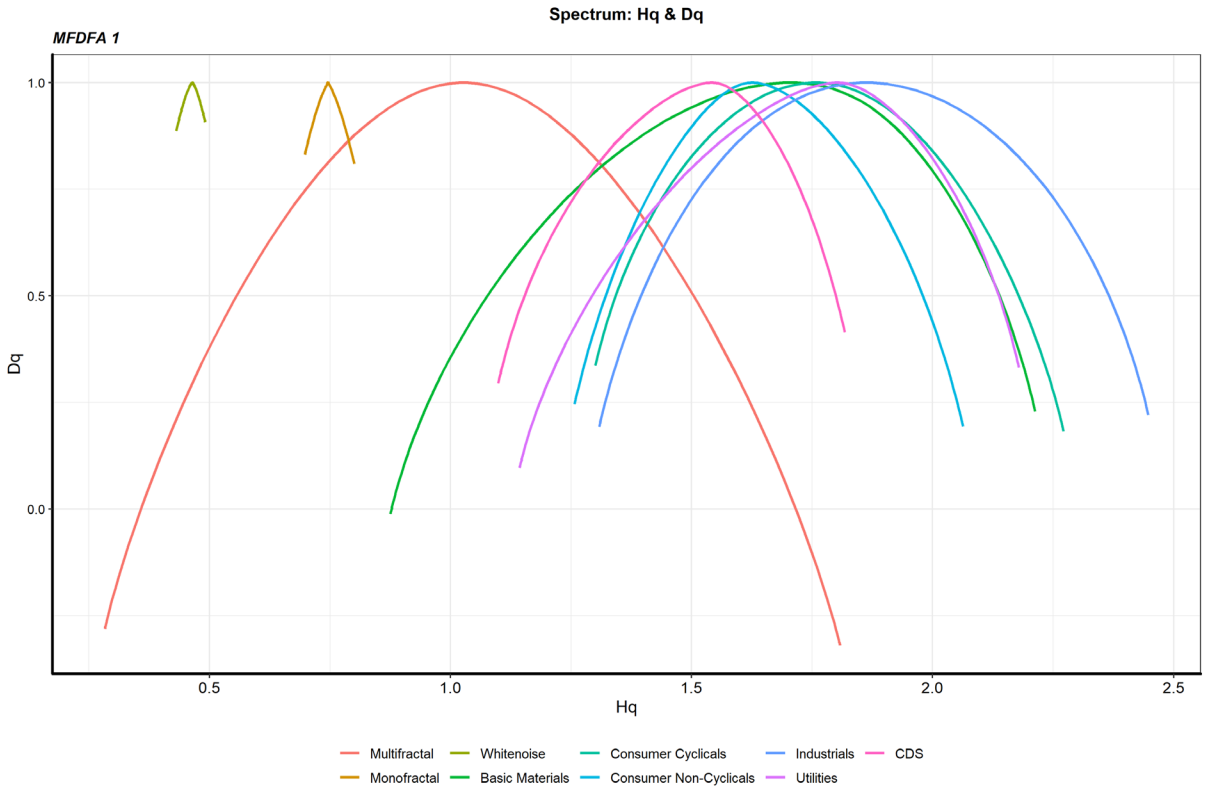


Figure 2-5. Multifractal spectrum.

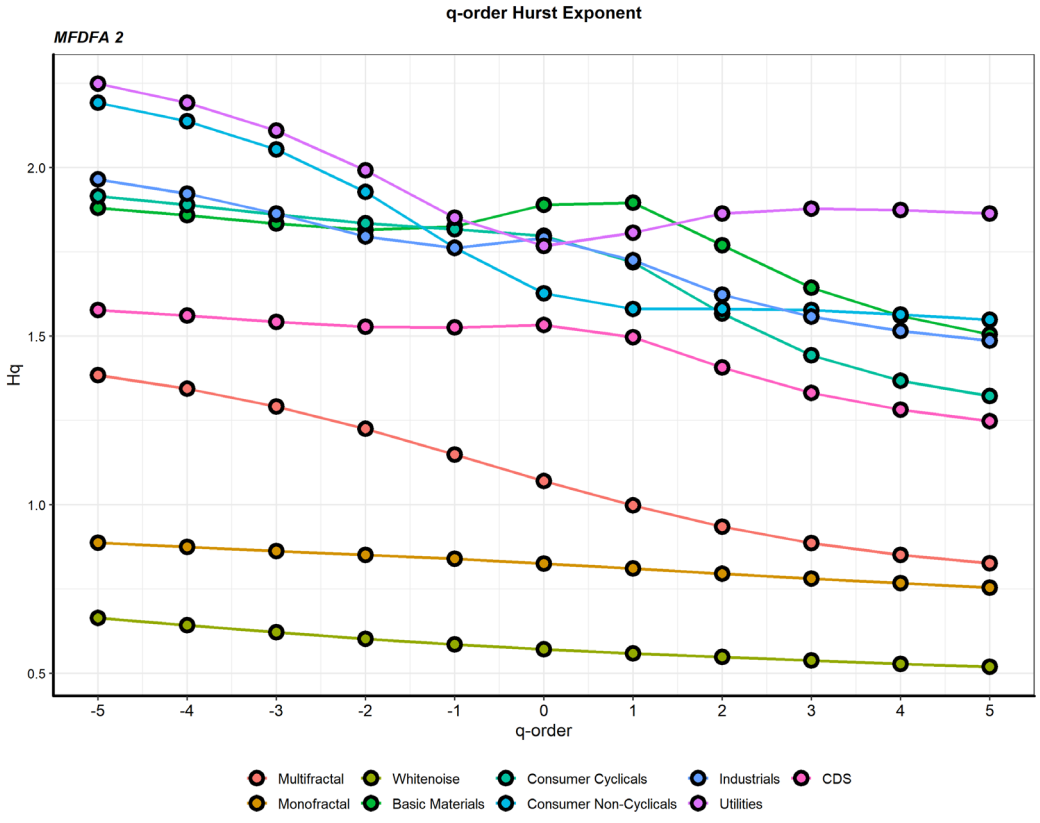
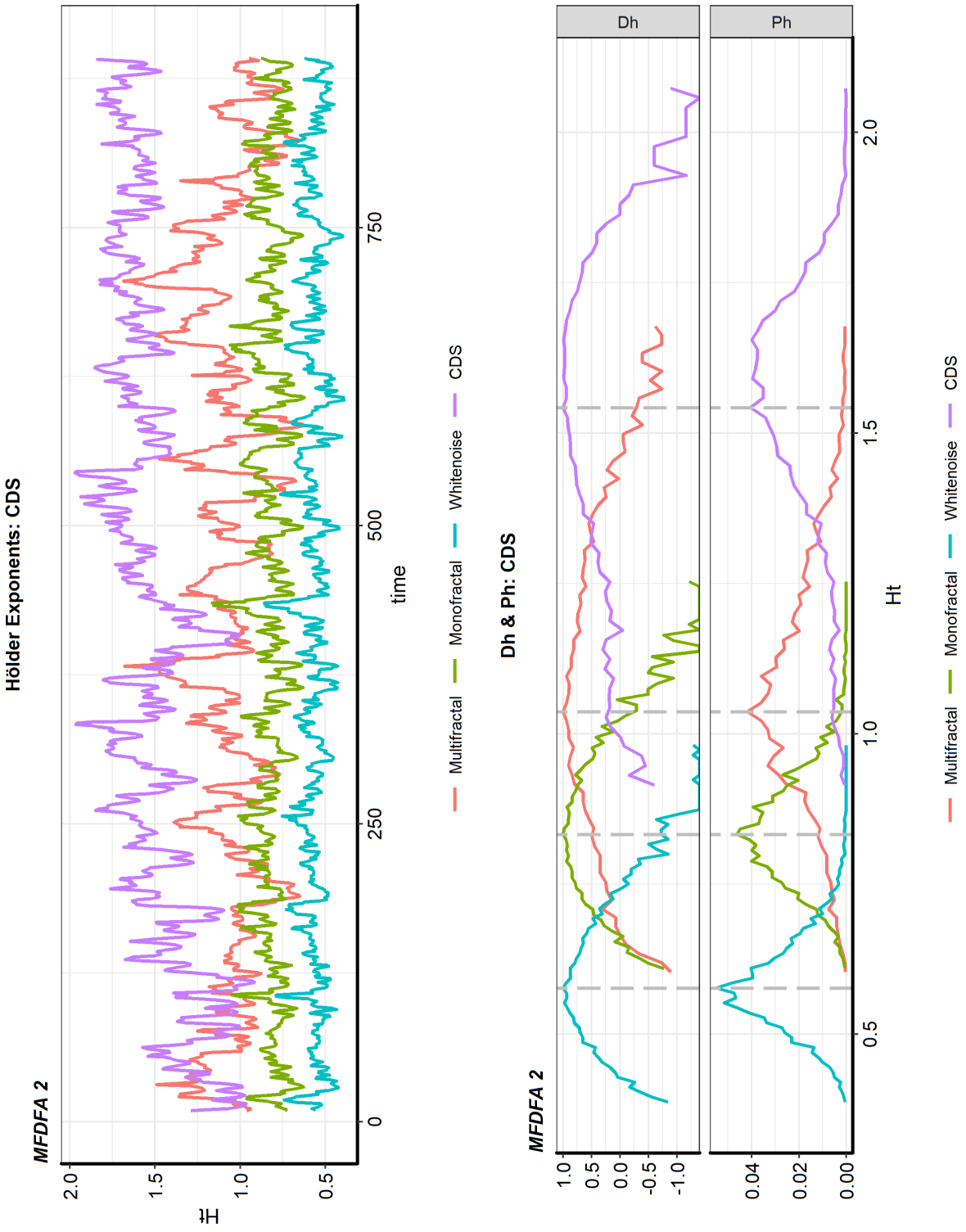
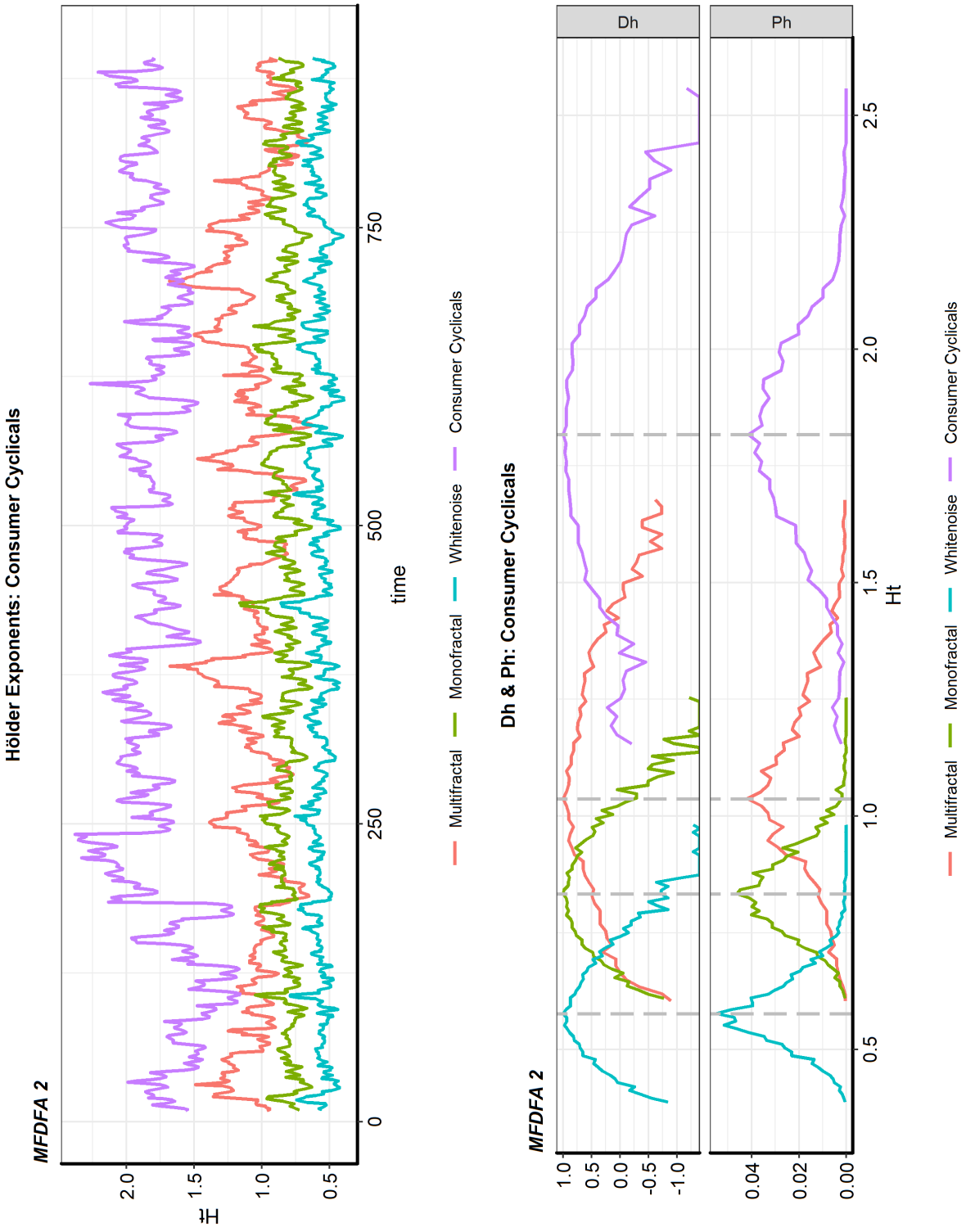


Figure 2-6. Multifractal spectrum.



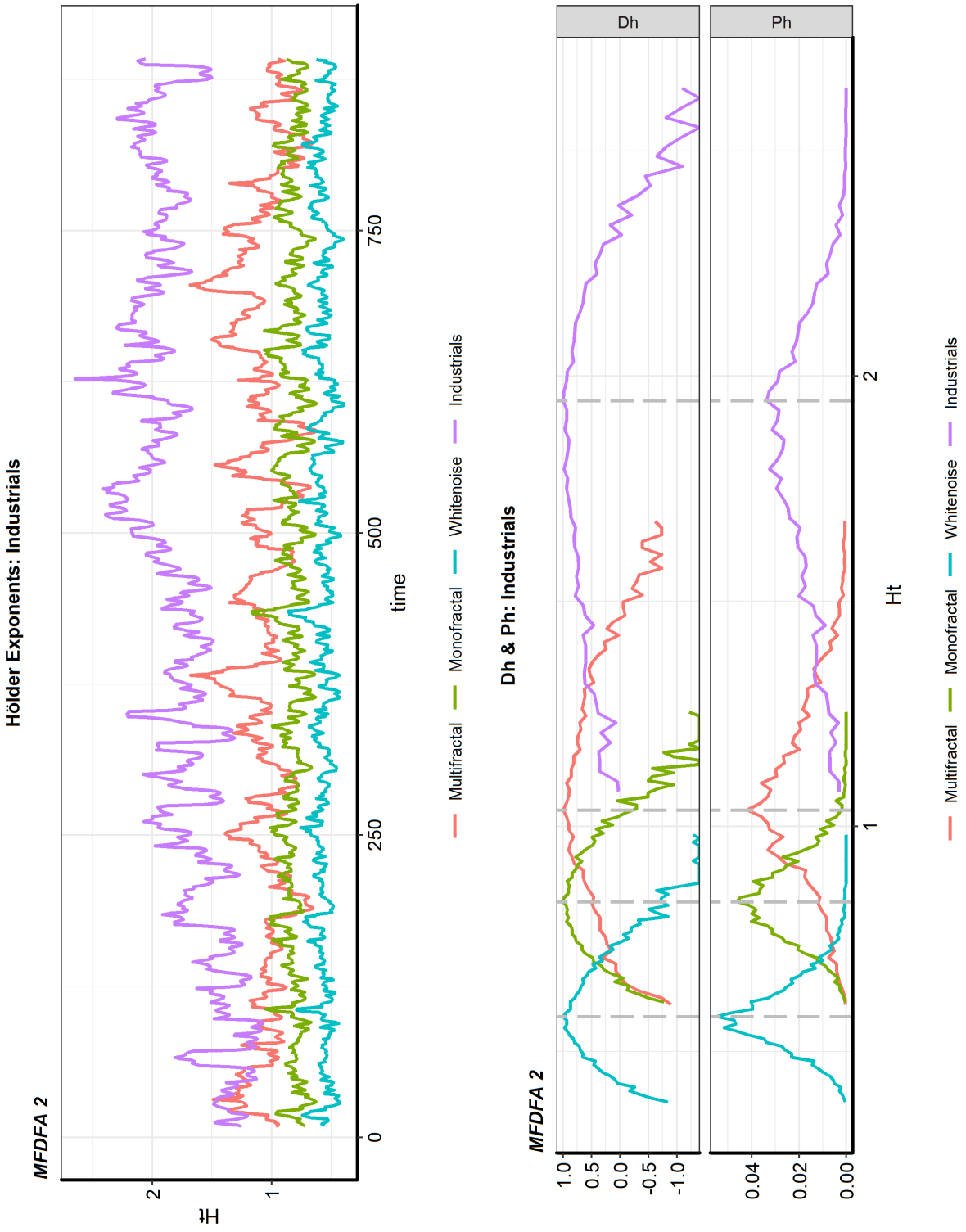
(a) CDS

Figure 2-7. Hölder exponents, probability distributions (Ph), multifractal spectrum (Dh). Besides, the generalized Hurst exponent results present in *Table 2-5*.



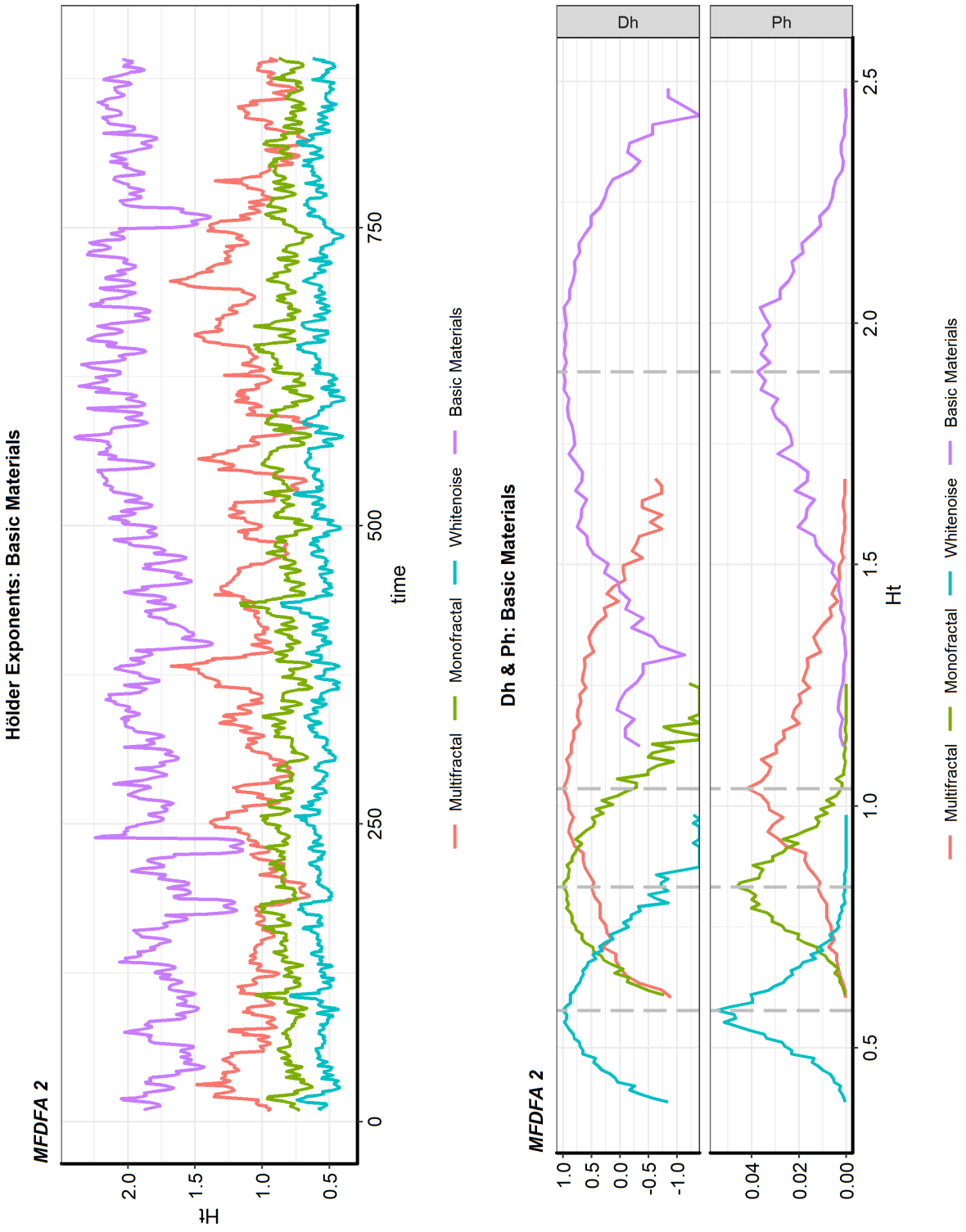
(b) Consumer Cyclicals

Fig. 2-7. (Continued)



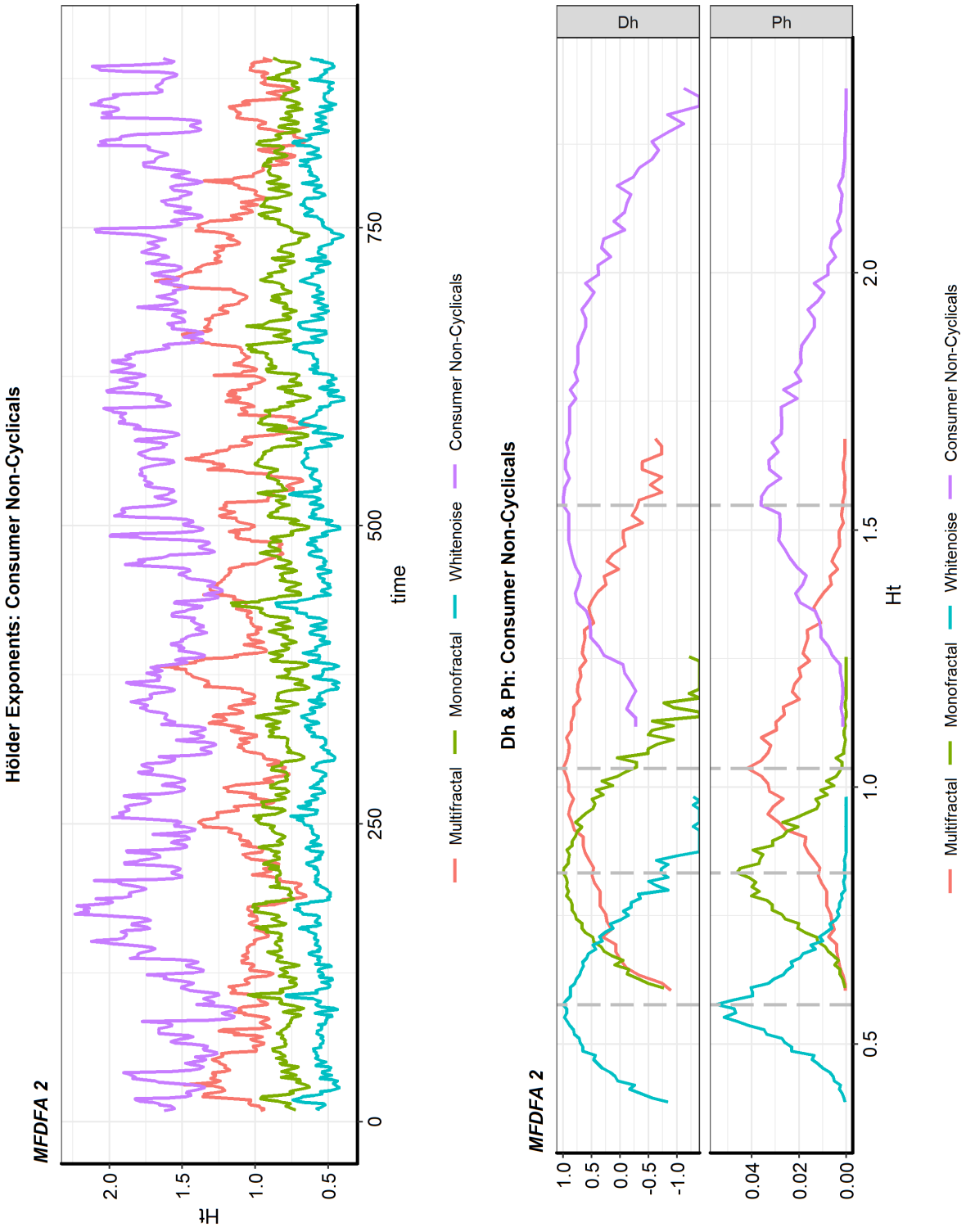
(c) Industrials

Fig. 2-7. (Continued)



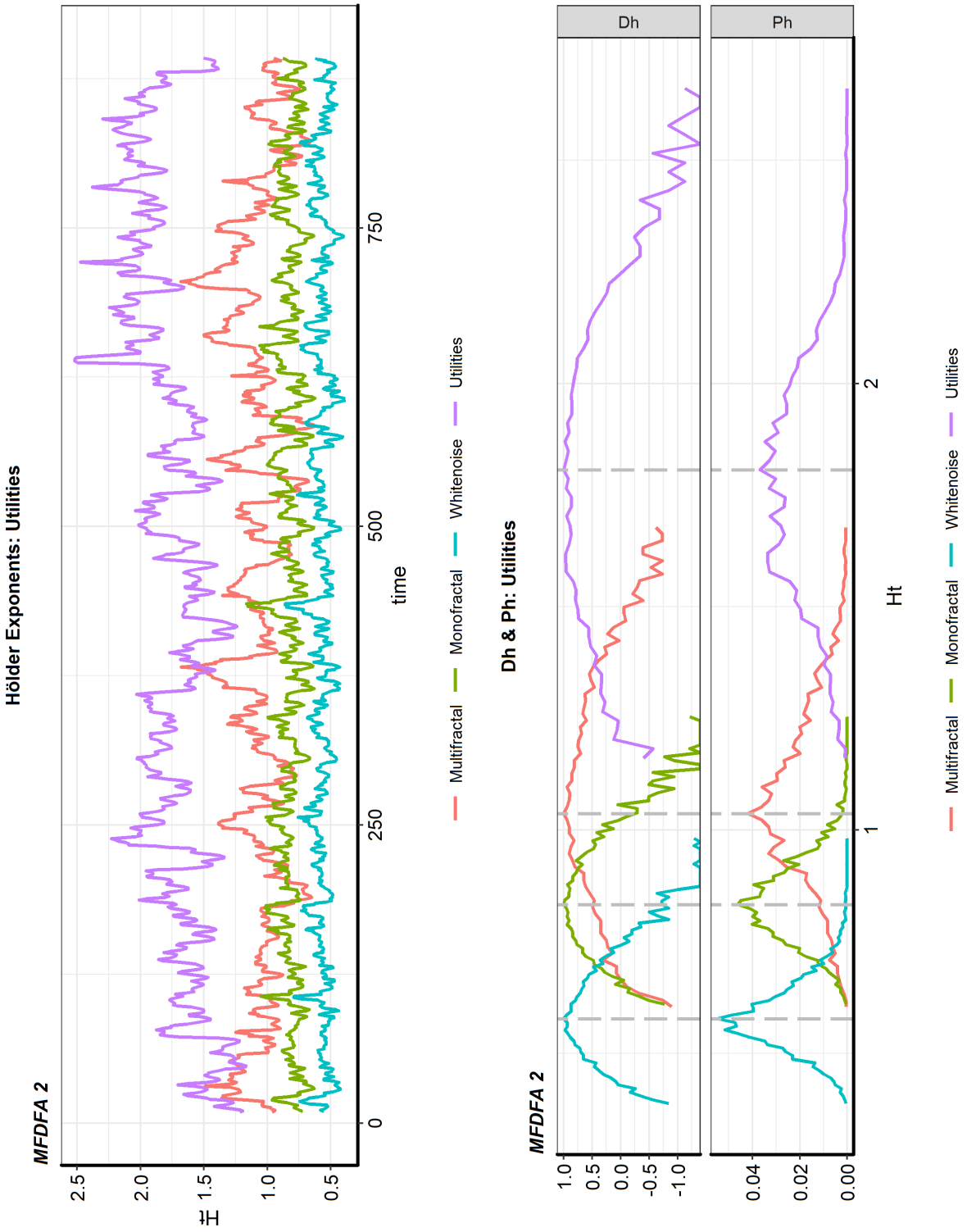
(d) Basic Materials

Fig. 2-7. (Continued)



(e) Consumer Non-Cyclicals

Fig. 2-7. (Continued)



(f) Utilities

Fig. 2-7. (Continued)

Table 2-5. Local Hurst exponent results.

	H_t
Multifractal	1.0359
Monofractal	0.8324
White-noise	0.5766
CDS	1.5418
Consumer Cyclicals	1.8167
Industrials	1.9448
Basic Materials	1.8989
Consumer Non-Cyclicals	1.5482
Utilities	1.8060

The spectrums of exponents are constructed to specify the multifractal behavior of the series. Figure 2-7 presents the local Hurst exponents, the probability distribution (Ph), and the multifractal spectrum (Dh). The multifractal spectrum tells that PDs and CDS indicate a high degree of irritability and uncertainty. According to Matia et al. (2003), "there are two factors to multifractal features: long-range temporal correlations for small and large fluctuations and the fat-tailed probability distributions" ([45] [46]). The amplitude of the multifractal fractal spectrum (Dh) is described via differentiation among the max and min probability ($\Delta\alpha = \alpha_{\max} - \alpha_{\min}$). The longer $\Delta\alpha$, the more uneven the distribution of time series is; hence, the stronger the multifractality is. The multifractal spectra with narrower amplitudes reveal indicative long-term and short correlations. Our findings (MF-DFA-1 and MF-DFA-2) suggest that the widths of multifractal spectra evidence strong multifractality in PDs and CDS.

2.3.2.2. Multifractal detrended cross-correlation analysis

In Section 2.3.1, we demonstrated the existence of cross-correlation between CDS and PDs. Besides, Section 2.3.2.1 manifests that PDs and CDS series have multifractal characteristics. This section will hire MF-DCCA to study the multifractal detrended cross-correlation CDS vs. probability of default series. The scale q is set from -10 to 10, and the step size is set to 1 ([47], [48]). Figure 2-8 is the log-log plots of the fluctuation function $F_q(s)$ versus time scale s. Every line fits the logarithmic line of $F_q(s)$ vs. s for $q \in [-10,10]$, which provide evidence of power-law cross-correlation among CDS and PDs.

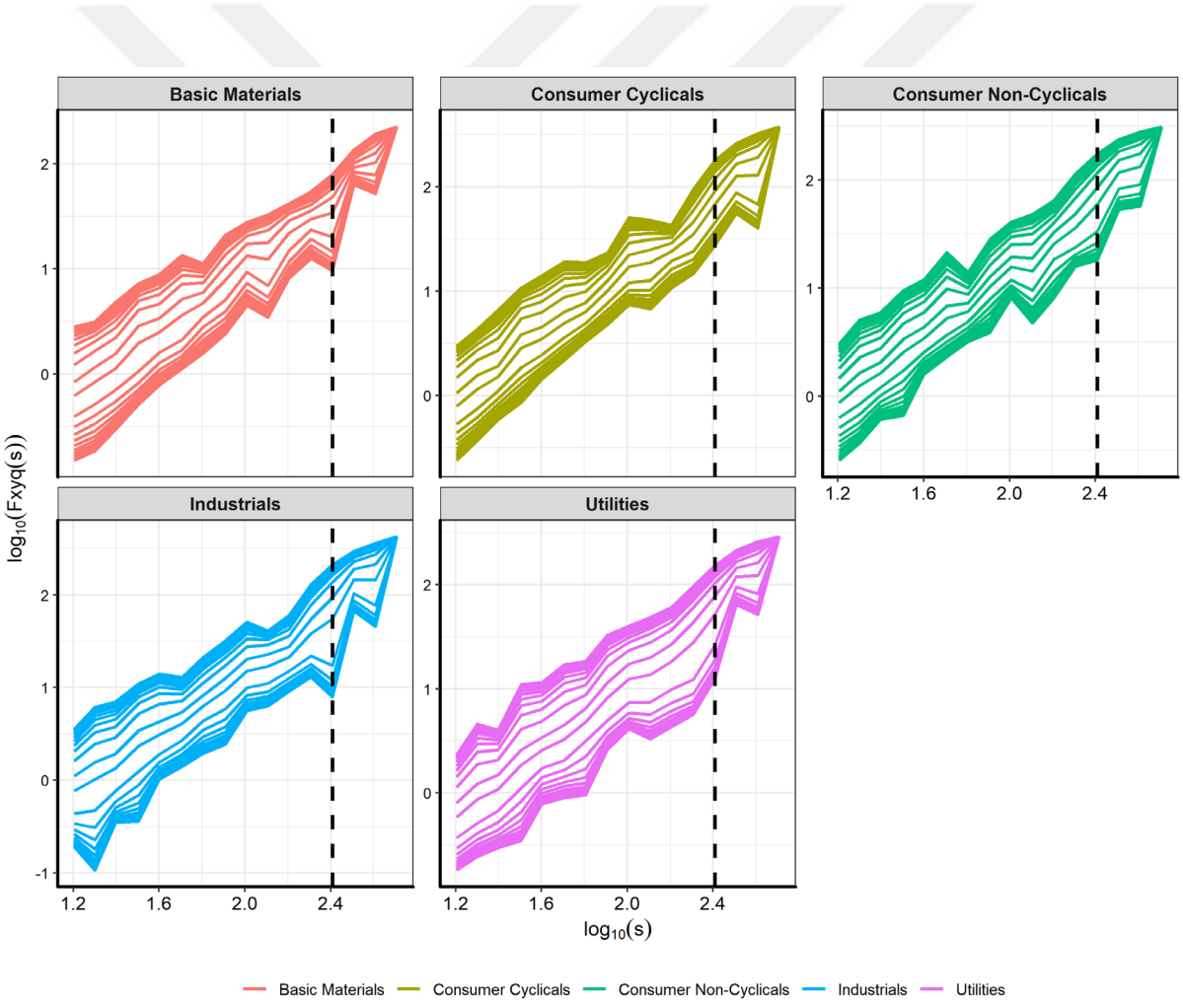


Figure 2-8. $F_{xy}(s)$ versus s.

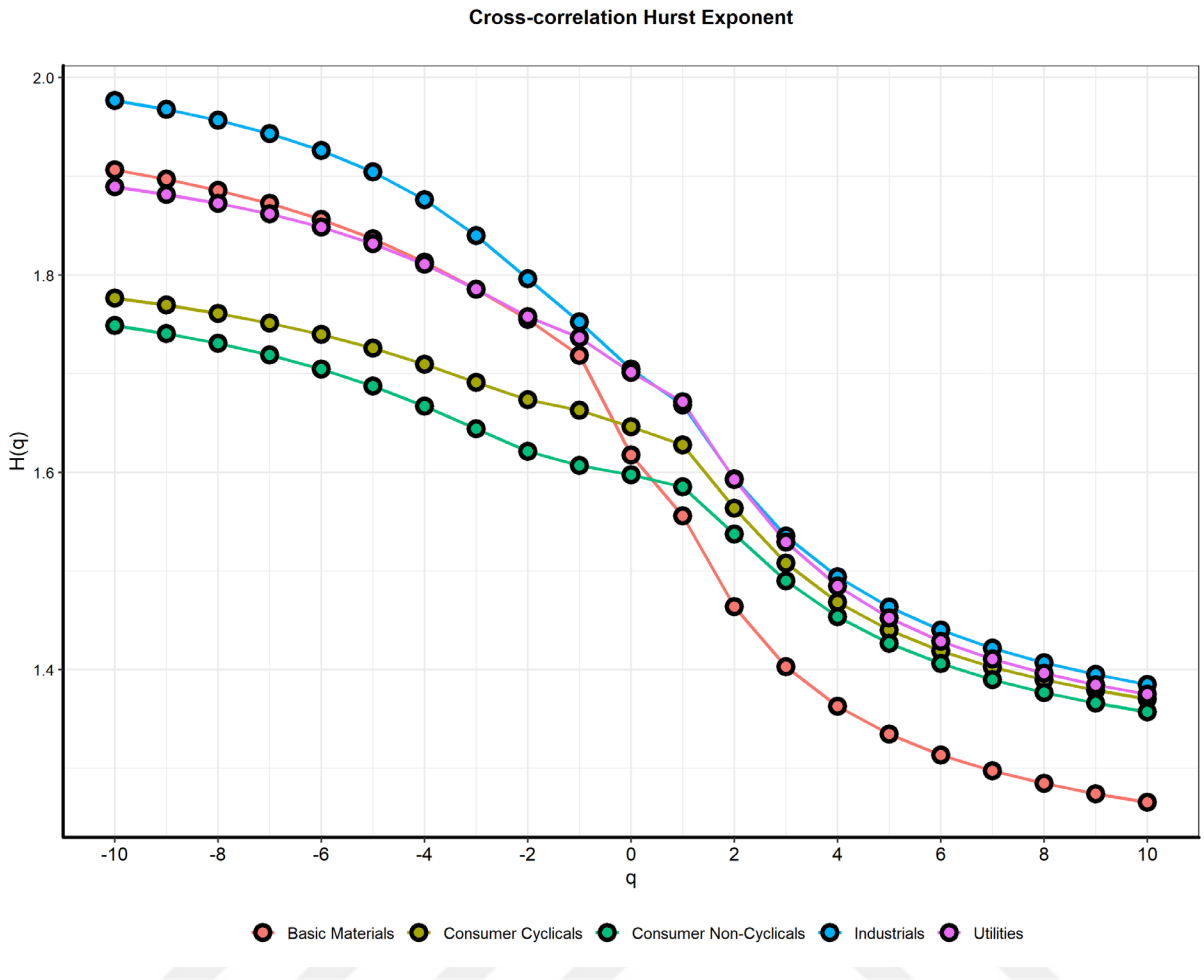


Figure 2-9. Cross-correlation Hurst exponents, $H_{xy}(q)$.

Figure 2-9 shows the relationship among the scaling exponents and q. When $q = 2$, MF-DCCA is equal to DCCA, and the bivariate Hurst exponent $H_{xy}(q)$ has similar features and interpretation to the univariate Hurst exponent. All $H_{xy}(2)$ pairs are almost similar and greater than 1, telling that they may be the same volatile degree. The variety of the Hurst exponents means a cross-correlation multifractality between pairs. Since the exponent results in the negative region of q-values are larger than the positive region, it can be showed that small-fluctuations are more cross-correlated than the large ones.

Figure 2-10 presents the scaling exponents with q varying from -10 to 10. In all pairs, decreasing long-term (red line) scaling exponents are greater than short-term (blue line) scaling exponents. It means that the cross-correlation is multifractal in the long-term. On the

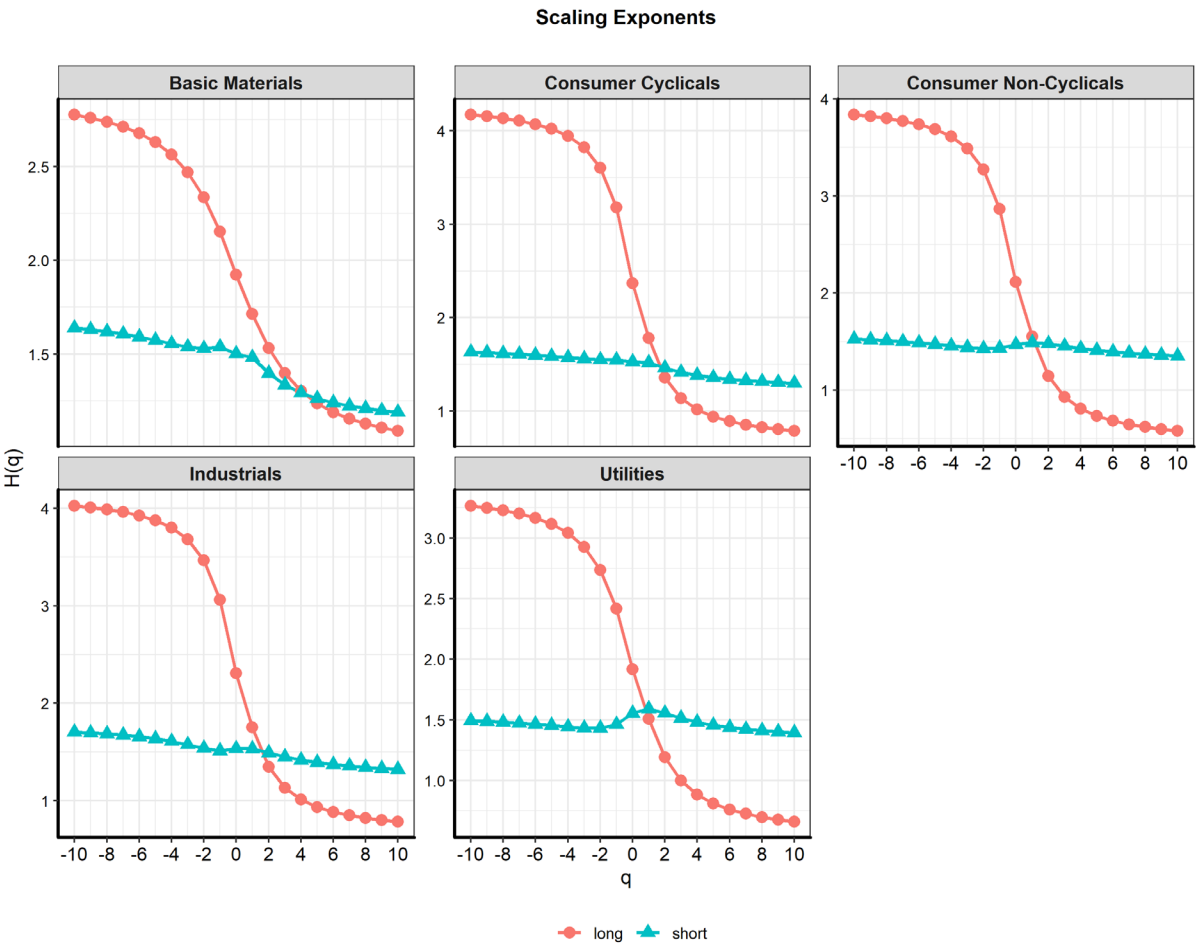


Figure 2-10. Scaling exponents with q varying from -10 to 10.

other hand, short-term exponents are weakly dependent on q, indicating that short-term cross-correlation is weakly multifractal.

One of the multifractality indicators Renyi exponent is estimated based on Eq. (2-20) and designates Figure 2-11- 2-12. According to Figure 2-11, $\tau_{xy(q)}$ is a nonlinear curve of all pairs dependent on q. However, from Figure 2-12, we find pairs expose a multifractal cross-correlation in the both long and short terms $\tau_{xy(q)}$ is approximately linear, which means a nearly monofractal cross-correlation in the sort-term.

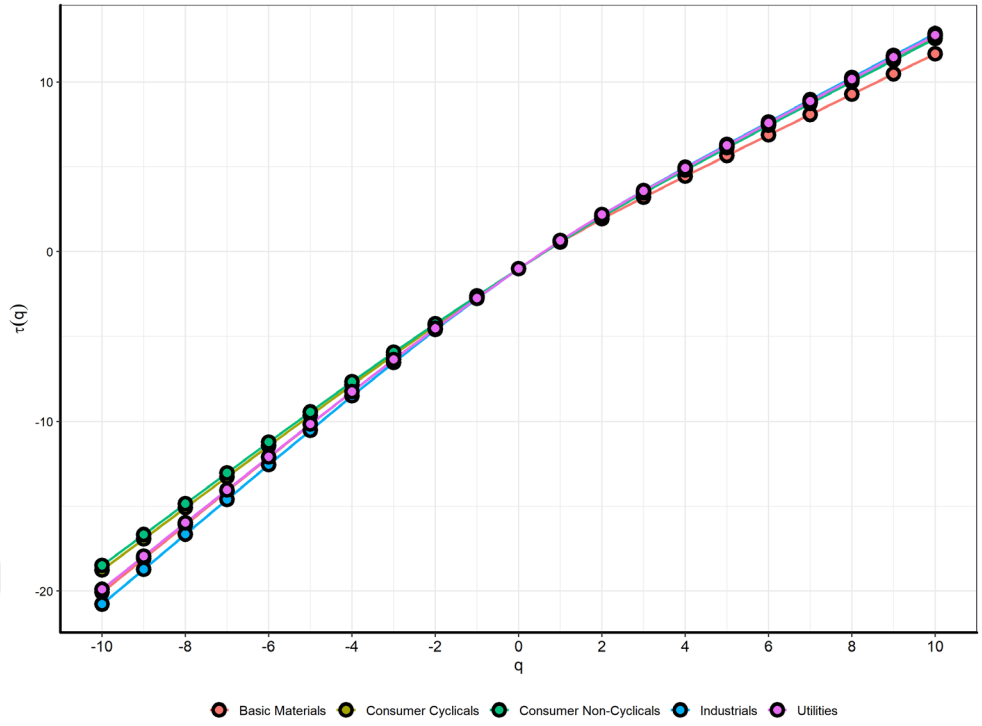


Figure 2-11. The relationship between $\tau_{xy(q)}$ and q.

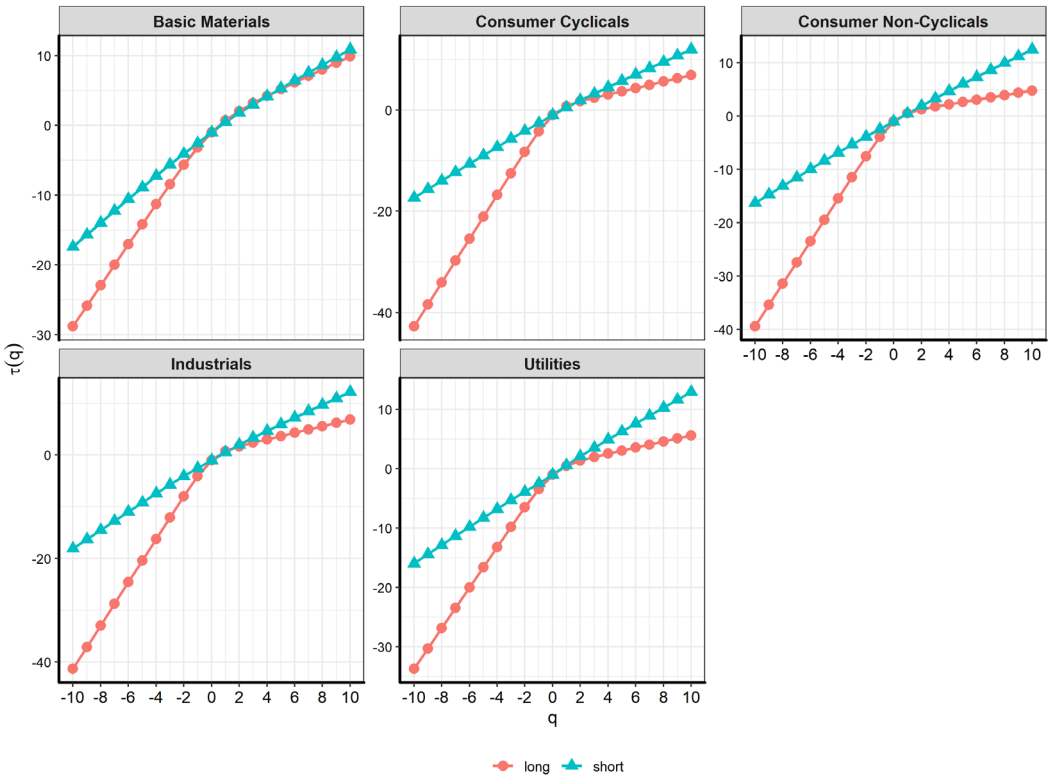


Figure 2-12. The relationships between $\tau_{xy(q)}$ and q.

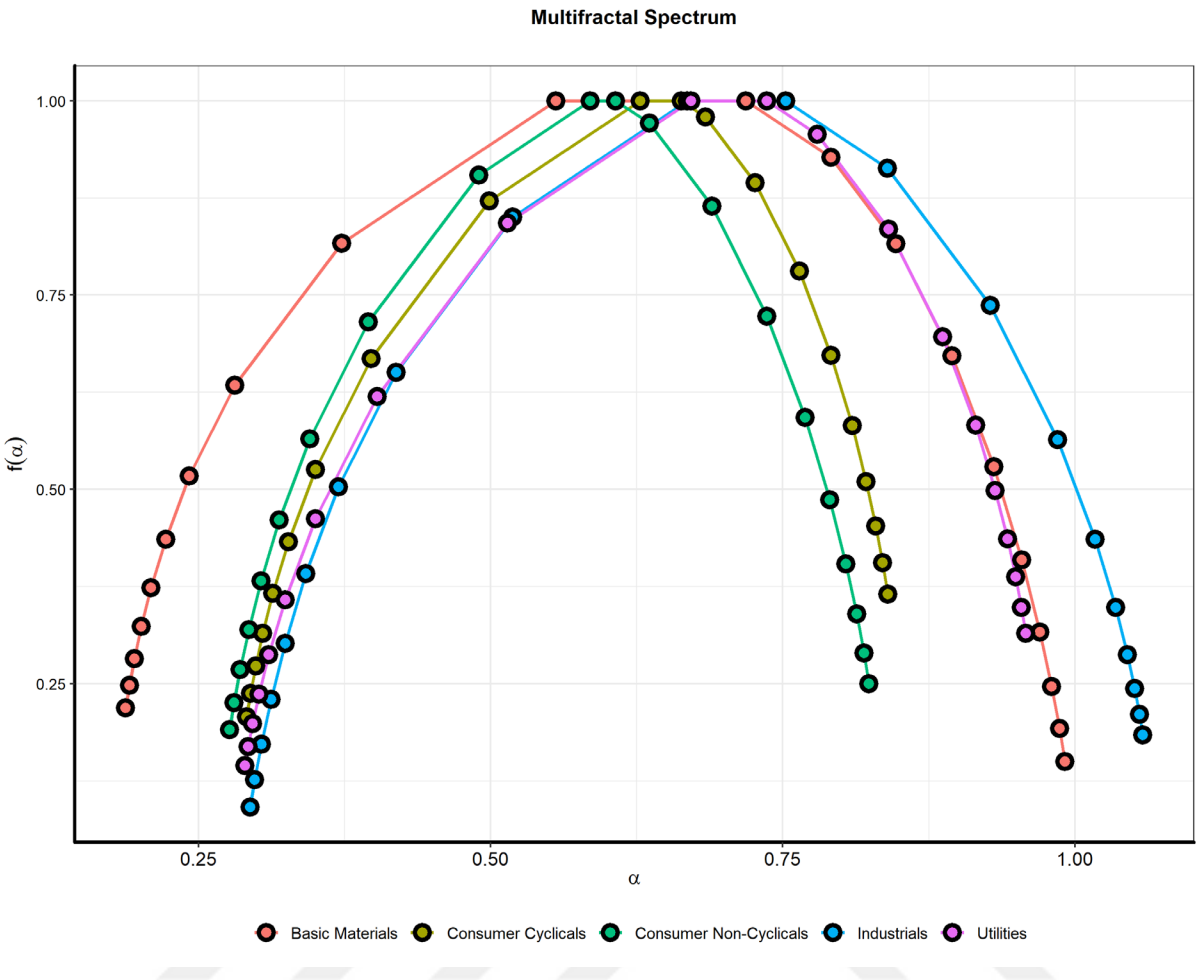


Figure 2-13. The multifractal spectrum, $f_{xy}(\alpha)$.

Multifractal spectrum examination performs as before in Section 2.3.2.1. The multifractal spectrum estimates from Eq. (2-22). The wide spectrum proposes forceful multifractality, and the smaller one symbolizes weak behavior. If the spectrum seems like a point, it is monofractal ([47], [48]). Figure 2-13 indicates that there are multifractal properties for all cross-correlation pairs. Furthermore, as shown in Figure 2-14, the long-term multifractal spectrums' width is highly larger than the short-term. All findings tell us, especially long-term cross-correlation in all pairs exhibits multifractal behavior.

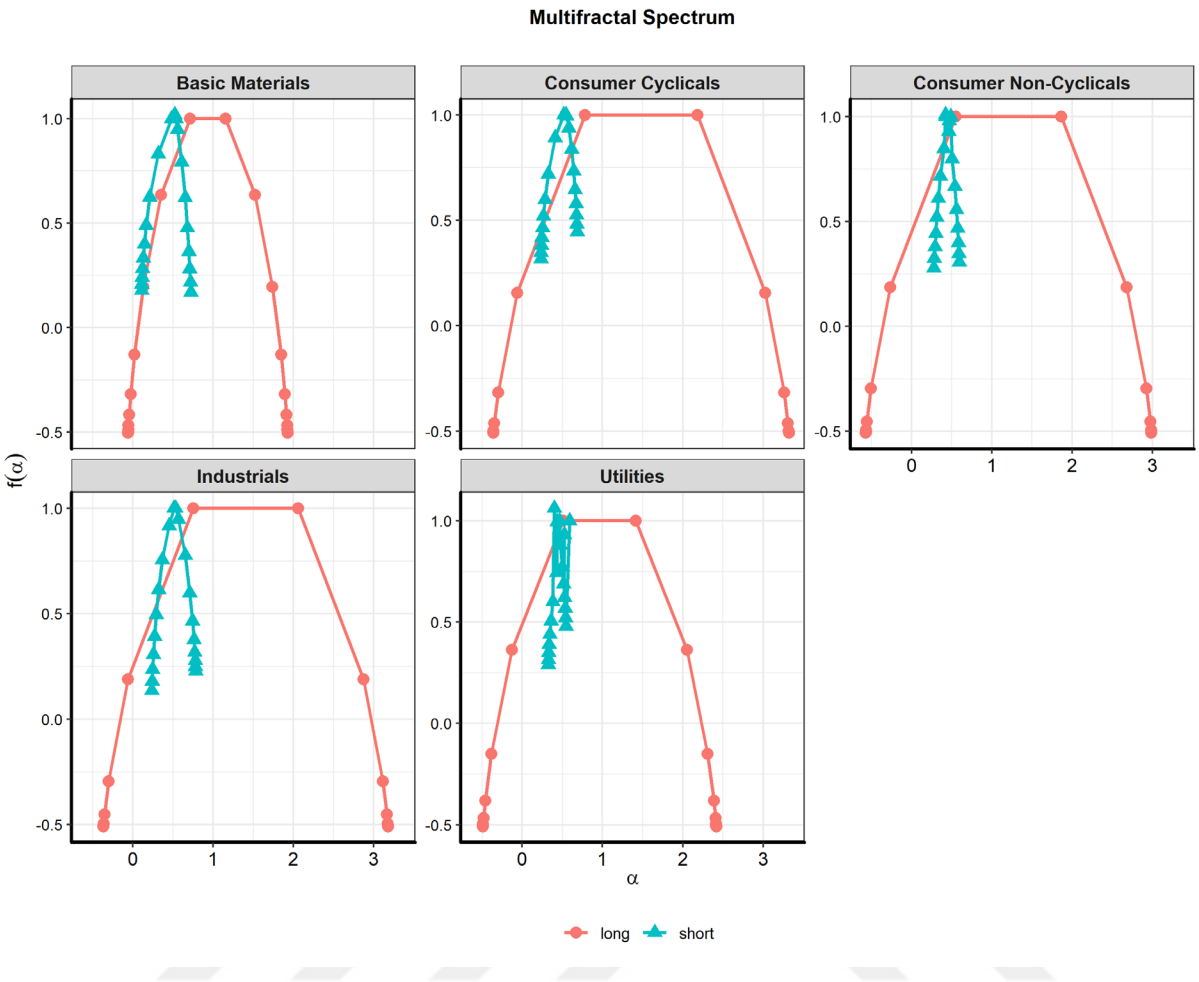


Figure 2-14. The multifractal spectra both in the long term and short term.

2.3.2.3. Multifractal detrended moving average cross-correlation analysis

This section study the multifractal detrended moving average cross-correlation CDS vs. probability of default series. The scale q is set from -10, 0, and 10. "We investigate three specific cases in this study.

1. $Q = 0$ refers to the backward-moving average, in which the moving average function $\widetilde{Z}(t)$ is calculated over all the past $n - 1$ data points of the series.
2. $Q = 0.5$ corresponds to the centered-moving average, where $\widetilde{Z}(t)$ contains half past and half future information in each window.
3. $Q = 1$ is called the forward-moving average, where $\widetilde{Z}(t)$ considers the trend of $n - 1$ data points in the future" [40].

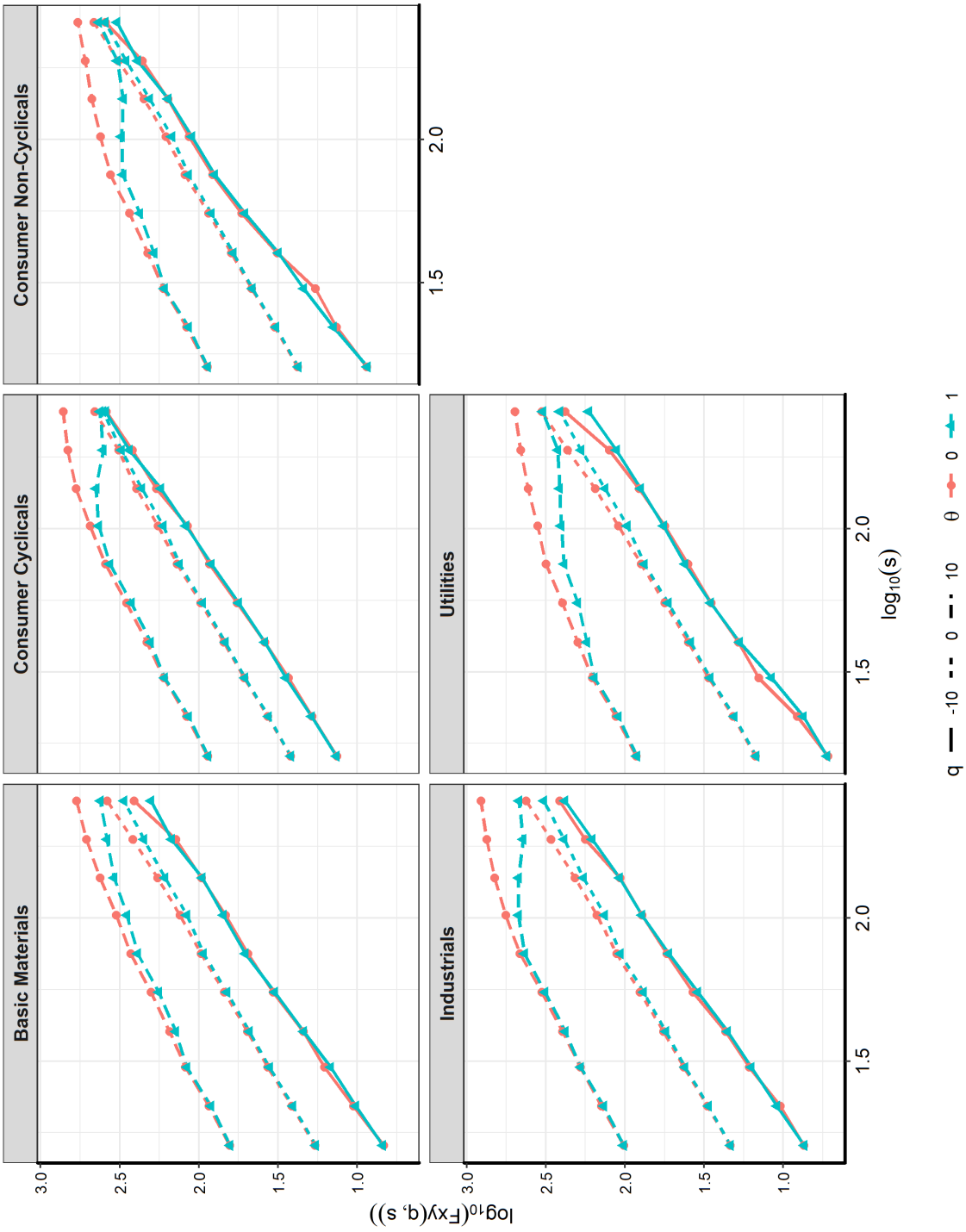


Figure 2-15. $F_{xy}(q, s)$ versus s.

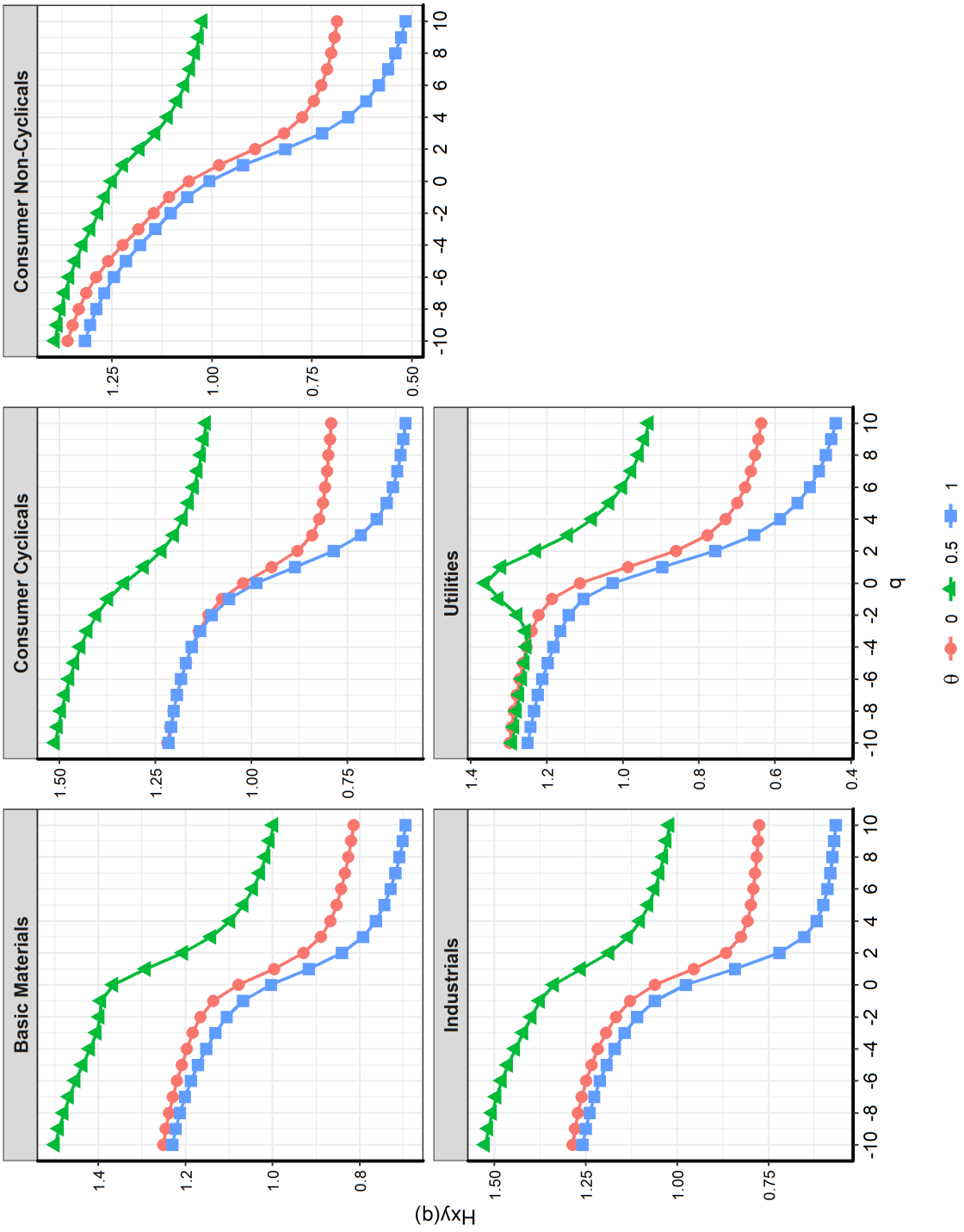


Figure 2-16. Cross-correlation Hurst exponents, $H_{xy}(q)$.

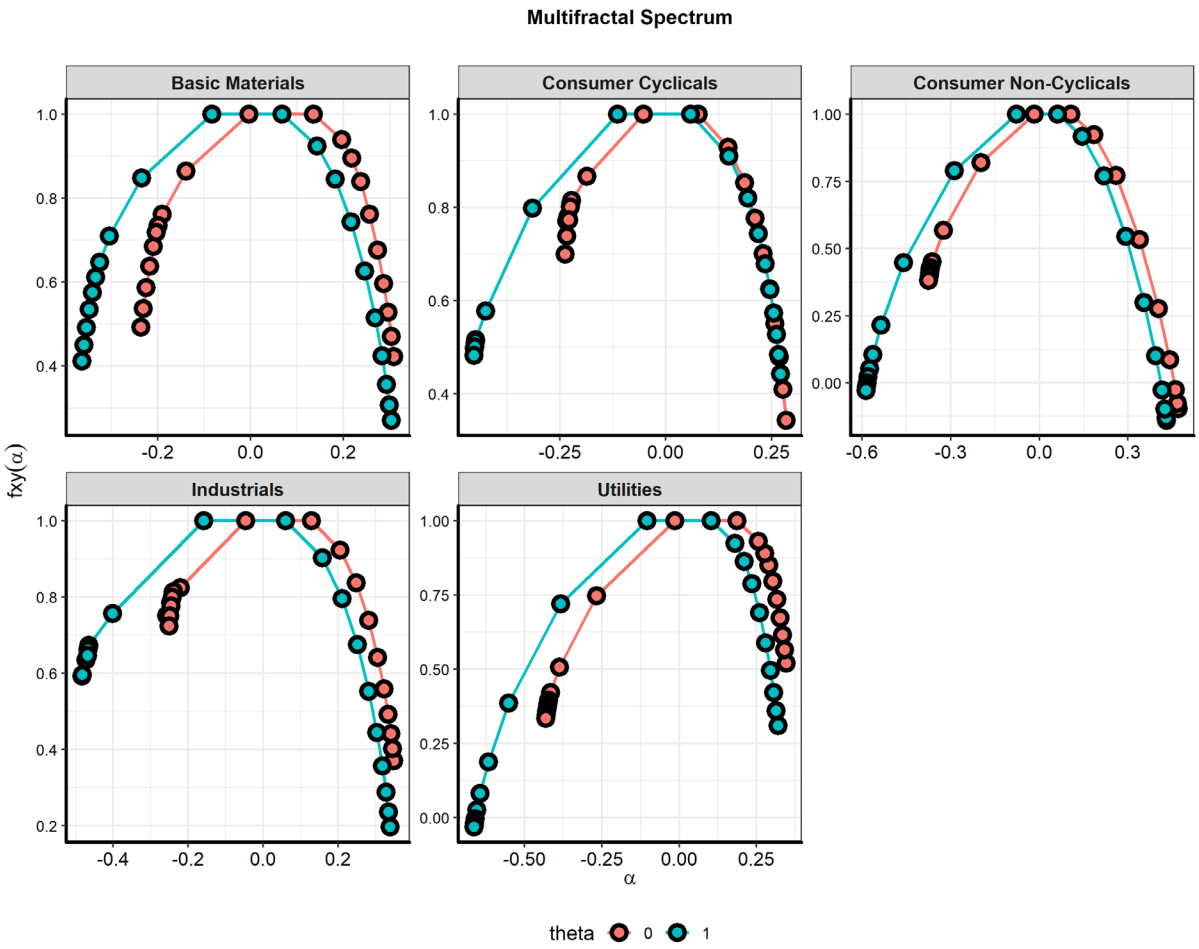


Figure 2-17. The multifractal spectrum, $f_{xy}(\alpha)$.

Figure 2-15 illustrates in log-log scale the dependence of the fluctuation functions $F_q(s)$ with respect to the scale s for $q \in [-10,0,10]$ for the volatilities. Power-law scaling is observed in the fluctuation functions for the MF-X-DMA algorithms with $Q = 0$. For $Q = 1$, there is a crossover in all curves. In Figure 2-16, the two functions are monotonically declining and close to each other. When $q = 2$, Hq is between 0.75 and 1, revealing a very strong linear long-term memory in the cross-correlation.

Figure 2-17 gives all multifractal spectrums. As in the previous sections, large singularity means that the cross-correlation between pairs exhibits multifractal behavior. According to the MF-DCCA and MF-X-DMA analysis, long-term cross-correlation in all CDS and PDs pairs show multifractal nature.

2.3.2.4. The Hölder exponent analysis

Critical events like shocks, booms, jumps in the time series cause significant and sudden changes. Hölder exponents can be employed to determine the local regularity of time series. It is a powerful detection tool for critical issues.

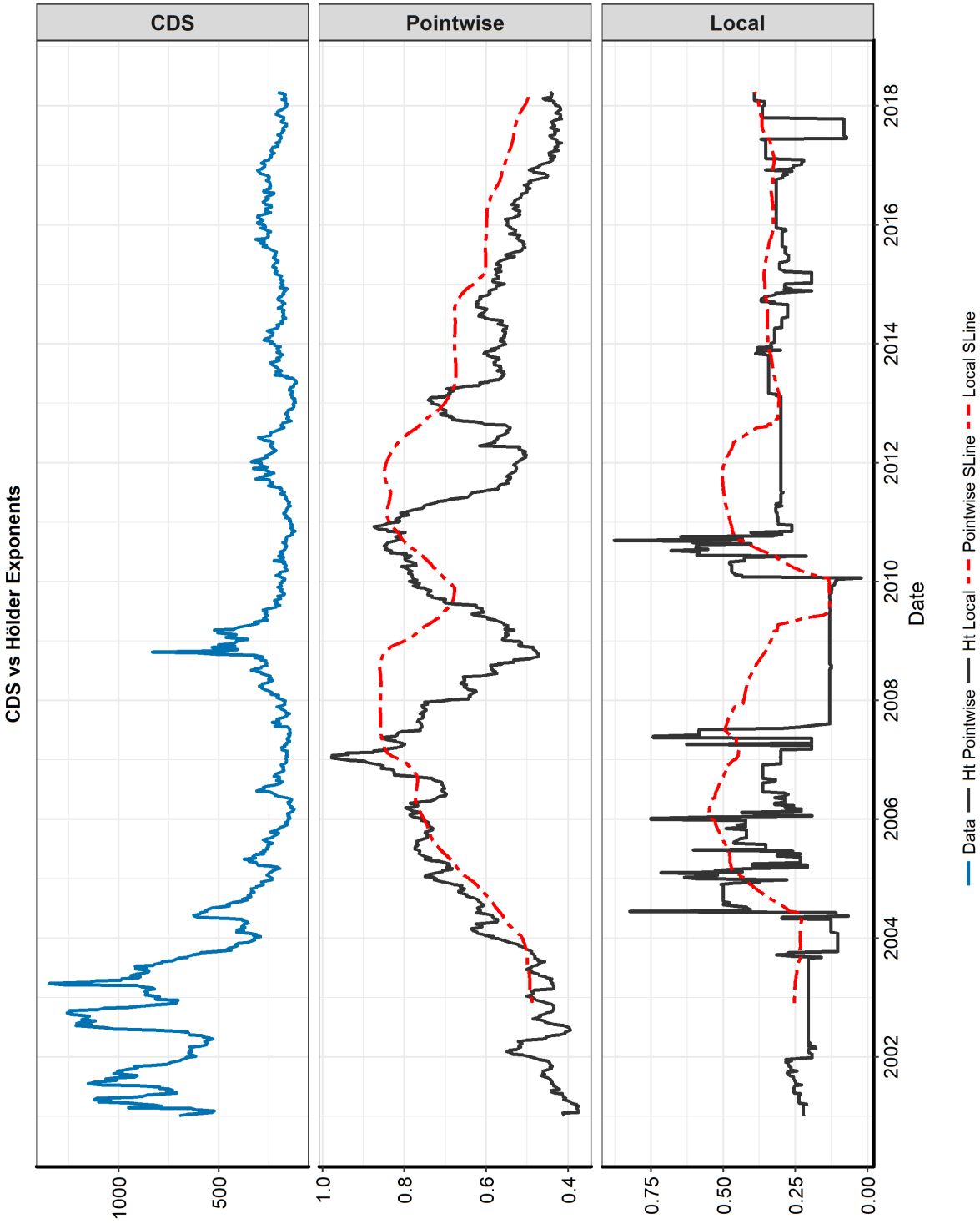
In Section 2.3.1, we have recognized that the CDS and sectoral default probabilities are multifractal. Many studies have pointed out that financial series exhibit multifractal features, plus consequently, the Hölder exponents can be determined [49]. For this reason, the estimation of the pointwise and local Hölder exponents proposed in Section 2.2.2.4 is significant. The Fraclab package implements for the prediction of the Hölder exponents [50]. Furthermore, Kuperin et al. [35] present for the univariate critical point predicting, called the signal line. The signal line s_t is evaluated as the sum of average Hölder exponents in the previous to t time period and k standard deviations in the same time period,

$$s_t = \overline{H}_t + k\left(\frac{1}{h-1}\sum_{i=1}^{h-1}(\overline{H}_t - H_{t-i})^2\right)^{(1/2)} \tag{2-29}$$

and,

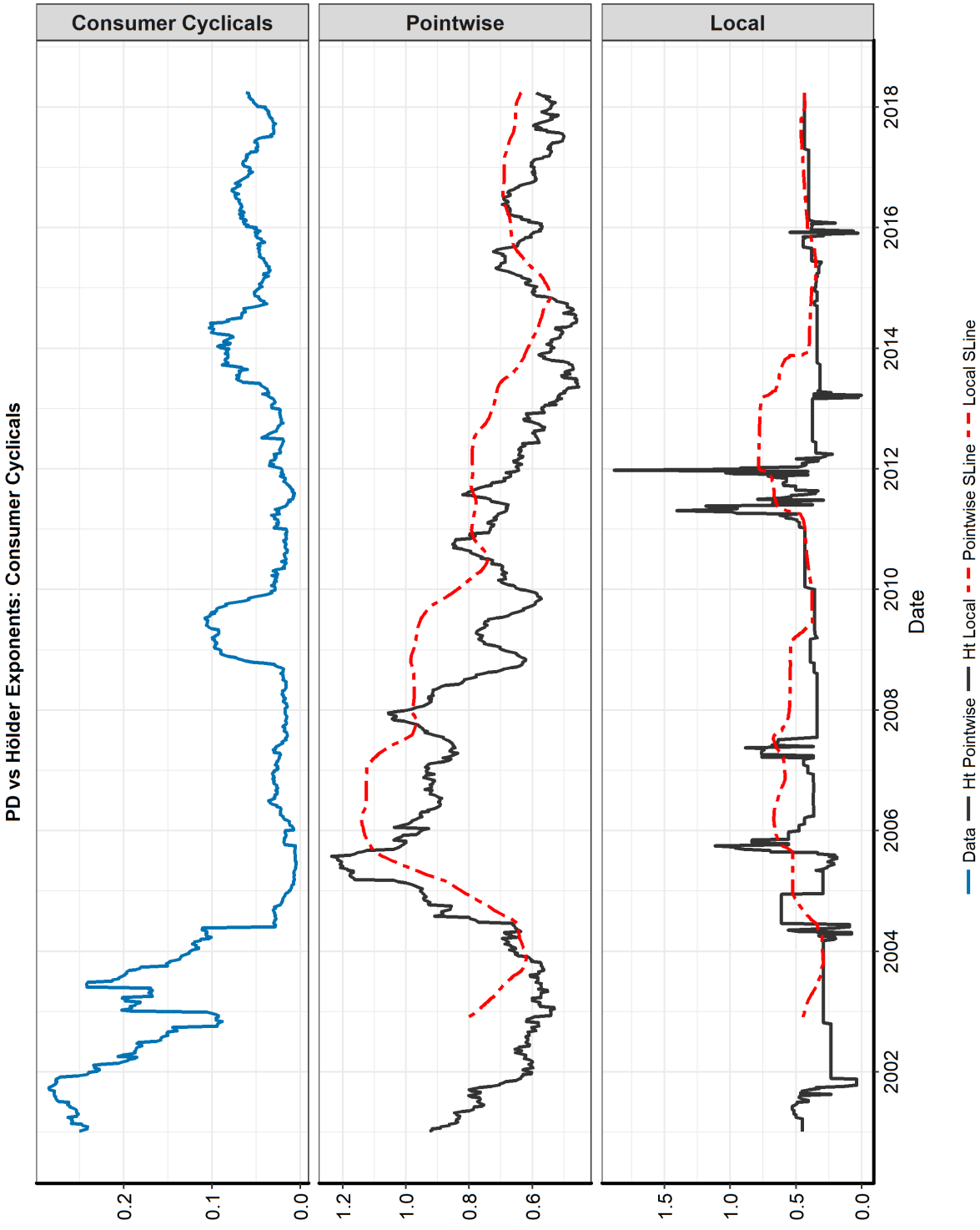
$$\overline{H}_t = \frac{1}{h}\sum_{i=0}^{h-1} H_{t-i} \tag{2-30}$$

where H_t is the value of Hölder exponent at time t. k and h are "the signal line-height" and "the history of the signal line," respectively. When the Hölder exponent crosses the signal line bottom-up, the signal occurs. These values of the coefficient of proportionality have been optimized in analytical practices [35]. In the analysis, parameters are set as $k = 1$ and $w = 100$. Figure 2-18 is consists of level, pointwise, local Hölder exponents, and their signal lines.



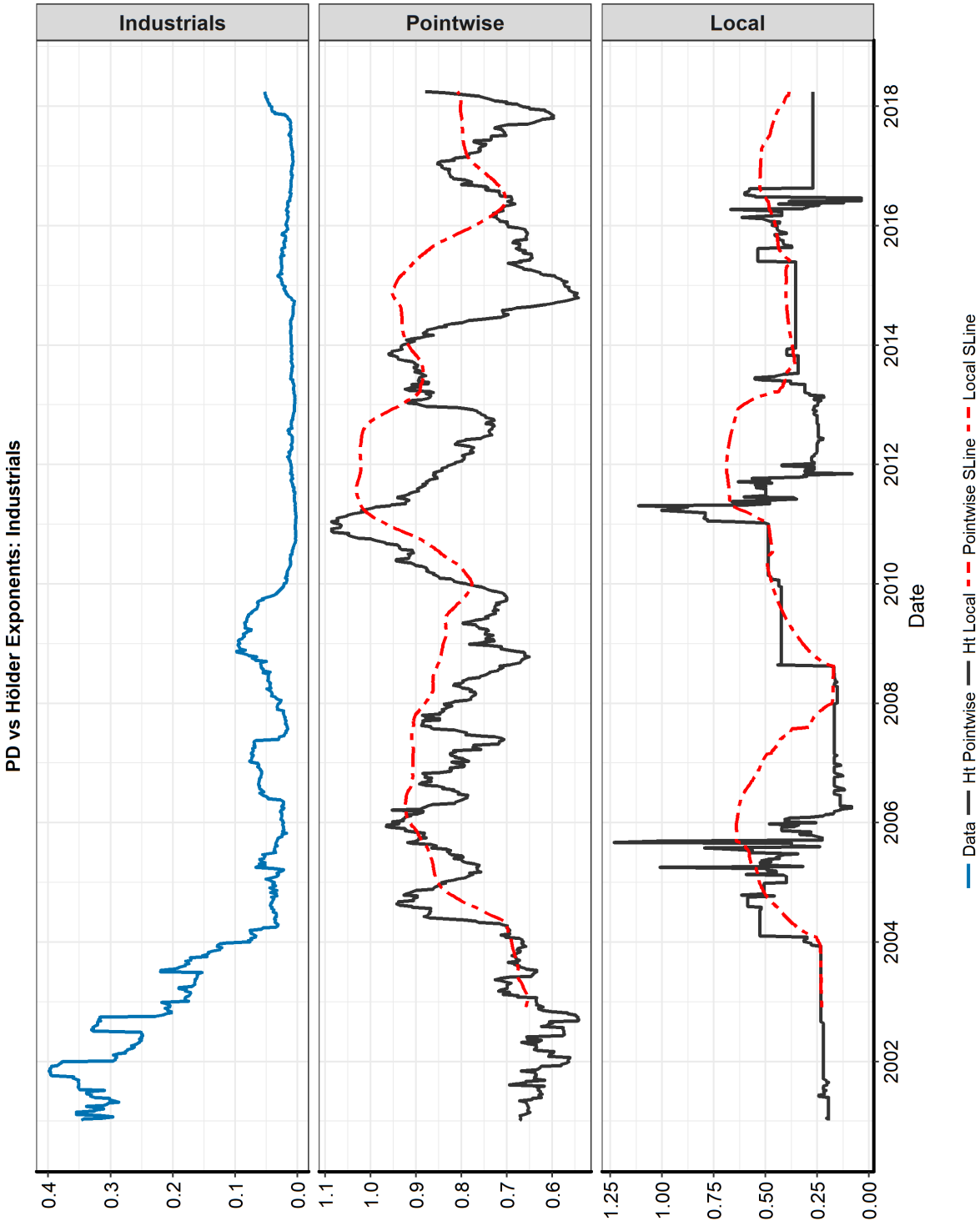
(a) CDS

Figure 2-18. Local and Pointwise Hölder exponents.



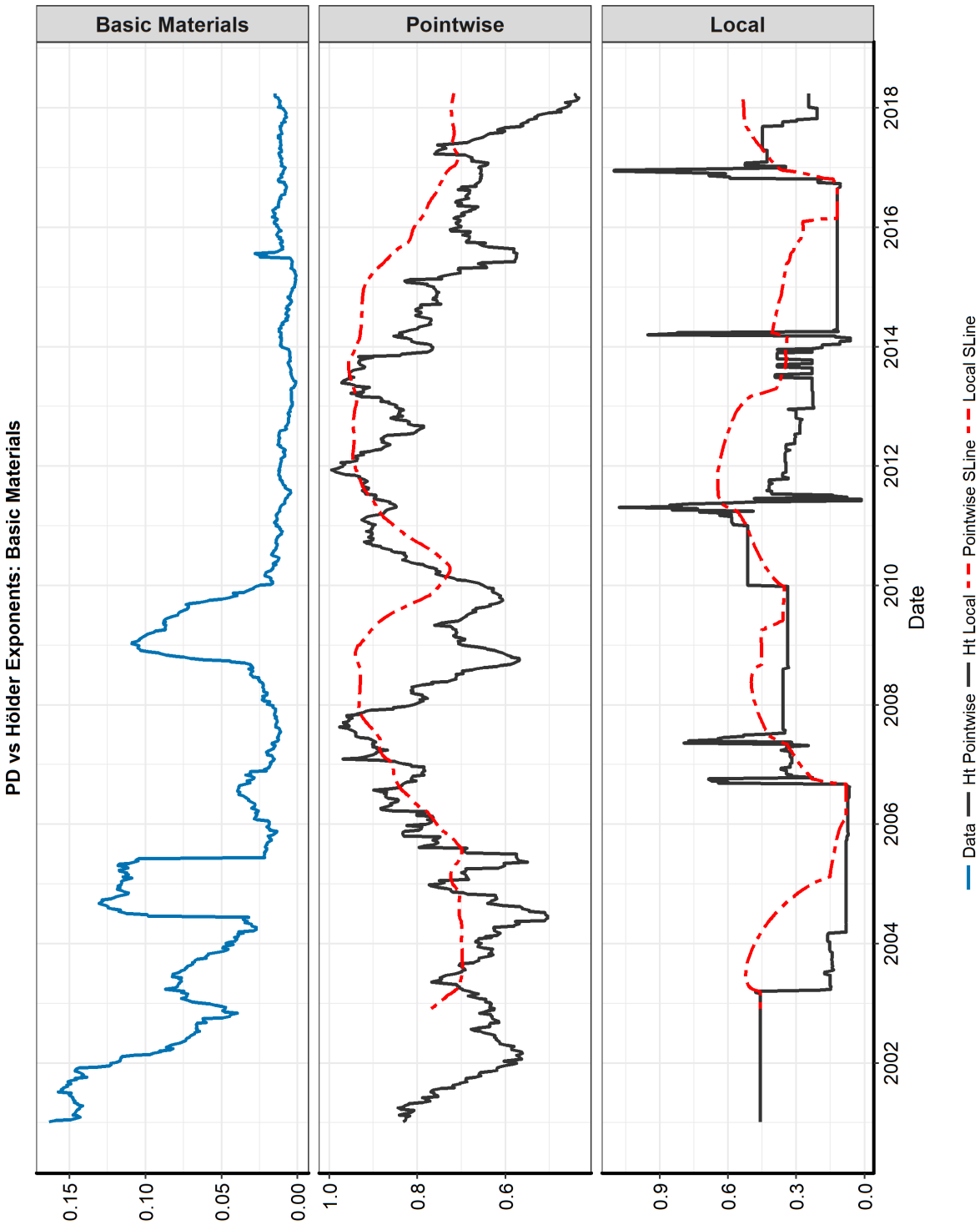
(b) Consumer Cyclicals

Fig. 2-18. (Continued)



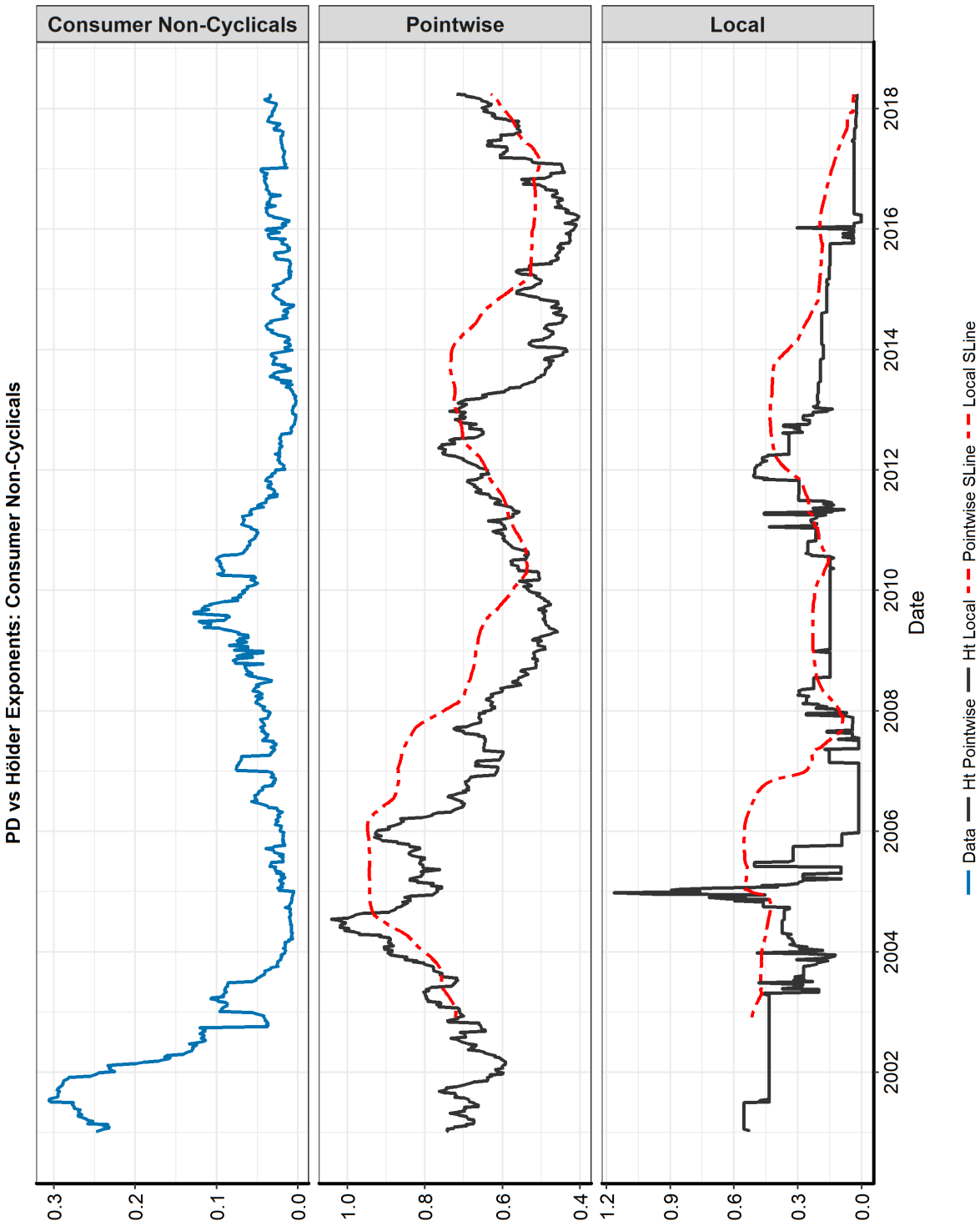
(c) Industrials

Fig. 2-18. (Continued)



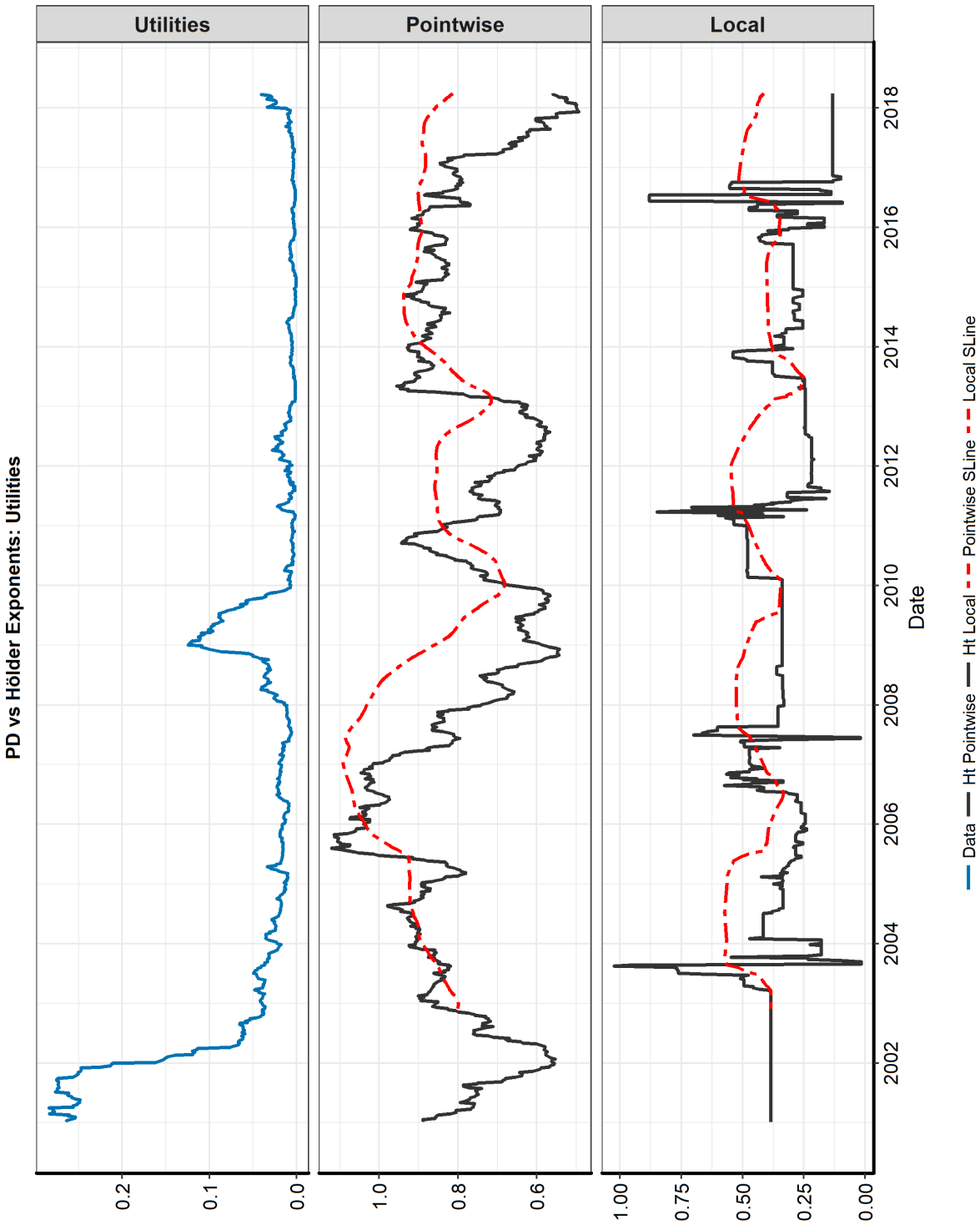
(d) Basic Materials

Fig. 2-18. (Continued)



(e) Consumer Non-Cyclicals

Fig. 2-18. (Continued)



(f) Utilities

Fig. 2-18. (Continued)

According to pointwise and local Hölder exponents of CDS and their signal lines (Figure 2-18(a), local Hölder exponents generate more signals than pointwise Hölder exponents. It appears that the pre-crisis or trend reversals have successfully detected local Hölder exponents. Local Hölder exponents of all sectors (Figure 2-18(b)-(f)) indicate similar critical points. There are univariate signals, especially before the 2008 mortgage crisis and the 2009 debt crisis. On the other hand, some flags are only due to trend reversals.

2.3.3. Wavelet analysis

Three of the wavelets, namely Morlet, Paul, and DOG[4] wavelets, are nonorthogonal. Morlet and Paul are both complex, unlike the DOG, which is real. Complex wavelets (Morlet and Paul) can better capture oscillations as they provide knowledge about amplitude and phase. Real wavelet (DOG) consists of only one element (real component) and is used to distinguish between peak and discontinuities. Hereafter, the stage of real wavelets is uncertain. When the graphs of the Hölder (also q-order Hurst exponent) exponents examine, peaks appear to be pretty clear. To distinguish positive and negative peaks, DOG overlays other wavelet families. As the order rises, the power of determining the relationship decreases. For $m = 2$, DOG finds the cleared link for q-order Hurst exponent, pointwise, and local Hölder exponents.

We investigate the relations between CDS and sectoral default probabilities in the time-frequency domain in this sub-chapter. The wavelet power spectrum (CWT) is reviewed univariate the energies of the series. The CWT findings are presented in Section 2.6. The cross-wavelet transform (XWT) will reveal the energy relations of the multivariate series. Wavelet coherence (WTC) is employed to reduce the time-frequency link between CDS and PDs. XWT and WTC findings are provided in Section 2.7 and Section 2.3.3.1, respectively. All analyzes consist of four components.

[4] derivative of Gaussian

— upper-left: Level,

— upper-right: q-order Hurst exponent,

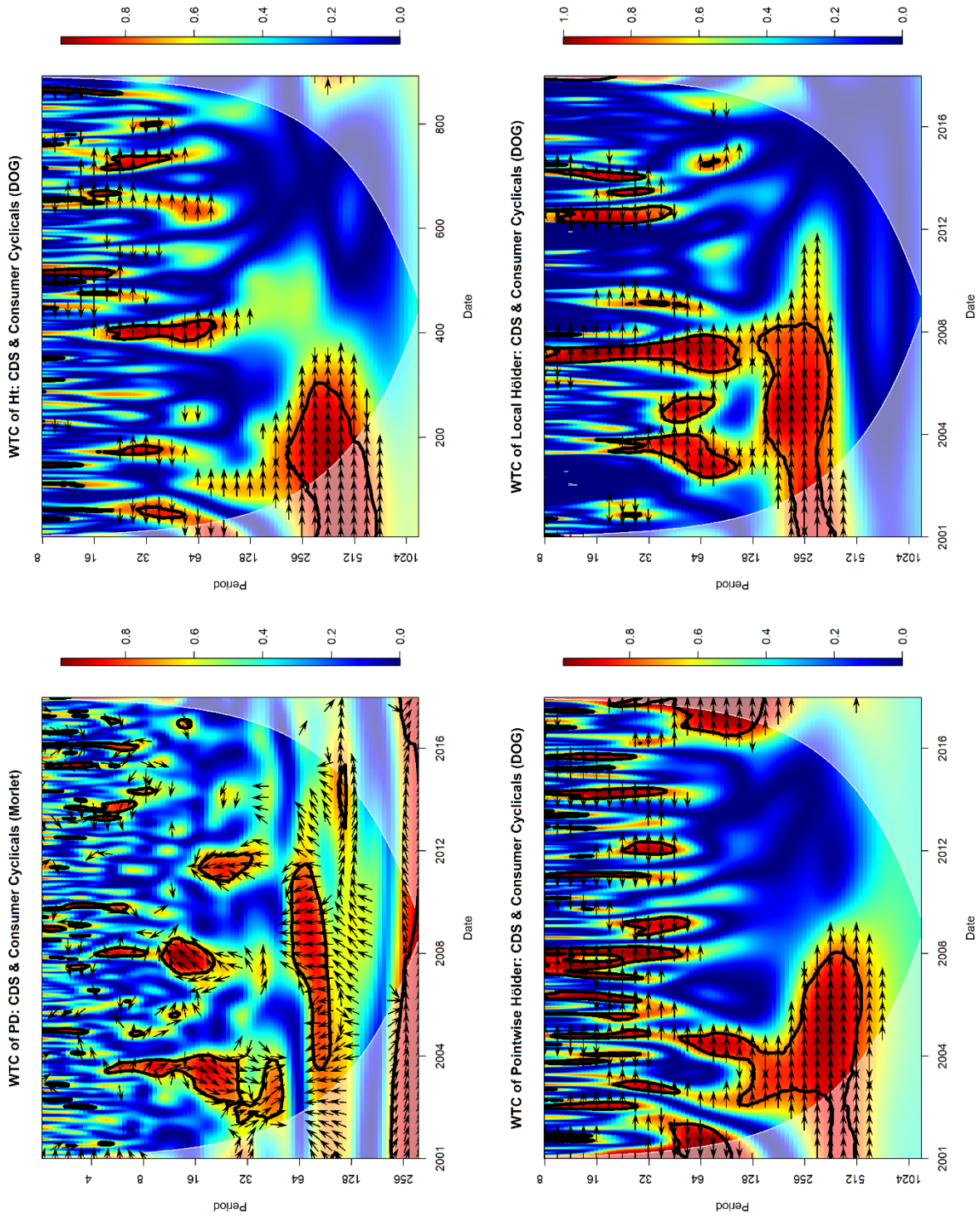
— bottom-left: Pointwise Hölder exponent,

— bottom-right: Local Hölder exponent.

2.3.3.1. Wavelet coherence

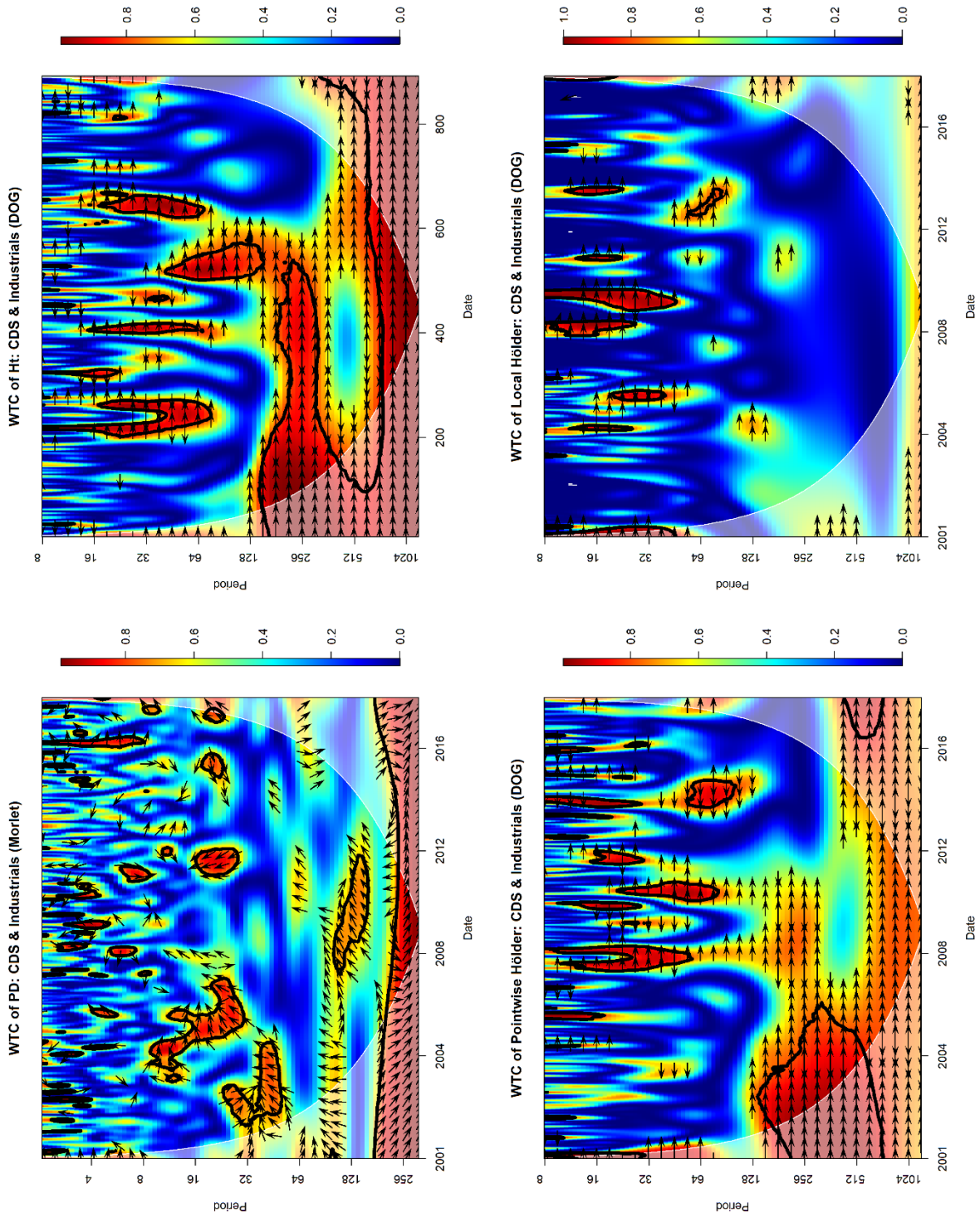
For the pair of CDS and default probability of Consumer Cyclicals (upper-left of Figure 2-19(a)) and in the significant field noted through a black border, during 2003 and 2004 in high frequency for 1 - 4 months cycle, the arrows show the direction of right-down, and in the 4 - 8 months period the arrows are pointing left-down, meaning the series are in phase and out of phase, respectively. Around 2004 - 2012, in low frequency for 1.3 - 2.6 years cycle, the arrows are pointing right, meaning the series is in phase. Around 2008 and 2012, the arrows are pointing right-up in high frequency for a 2 - 8 months cycle. According to all significant regions, the probability of default of Consumer Cyclicals is leading. For the pair of exponents of CDS and Consumer Cyclicals (Figure 2-19(a)), whole exponents exhibit similar results. The wavelet coherence generated by three different multifractal exponents detect the 2001 Turkish banking crisis, 2008 mortgage, and 2009 debt crises. The WTCs produced via q-order Hurst and pointwise Hölder exponents identify more relations than local Hölder exponents. The local Hölder exponents are more successful in determining the periods of crisis with high fluctuations. On the other hand, pointwise Hölder exponents can recognize as tinier fluctuations. Hence, it gives remarkable signals for 2018 despite the Cone of Influence effect.

Figure 2-19(b) consists of the pair of CDS and PD of Industrials. According to the level (upper-left of Figure 2-19(b)), during 2003 and 2004 in high frequency for 8 months - 1 year cycle, the arrows are pointing right-up; between 2004 and 2007 in high frequency for 2 - 8 months cycle the arrows are pointing right-up. From 2008 to 2012, in low frequency for the



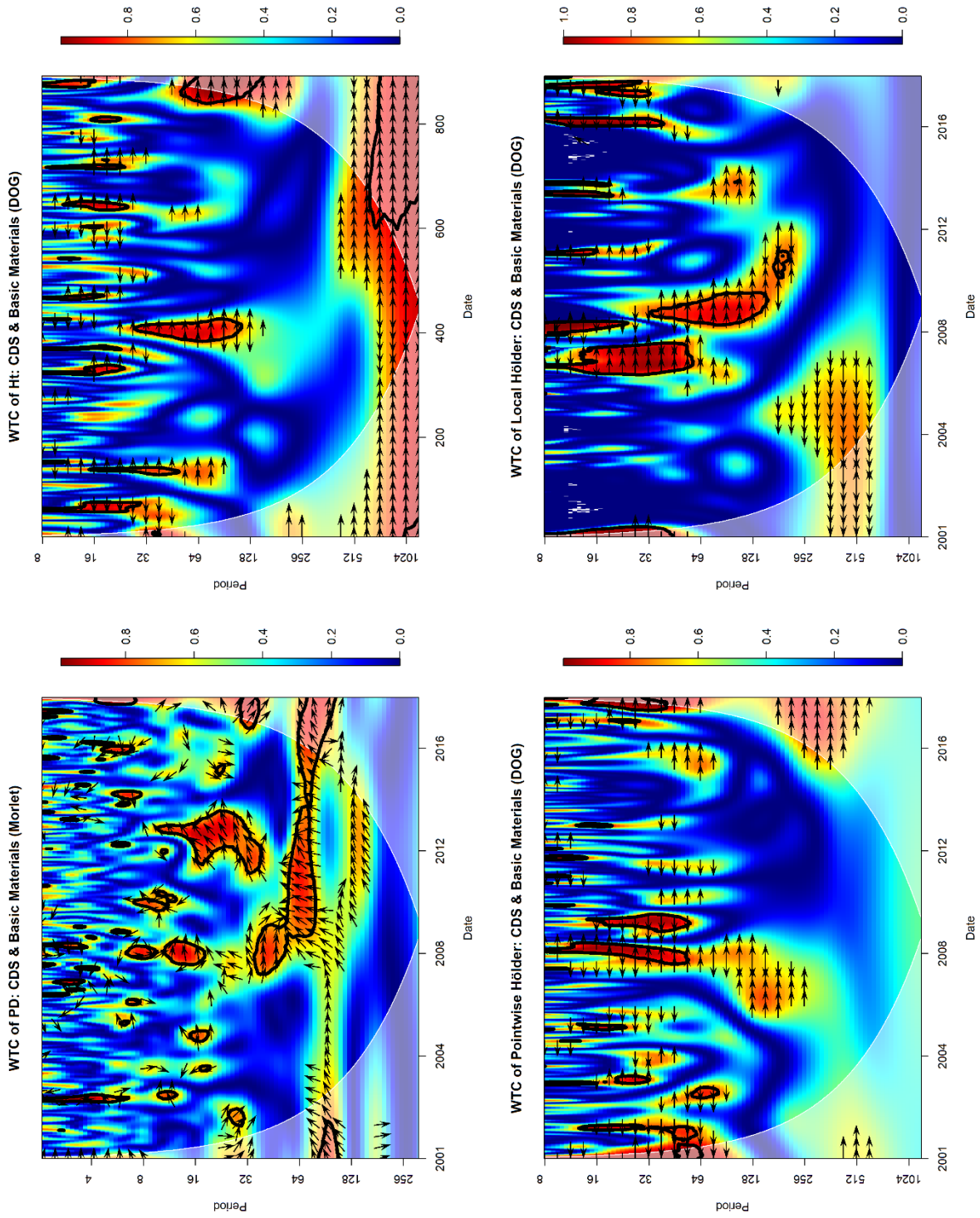
(a) WTC: CDS versus Consumer Cyclicals

Figure 2-19. The wavelet coherences of all series.



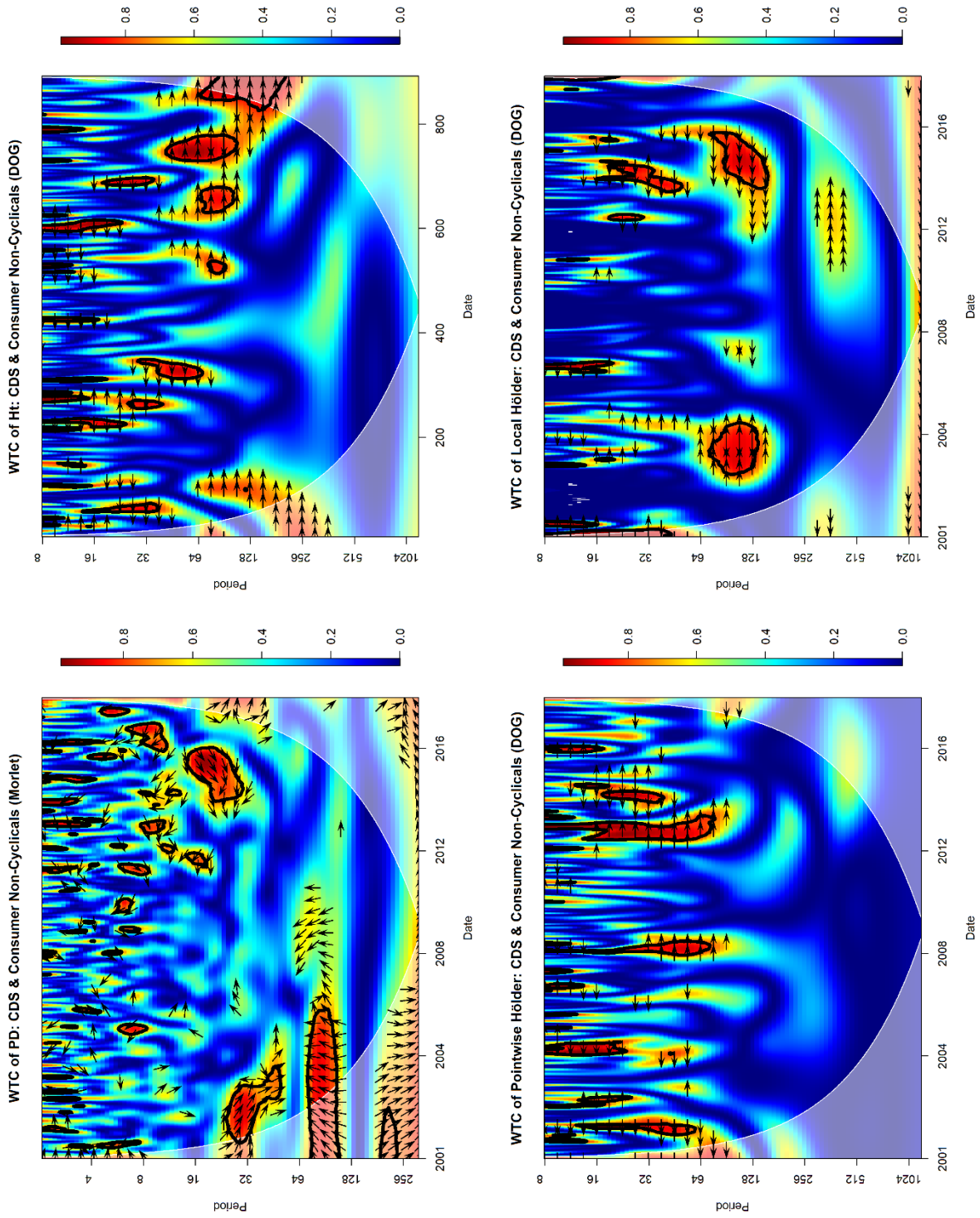
(b) WTC: CDS versus Industrials

Fig. 2-19. (Continued)



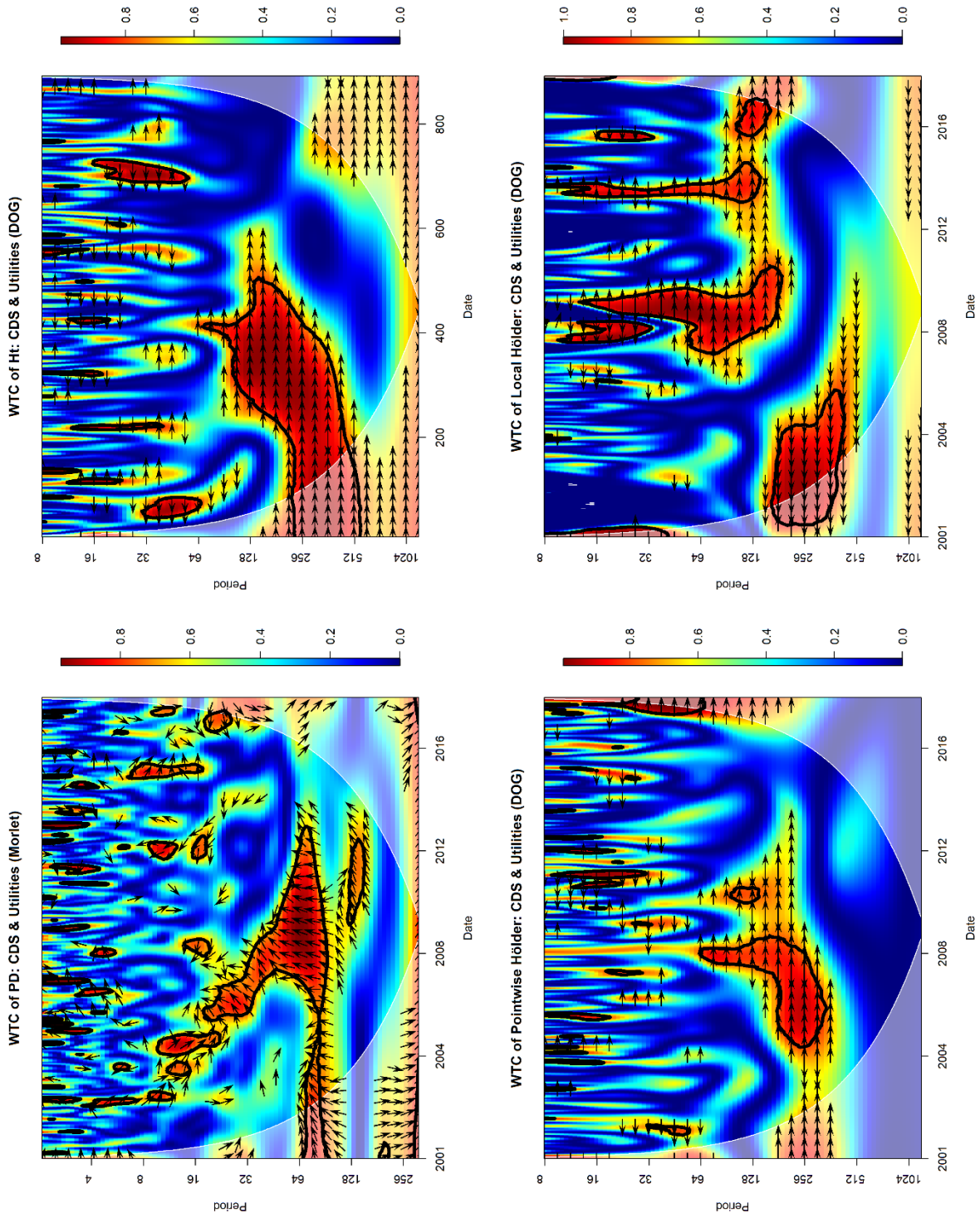
(c) WTC: CDS versus Basic Materials

Fig. 2-19. (Continued)



(d) WTC: CDS versus Consumer Non-Cyclicals

Fig. 2-19. (Continued)



(e) WTC: CDS versus Utilities

Fig. 2-19. (Continued)

2 - 2.6 years cycle, the arrows are pointing right-down. According to all significant regions, the probability of default of Industrials is leading. A couple of exponents of CDS and Industrials captured all the financial crises like Consumer Cyclicals. As in the WTCs of Consumer Cyclicals results, q-order Hurst and pointwise Hölder exponents have generated more signals than required by the constructs. Local Hölder exponents have revealed associations obviously between the high frequency from CDS and the Industrials sector during all financial crises. According to the local Hölder exponents (bottom-right of Figure 2-19(b)), in the financial crisis period in high frequency for 2 months - 1 year cycle, the arrows are pointing right, showing the exponents are in phase.

For the pair of CDS and Basic Materials' default probability (upper-left of Figure 2-19(c)), between 2008 and 2018 in low frequency for 1 - 2 years cycle and around 2012 - 2013 in high frequency for 4 months - 1 year cycle, the arrows are pointing right-up showing that CDS and Basic Materials are in phase, and Basic Materials is leading. Like the other cases, the wavelet coherence created by three various multifractal exponents catches the 2001 Turkish banking crisis, the 2008 mortgage, and the 2009 debt crisis for Basic Materials. Another remarkable point is that all exponents gave signals for the high frequency in 2018.

Figure 2-19(d) presents a couple of CDS and Consumer Non-Cyclicals. For the pair of CDS and Consumer Non-Cyclicals' default probability (upper-left of Figure 2-19(d)) in the significant field noted through a black border, between 2001 - 2006 in low frequency for 1.3 - 2.6 years, the arrows are pointing left-up (in-phase and Consumer Non-Cyclical leading). Around 2002 - 2004 in a high frequency 8 months - 1 year cycle, the arrows are right-down, meaning exponents are positively correlated, and Consumer Non-Cyclicals is lagging. Nearby 2014 - 2016 in high frequency for 4 - 8 months cycle arrows are pointing left-down. In this region, CDS and the probability of default are out of phase the first time. Consumer Non-Cyclicals' default probability is leading. Although the q-order Hurst and pointwise Hölder

exponents give detailed results, the local Hölder exponent results are different in Consumer Non-Cyclical. The local Hölder exponents not only identify the crisis periods of interest but also discover the sectoral breaks in 2004 and 2014. Around 2004 and 2014, in low frequency for 1.3 - 2.6 years cycle, the arrows point positive and negative correlation, respectively.

Figure 2-19(e) is related to the pair of CDS and the probability of default of Utilities. According to the level (upper-left of Figure 2-19(e)), between 2008 - 2012 in low frequency for 1 - 1.3 years cycle, the arrows are pointing right-up meaning series are positively correlated, and Utilities is leading. According to q-order Hurst and pointwise Hölder exponents, their findings are not much dissimilar. On the other hand, the WTC of local Hölder exponents (bottom-right of Figure 2-19(e)) is different from other sectors. The local Hölder exponents capture all financial crises in both high and low frequencies. Around 2014, in both frequencies for 4 months - 2.6 years, the arrows point series exhibit a positive relationship.

2.4. Large-Scale Forecast

Based on the wavelet coherence analysis, we indicated that local Hölder exponents of CDS and the probability of default of Consumer Cyclical, Basic Materials, and Utility sectors highly correlate in mortgage and debt crisis periods in low frequency. In this section, the regions specified on the wavelet coherence will explore deeply. Forecasting relationships within the windows determined at a low frequency based on wavelet coherence are called large-scale forecasts. The selected windows are detailed present in *Table 2-6*. All panes except Consumer Cyclical contain US sub-prime and European sovereign crisis periods. The first window consists of CDS and Consumer Cyclical. The window details in Section 2.4.1 are between 2004 and 2008 in low frequency for 2.5–5 years cycle in Figure 2-20. CDS versus Basic materials (Section 2.4.2) and Utilities (Section 2.4.3) windows from 2006 to 2011 in low frequency for the 1.2–2.5 years cycle are presented in Figures 2-22 and 2-24.

Table 2-6. Window definitions.

CDS and PD	TP	SP	Length	Correlation
Consumer Cyclicals	2004-2008	128-256	209	0.5850
Basic Materials	2006-2011	64-128	224	0.5787
Utilities	2006-2011	64-128	224	0.5045

Note. TP and SP denote the time period and scale period, respectively. Correlation denotes Pearson's product-moment correlation.

The time series from the region of interest should be extracted to perform scale-by-scale analysis [36]. Primarily, all local Hölder exponents are extracted into time and frequency domains by continuous wavelet transform. Scale and octave-voice matched with each other by using a wavelet scalogram. Consequently, the series corresponding to the selected region is obtained via inverse wavelet transform for only related octave-voice.

In multivariate time series models, we need to manually verify the high connection among the variables using wavelet coherence and showing numerically. Multivariate time series analysis estimates synchronically multiple time series. In particular, VARMA models are available to recognize dynamic connections between variables [26]. Furthermore, long memory characteristics are not taken into consideration when the usual VARMA models are applied. Therefore, VFARIMA is employed to examine the behavior of local Hölder exponents during crisis periods. Vector-type models not only make a forecast using the history of the related data but also consider other dependent variables. For this reason, they give pretty reliable results in economic data forecasting than comparable models [27]. We fit and forecast 12-step-ahead (weekly basis) for all panes by using the following models: VFARIMA, VARMA, FARIMA, and ARMA

The m-variate process x_t is a vector fractionally autoregressive integrating moving average $VFARIMA(p, d_1, d_2, .. d_m, q)$ the process if [51]

$$\Phi(B)\Delta^d(B)(x_t - \mu) = \Theta(B)\epsilon_t \tag{2-31}$$

where B is the lag operator, μ is the mean vector, ϵ_t is white noise with $E(\epsilon_t) = 0$ and $Var(\epsilon_t) = RR'$. The ARMA operators

$$\Phi(B) = \Phi_0 - \sum_{j=1}^{p} \Phi_j B^j \tag{2-32}$$

$$\Theta(B) = \Theta_0 + \sum_{j=1}^{q} \Theta_j B^j \tag{2-33}$$

where $\Phi(B)$ and $\Theta(B)$ are $m \times m$ matrix polynomials in B. The coefficients of polynomials $\Phi(B)$ and $\Theta(B)$ are assumed to satisfy the standard stationarity and invertibility conditions and are non-linear functions of some estimable parameters after imposed normalization and identification restrictions.

Three various procedures are employed to select the most appropriate model. First, we estimate the following error metrics: RMSE, MAE, ME, MPE, and MAPE. Then, QLIKE, standard (SE), and absolute (AE) errors graphs are created to measure forecast accuracy. Finally, we employ the model confidence set procedure of Hansen et al. to list suitable models. [52]

2.4.1. Consumer cyclical

The selected pane consists of local Hölder exponents of CDS and probability of default of Consumer Cyclicals from January 2004 to December 2007 in low frequency for 2.5–5 years cycle in wavelet coherence (right bottom of Figure 2-19(a)). In total, 209 observations are used. The top of Figure 2-20 indicates the converted series.

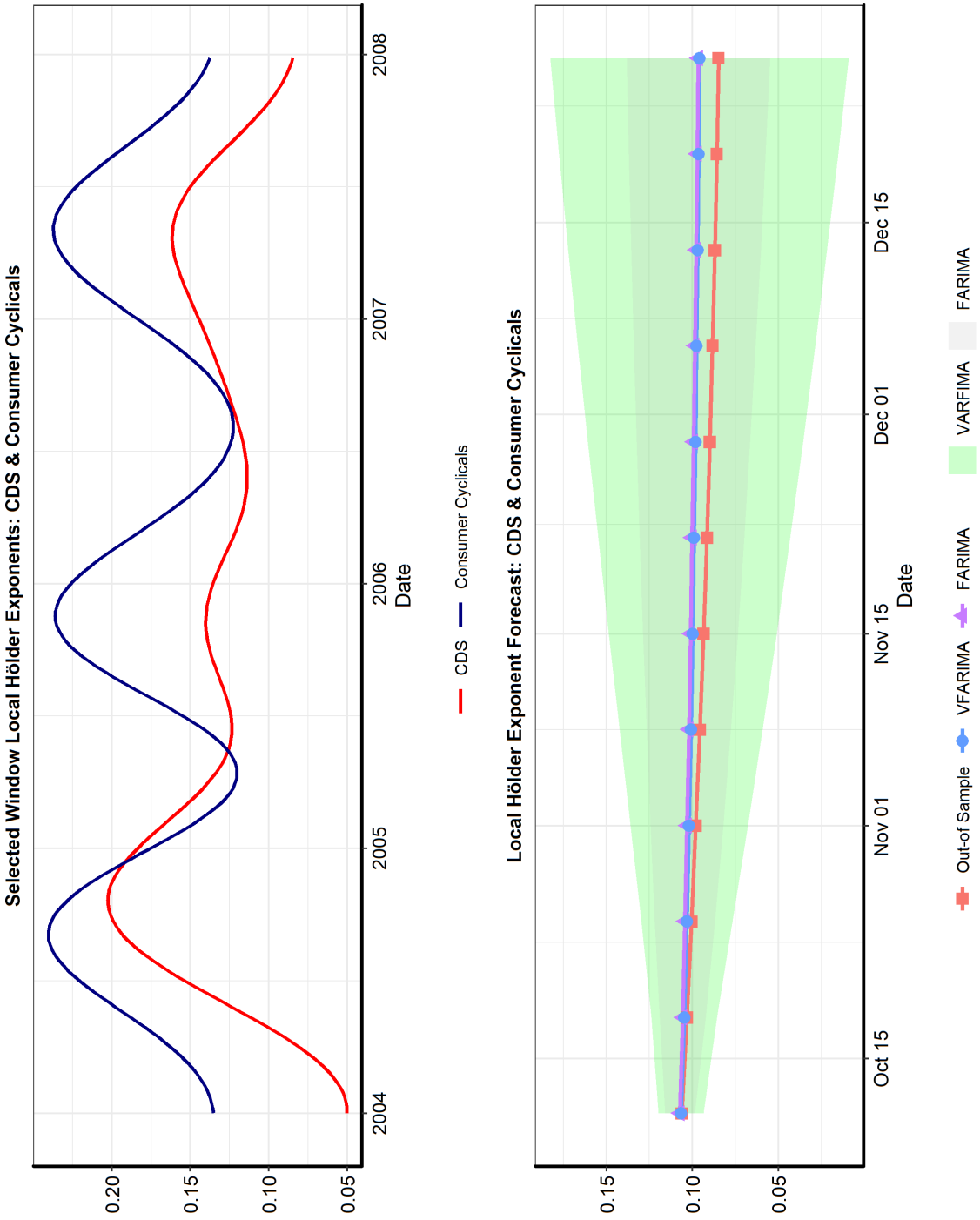


Figure 2-20. Selected window and forecast plot: CDS versus Consumer Cyclicals.

The local Hölder exponents of CDS and Consumer Cyclicals' PD fit and the local Hölder exponents of CDS predict 12-step-ahead (three months) by VFARIMA$(1, d_1, d_2, 1)$ and following benchmark models: VARMA(1,1), ARMA(1,1) and FARIMA$(1, d, 1)$. The bottom of Figure 2-20 exhibits the 12-step-ahead forecast results of models.

Table 2-7. Forecast performance comparison: CDS versus Consumer Cyclicals.

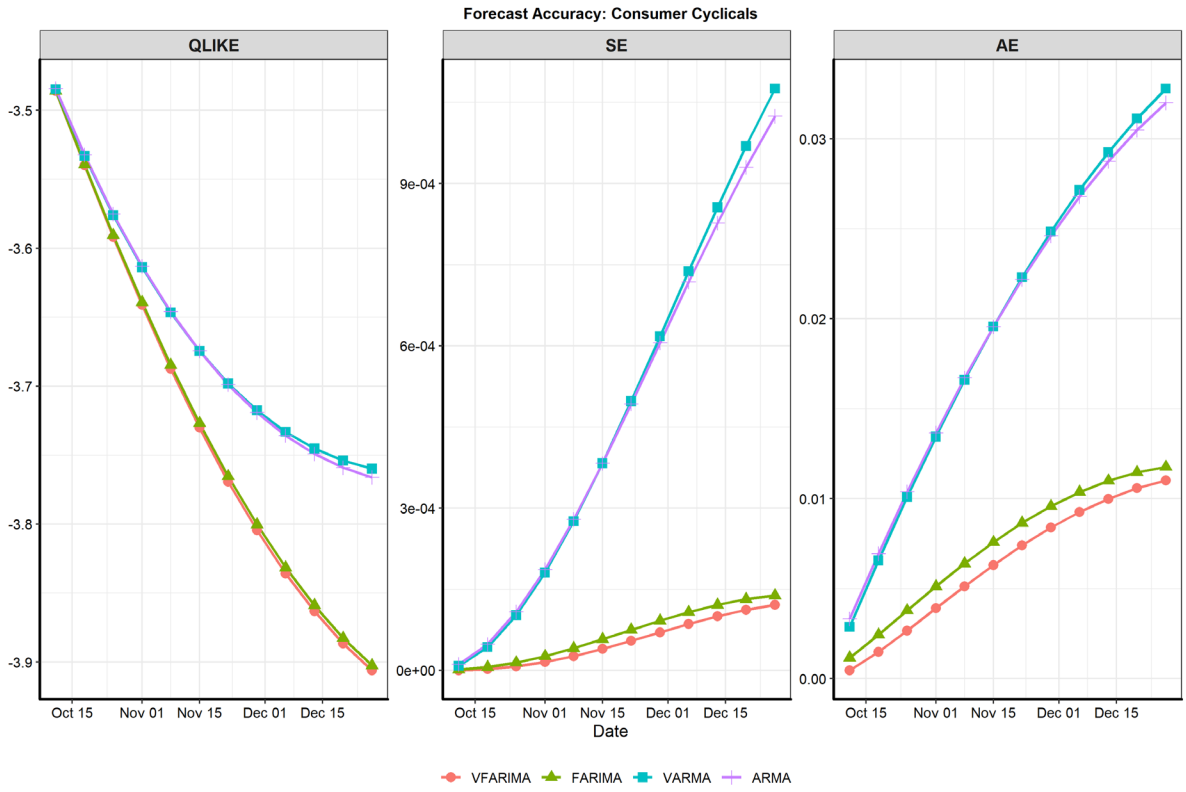
	Out of sample				
	RMSE	MAE	ME	MPE	MAPE
VFARIMA$(1, d_1, d_2, 1)$	0.00728	0.00639	-0.00639	-7.1152	7.1152
FARIMA$(1, d, 1)$	0.00823	0.00745	-0.00745	-8.2507	8.2507
VARMA(1,1)	0.02189	0.01972	-0.01972	-21.8736	21.8736
ARMA(1,1)	0.02163	0.01962	-0.01962	-21.7316	21.7316

The prediction performance examines three layers. Standard performance metrics are shown in *Table 2-7* and ranked using RMSE. In all metrics, the VFARIMA model outperforms the others. Besides, the forecast accuracy graph in Figure 2-21 also supports performance metric findings. On the other hand, the model confidence set table (*Table 2-8*) eliminated forecast results except for VFARIMA. Thence, VFARIMA$(1, d_1, d_2, 1)$ model has the best out-of-sample forecasting performance according to all criteria' results.

Table 2-8. Model confidence set: Consumer Cyclicals.

	M			R			
	Rank	v	MCS	Rank	v	MCS	Loss
VFARIMA$(1, d_1, d_2, 1)$	1	-11.97	1	1	-11.97	1	0.10011
FARIMA$(1, d, 1)$				eliminated			
VARMA(1,1)				eliminated			
ARMA(1,1)				eliminated			

Note. The confidence level is 95%, and the number of bootstrapped samples is 5000.



Note. SE and AE denote the square error and absolute error, respectively.

Figure 2-21. Forecast accuracy: CDS versus Consumer Cyclicals.

2.4.2. Basic materials

The selected region consists of local Hölder exponents of CDS and probability of default of Basic Materials from September 2006 to January 2011 in low frequency for 1.2–2.5 years cycle in wavelet coherence (right-bottom in Figure 2-19(c)). In total, 224 observations are used. The top of Figure 2-22 indicates the converted series.

The local Hölder exponents of CDS and default probability of Basic Materials fit, and the local Hölder exponents of CDS predict 12-step-ahead (three months) by VFARIMA$(1, d_1, d_2, 1)$ and following benchmark models: VARMA(1,1), ARMA(1,1) and FARIMA$(1, d, 1)$. The bottom of Figure 2-22 exhibits the 12-step-ahead forecast results of models.

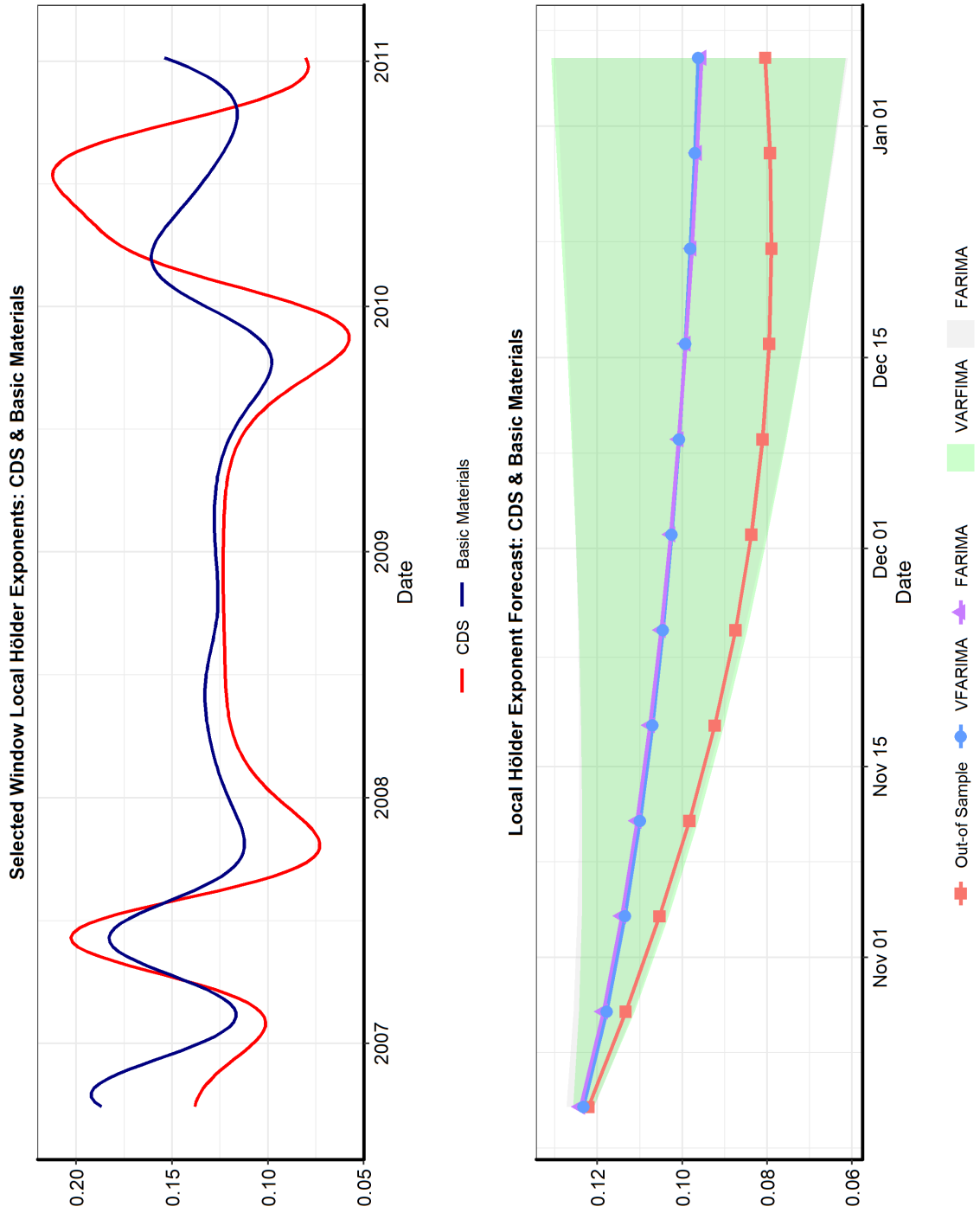


Figure 2-22. Selected window and forecast plot: CDS versus Basic Materials.

The estimate performance reviews three layers. Standard performance metrics are shown in *Table 2-9* and ranked using root mean square error (RMSE). In all metrics, the VFARIMA model outperforms the others. Besides, the forecast accuracy graph in Figure 2-23 also supports performance metric findings. According to the model confidence set table

(*Table 2-10*), VFARIMA and FARIMA models' results eliminated the forecast results except for VFARIMA and FARIMA. Nevertheless, the VFARIMA still outperforms according to the loss function results. Thence, VFARIMA$(1, d_1, d_2, 1)$ model has the best out-of-sample forecasting performance according to all criteria' results.

Table 2-9. Forecast performance comparison: CDS versus Basic Materials.

	Out of sample				
	RMSE	MAE	ME	MPE	MAPE
VFARIMA$(1, d_1, d_2, 1)$	0.01526	0.01401	-0.01401	-16.48002	16.48002
FARIMA$(1, d, 1)$	0.01532	0.01422	-0.01422	-16.64617	16.64617
VARMA(1,1)	0.04091	0.03917	-0.03917	-45.36246	45.36246
ARMA(1,1)	0.02857	0.02560	-0.02445	-29.45623	30.39653

Table 2-10. Model confidence set: Basic Materials.

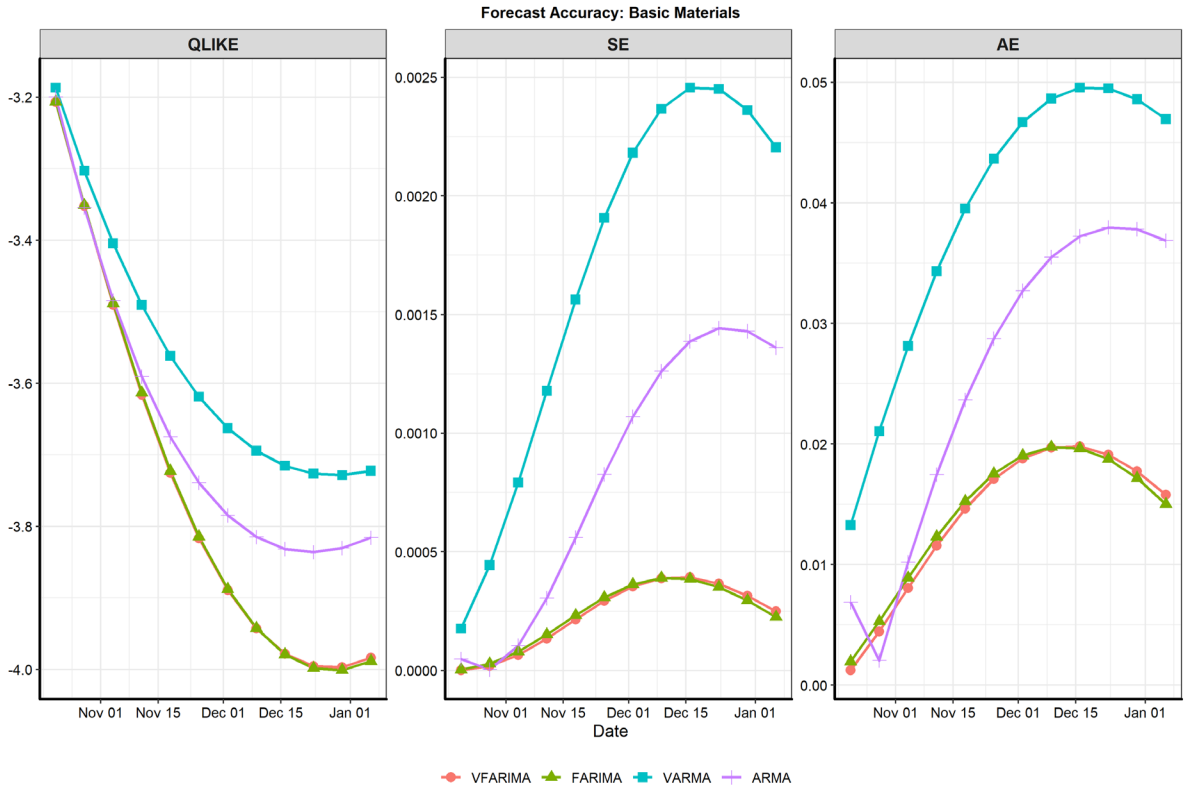
	M			R			
	Rank	v	MCS	Rank	v	MCS	Loss
VFARIMA$(1, d_1, d_2, 1)$	1	-1.17	1	1	-1.17	1	0.10582
FARIMA$(1, d, 1)$	2	1.17	0.2426	2	1.17	1	0.10604
VARMA(1,1)	eliminated						
ARMA(1,1)	eliminated						

Note. The confidence level is 95%, and the number of bootstrapped samples is 5000.

2.4.3. Utilities

The selected window consists of local Hölder exponents of CDS and Utilities default probability from September 2006 to January 2011 in low frequency for a 1.2–2.5 years cycle in wavelet coherence (right-bottom in Figure 2-19(e)). In total, 224 observations are used. The top of Figure 2-24 indicates the converted series.

The local Hölder exponents of CDS and Utilities' PD fit and the local Hölder exponents of CDS predict 12-step-ahead (three months) by VFARIMA$(1, d_1, d_2, 1)$ and



Note. SE and AE denote the square error and absolute error, respectively.

Figure 2-23. Forecast accuracy: CDS versus Basic Materials.

following benchmark models: VARMA(1,1), ARMA(1,1) and FARIMA$(1, d, 1)$. The bottom of Figure 2-24 exhibits the 12-step-ahead forecast results of models.

The prediction performance examines three layers. Standard performance metrics are shown in *Table 2-11* and ranked using root mean square error (RMSE). In all metrics, the

VFARIMA model outperforms the others. Besides, the forecast accuracy graph in Figure 2-25 also supports performance metric findings. On the other hand, the model confidence set table (*Table 2-12*) eliminated forecast results except for VFARIMA. Thence, the VFARIMA$(1, d_1, d_2, 1)$ model produces the most reliable out-of-sample estimate performance according to the results of all criteria.

Table 2-11. Forecast performance comparison: CDS versus Utilities.

	Out of sample				
	RMSE	MAE	ME	MPE	MAPE
VFARIMA$(1, d_1, d_2, 1)$	0.01155	0.00762	0.00744	9.2915	9.46008
FARIMA$(1, d, 1)$	0.01532	0.01422	-0.01422	-16.64617	16.64617
VARMA(1,1)	0.06070	0.05922	-0.05922	-67.91151	67.91151
ARMA(1,1)	0.02857	0.02560	-0.02445	-29.45623	30.39653

Table 2-12. Model confidence set: Utilities.

	M			R			
	Rank	v	MCS	Rank	v	MCS	Loss
VFARIMA$(1, d_1, d_2, 1)$	1	-4.21	1	1	-4.21	1	0.08438
FARIMA$(1, d, 1)$				eliminated			
VARMA(1,1)				eliminated			
ARMA(1,1)				eliminated			

Note. The confidence level is 95%, and the number of bootstrapped samples is 5000.

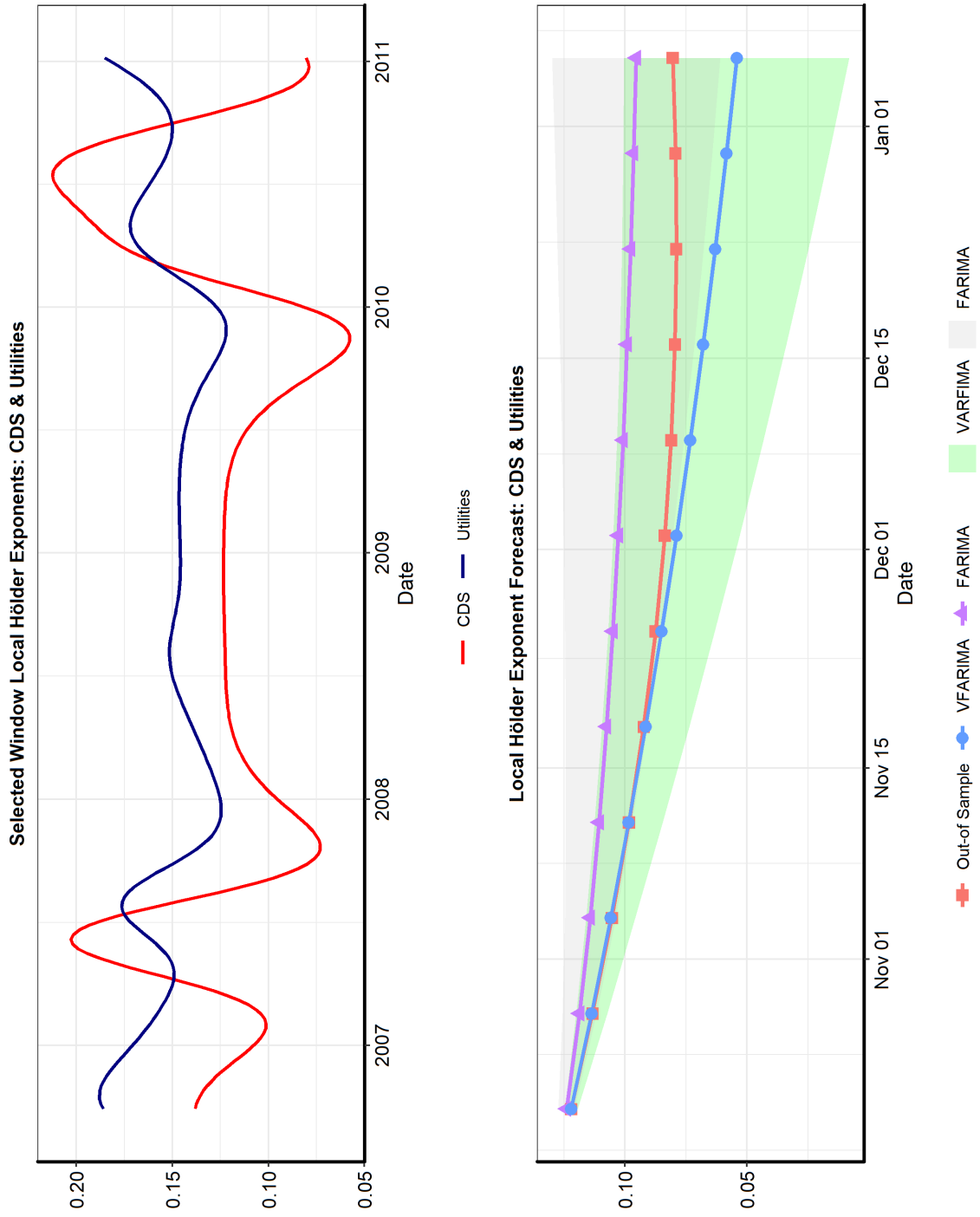
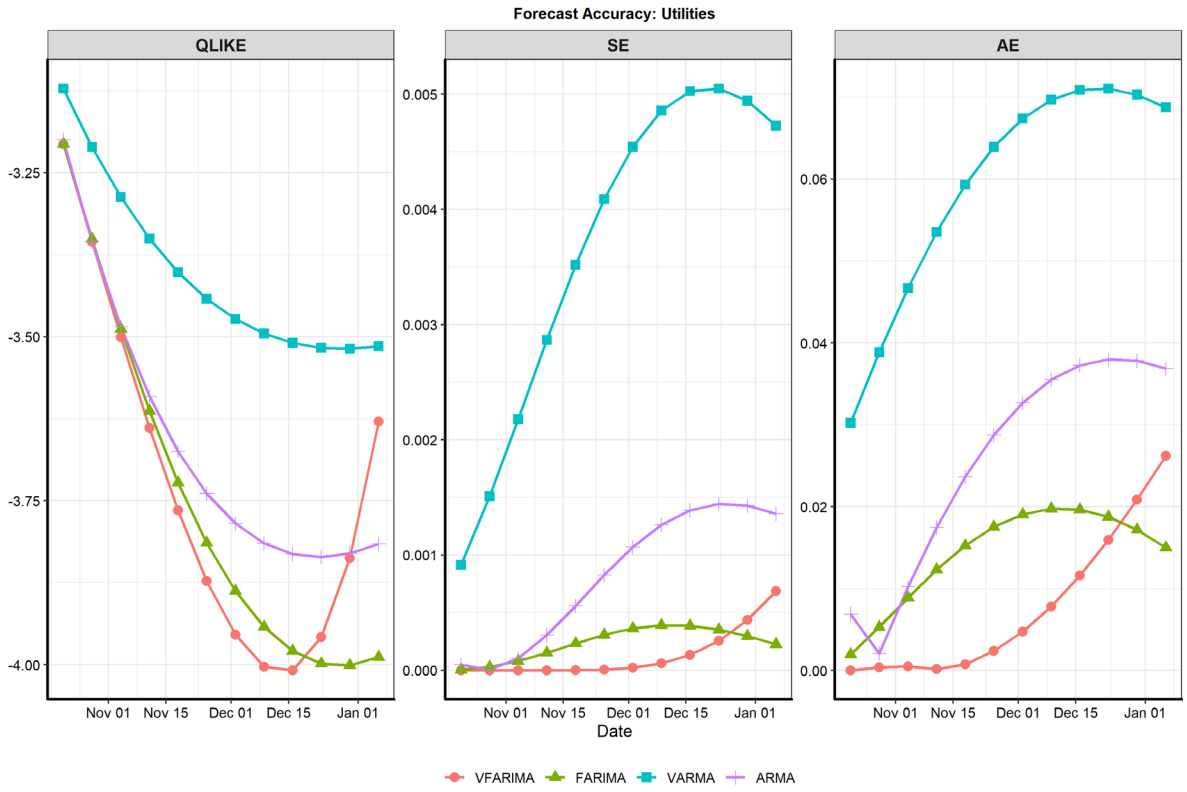


Figure 2-24. Selected window and forecast plot: CDS versus Utilities.



Note. SE and AE denote the square error and absolute error, respectively.

Figure 2-25. Forecast accuracy: CDS versus Utilities.

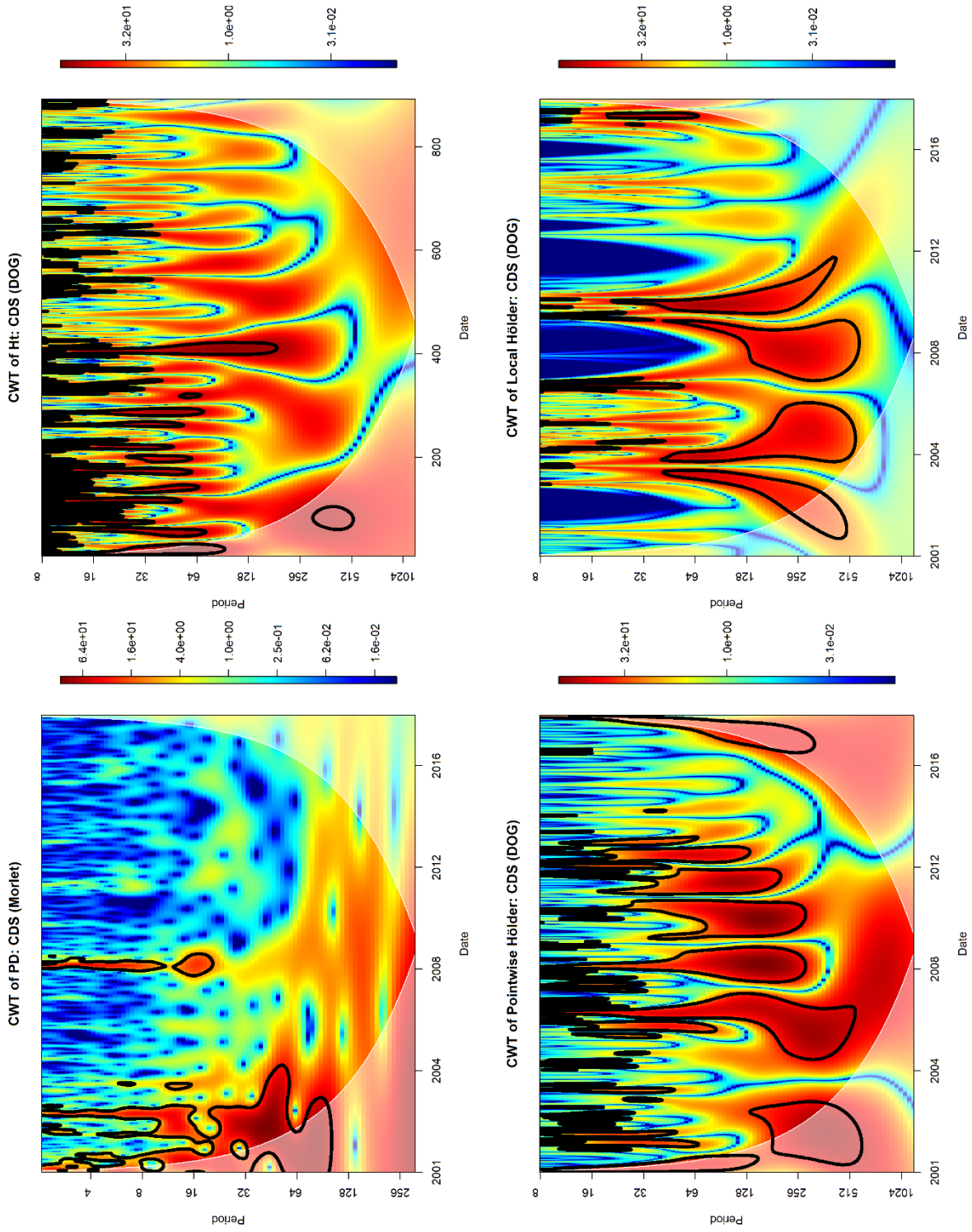
2.5. Conclusion

Within the chapter, the dynamic co-movements among CDS and sectoral default probabilities in the large-scale fluctuations have been reviewed to discover the sensitivities of sector behavior in crisis periods. First, the sectoral default probabilities estimate according to Moody's KVM expected default frequency methodology. Afterward, the series' multifractal features analyze according to the benchmark series, and we studied the multifractal cross-correlation between CDS and PDs. According to the multifractal analysis, it is revealed that all series have a multifractal behavior and long-term cross-correlation between all pairs exhibits multifractal nature. The q-order Hurst, pointwise, and local Hölder exponents are calculated for CDS and PSs that are recognized as having multifractal characteristics. The q-order Hurst, pointwise, and local Hölder exponents are used to define the fragilities of the

time series to determine the links between CDS and sectors. In this view, dynamic co-movements between the series are determined by wavelet coherence, considering the fragility, trend, and structural changes. The results symbolize that CDS explain by sectoral default probabilities in many time-frequency domains. As a result of the theoretical and fundamental contrasts between the exponents, the local Hölder exponent is selected to analyze crisis periods. However, according to local Hölder exponents, the co-movement of the CDS and PDs reveals all the financial crises in the analysis period. Another significant finding also discusses the lead-lag relationship: the sectoral default probability is the leading indicator to catch the financial crisis.

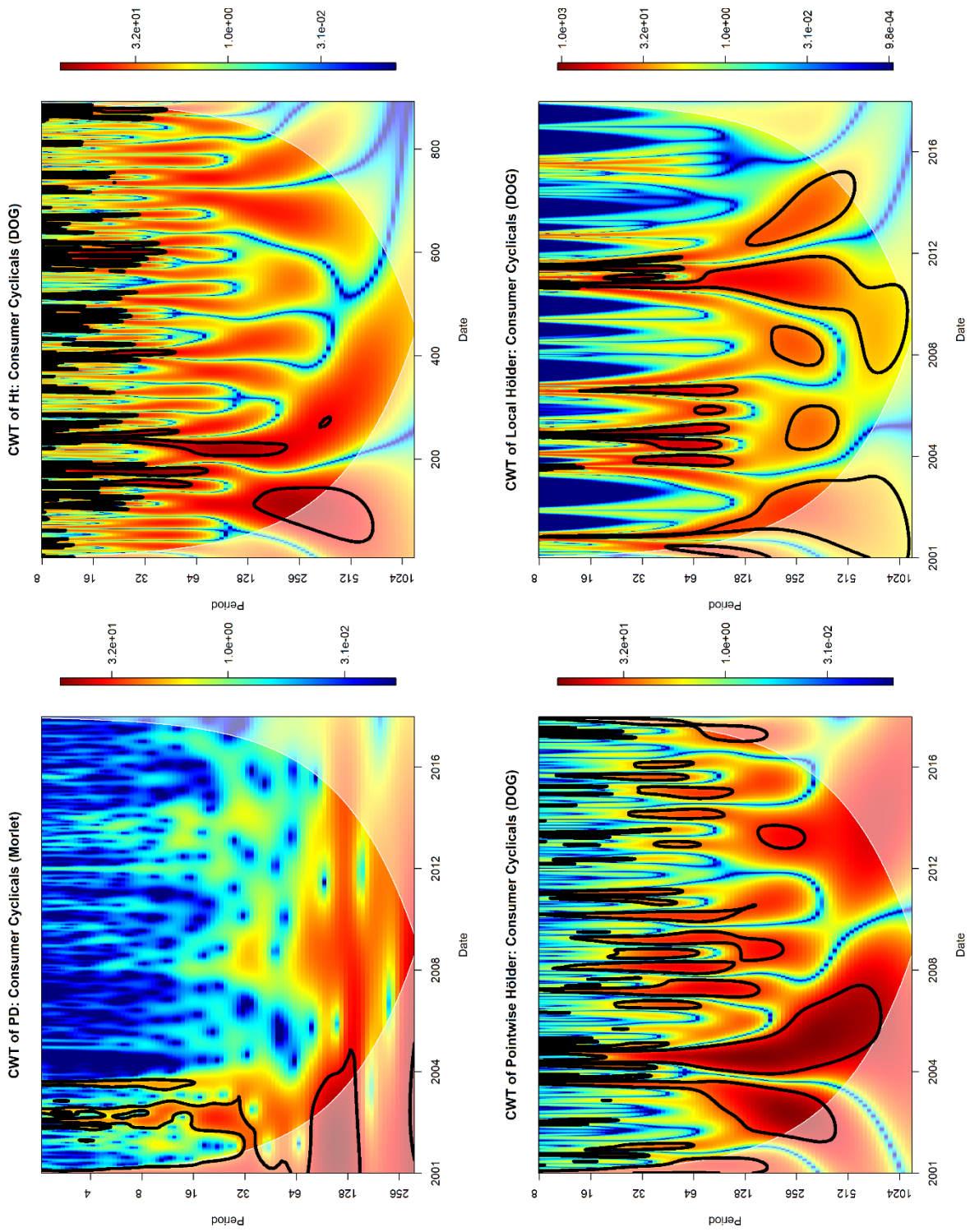
On the other hand, CDS versus Consumer Cyclical, Basic Materials, and Utility sectors have been used for large-scale forecasts in the 2008 US subprime mortgage crisis with the low frequency determined relations. The scale-by-scale analysis is performed on these views to create panes from local Hölder exponents. Then, we employed multivariate and univariate time series methodologies for 12-step- ahead (three months) prediction of the local Hölder exponents in chosen regions. The vector-type models perform better for modeling the macroeconomic series. Because the series show multifractal characteristics, the VFARIMA is better than the benchmark models, FARIMA, VARMA, and ARMA, in all selected windows.

2.6. Wavelet Power Spectra



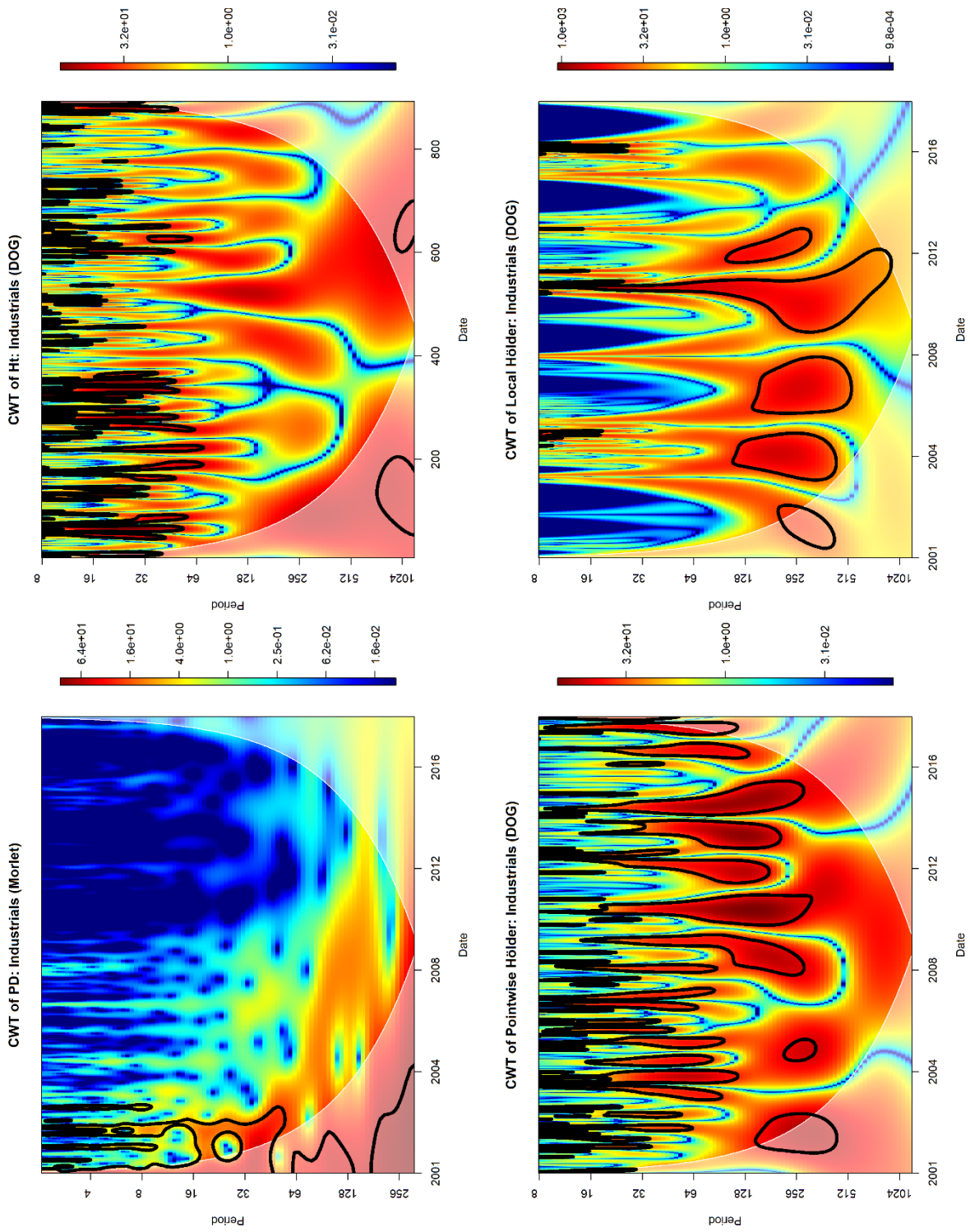
(a) CWT: CDS

Figure 2-26. Wavelet power spectra of all series.



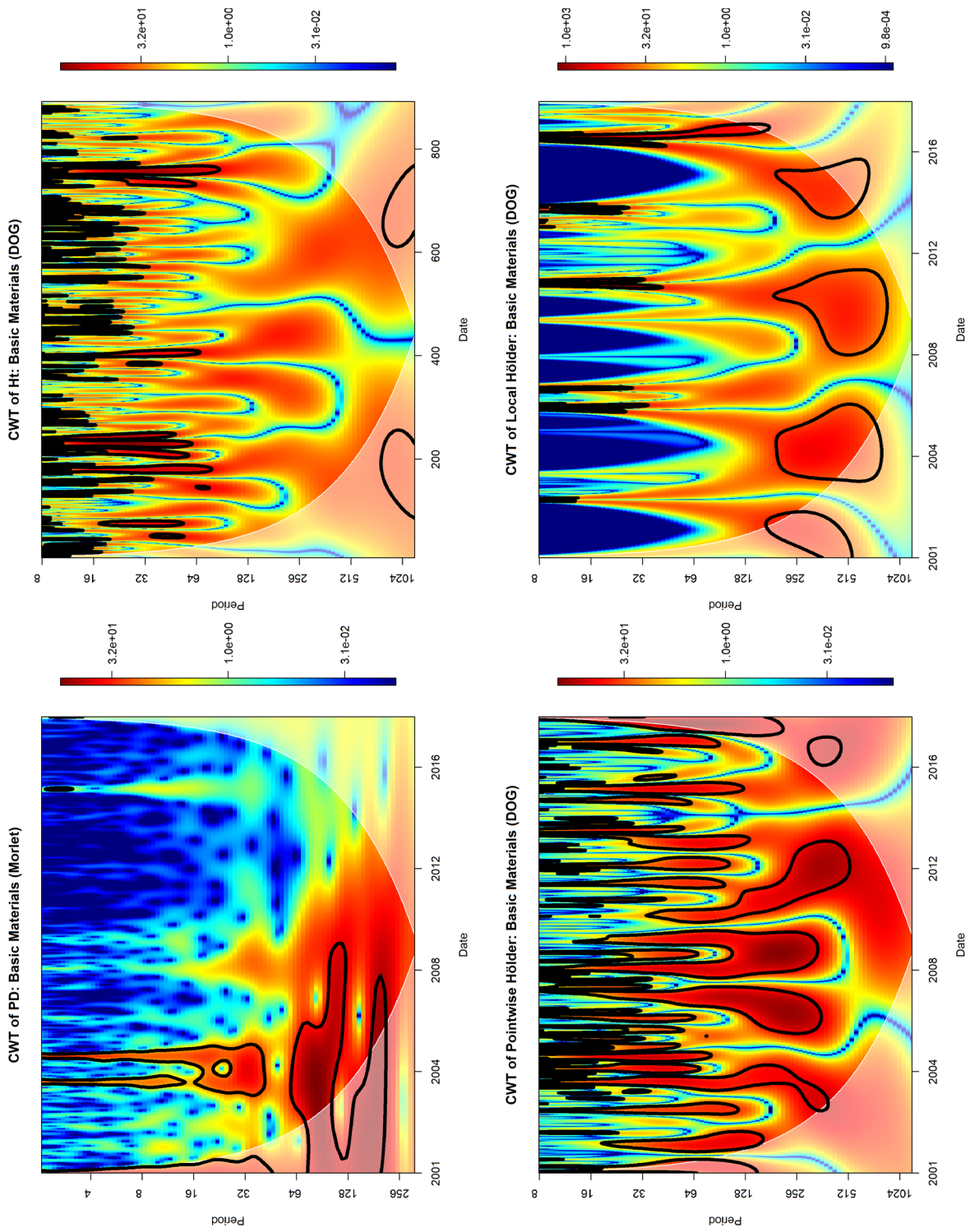
(b) CWT: Consumer Cyclicals

Fig. 2-26. (Continued)



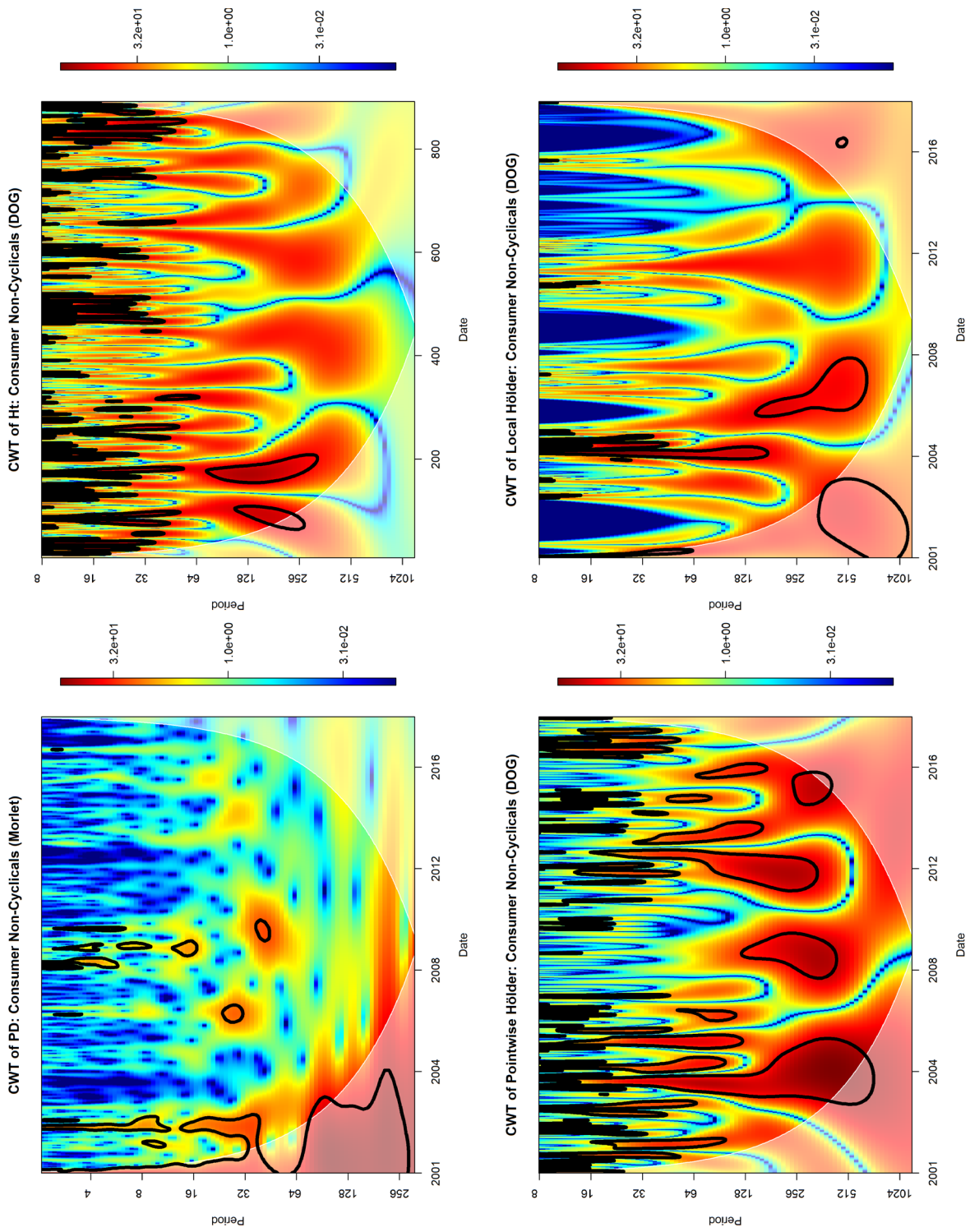
(c) CWT: Industrials

Fig. 2-26. (Continued)



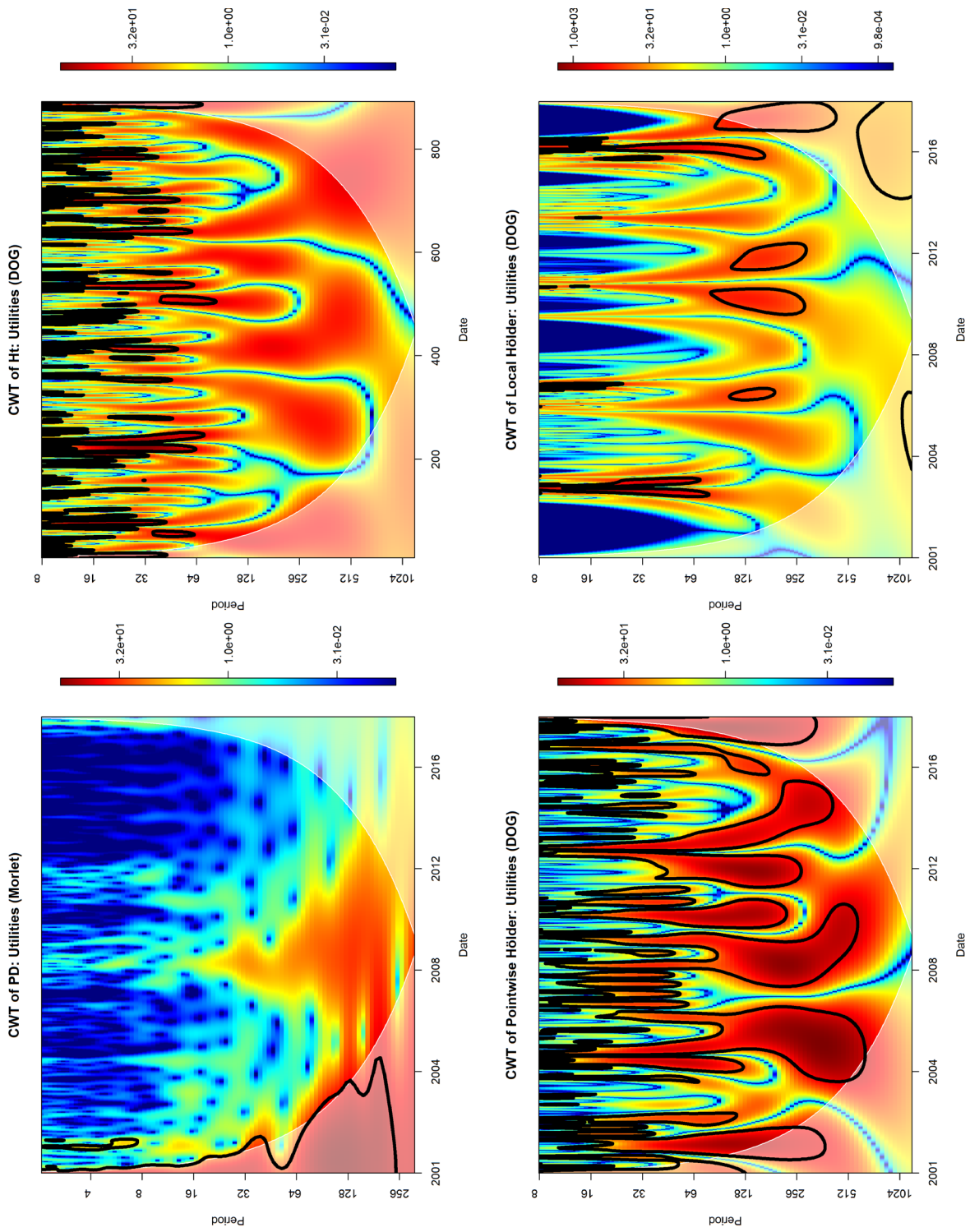
(d) CWT: Basic Materials

Fig. 2-26. (Continued)



(e) CWT: Consumer-Non-Cyclicals

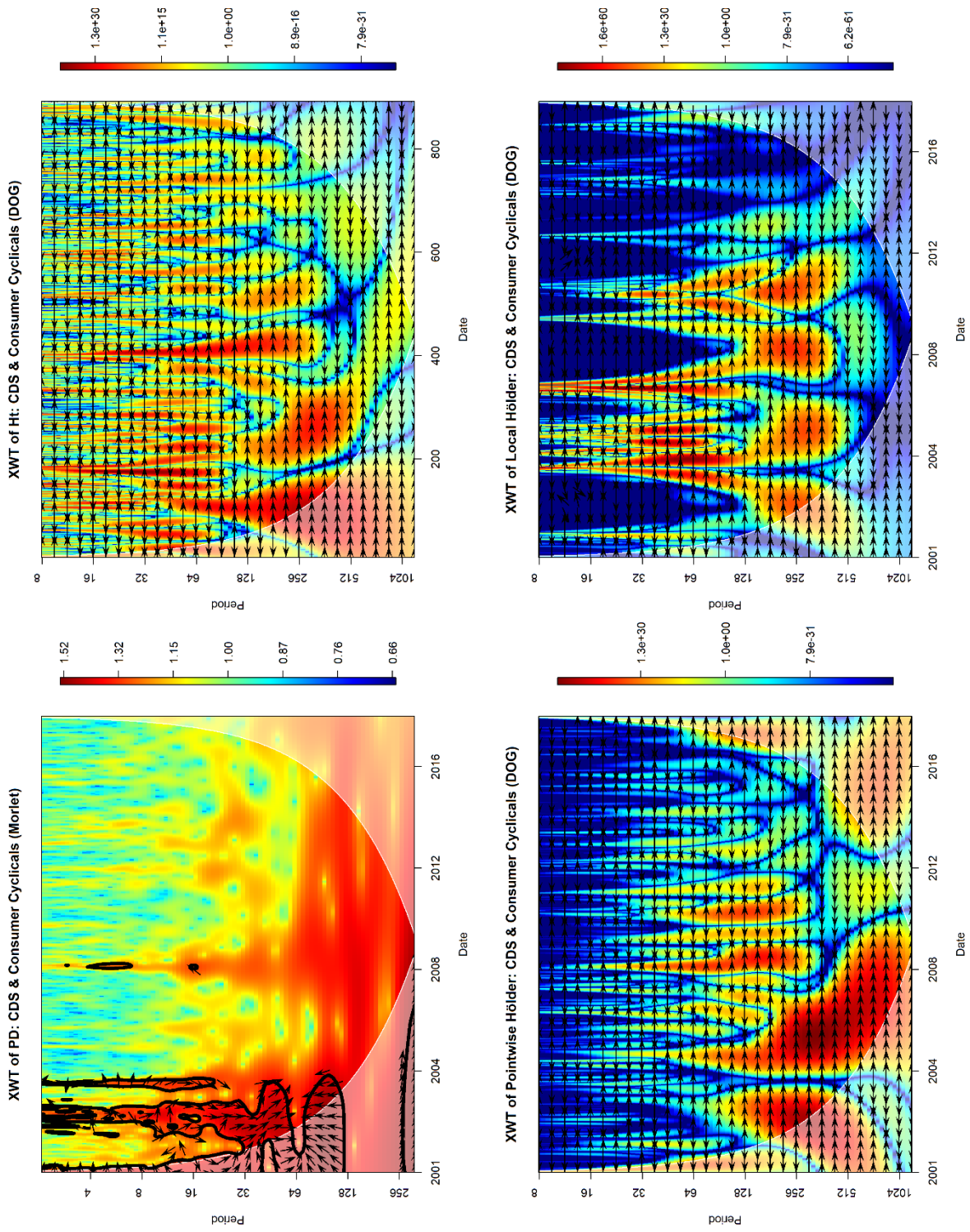
Fig. 2-26. (Continued)



(f) CWT: Utilities

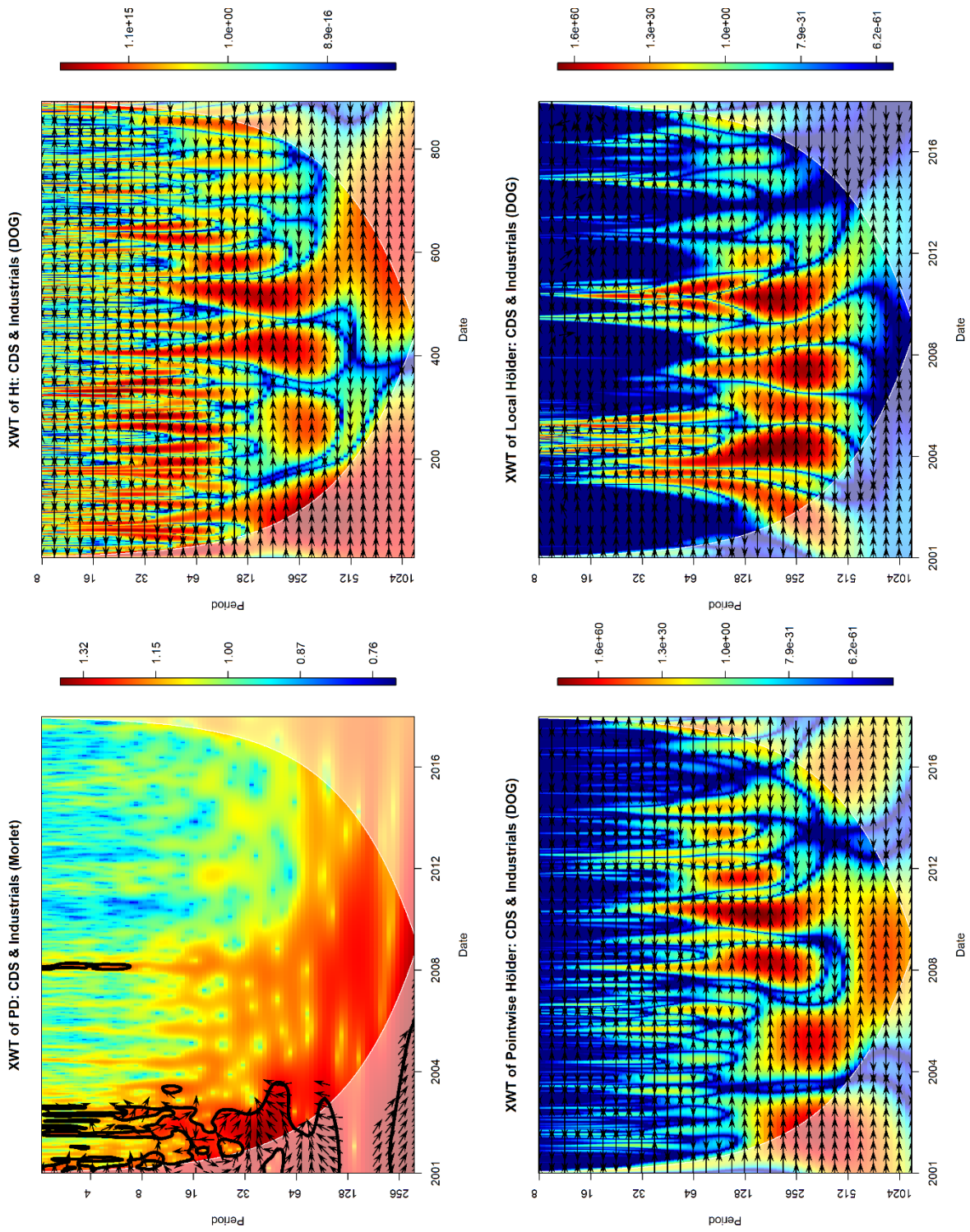
Fig. 2-26. (Continued)

2.7. The Cross-Wavelet Transforms



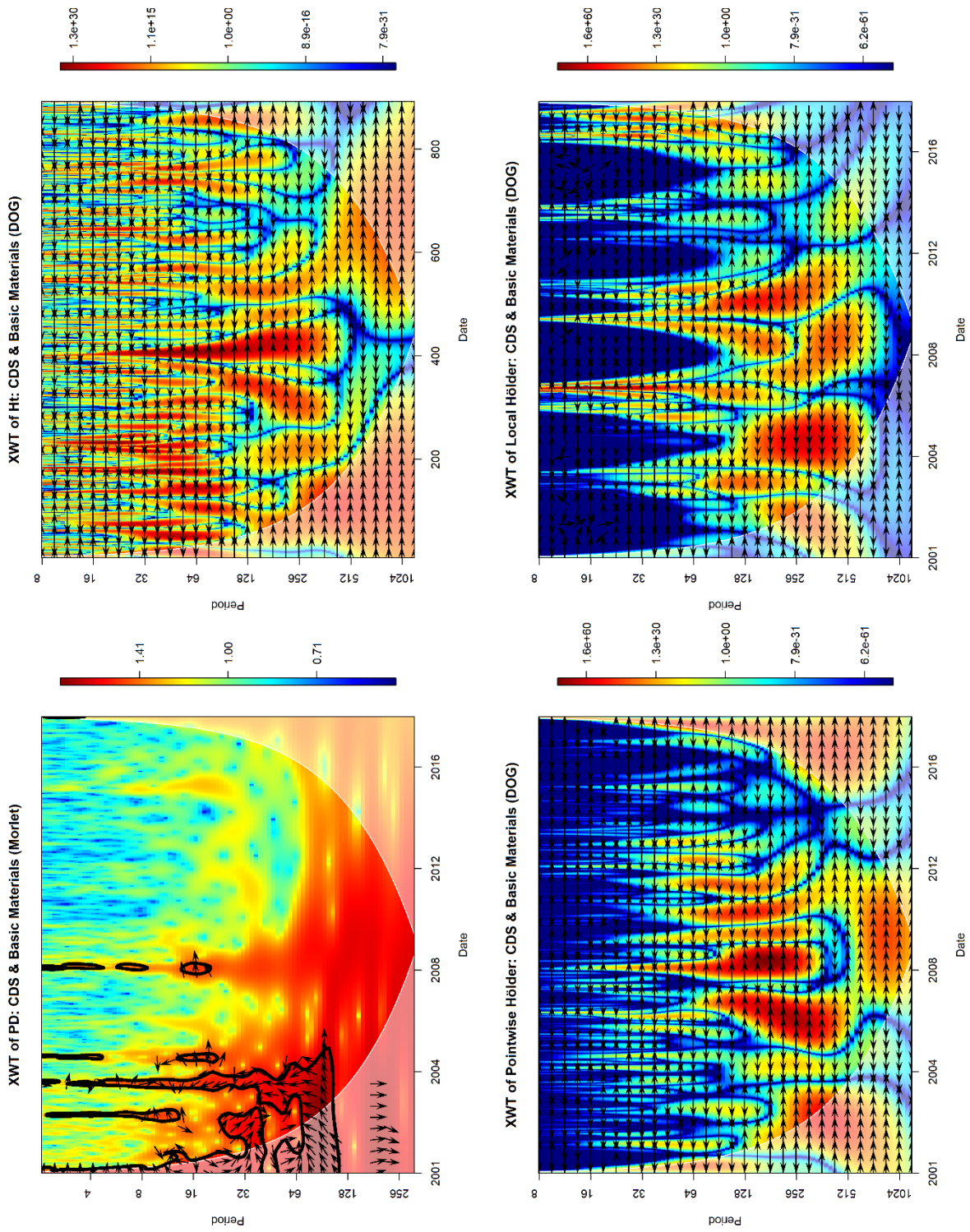
(a) XWT: CDS versus Consumer Cyclicals

Figure 2-27. The cross-wavelet transforms of all series.



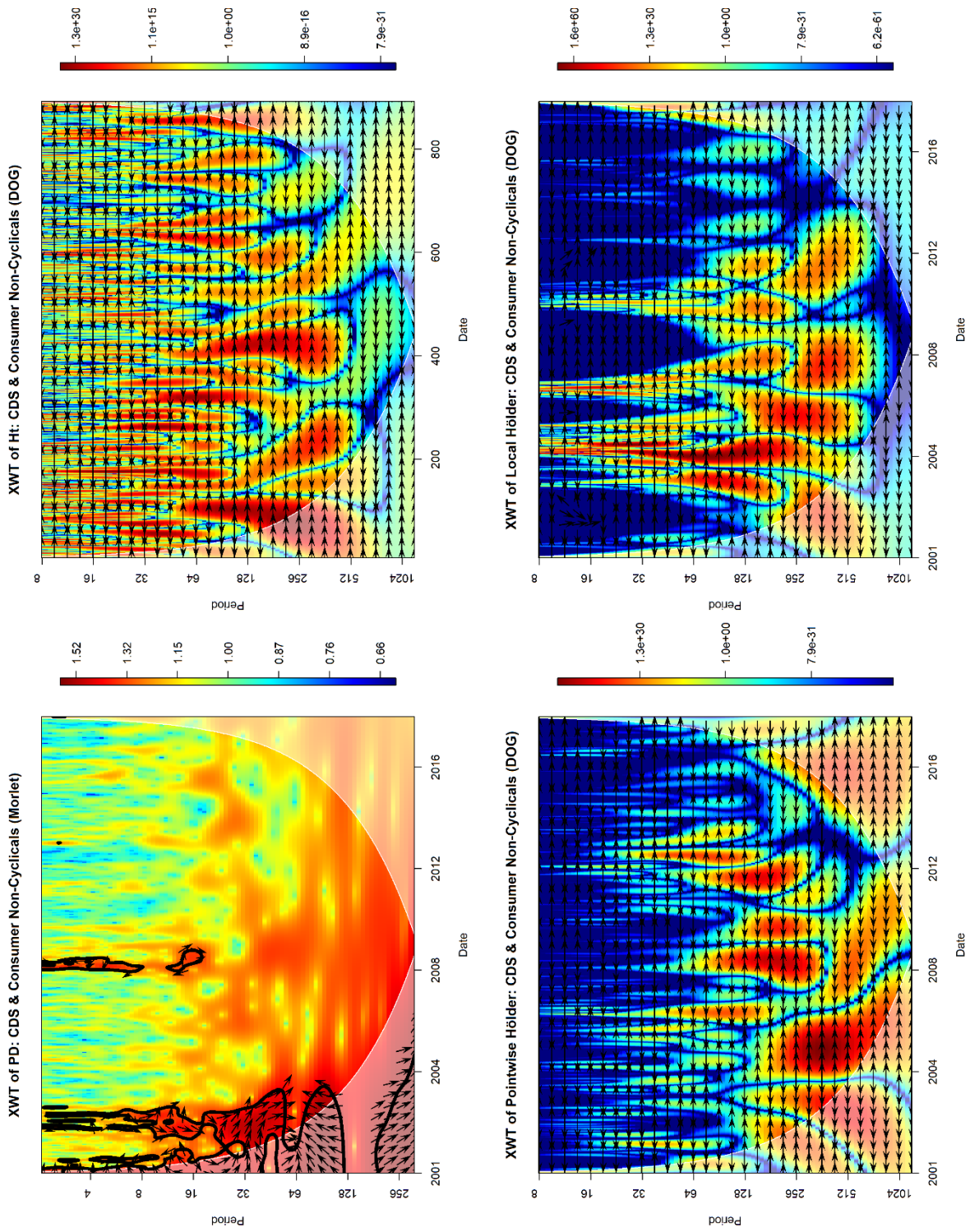
(b) XWT: CDS versus Industrials

Fig. 2-27. (Continued)



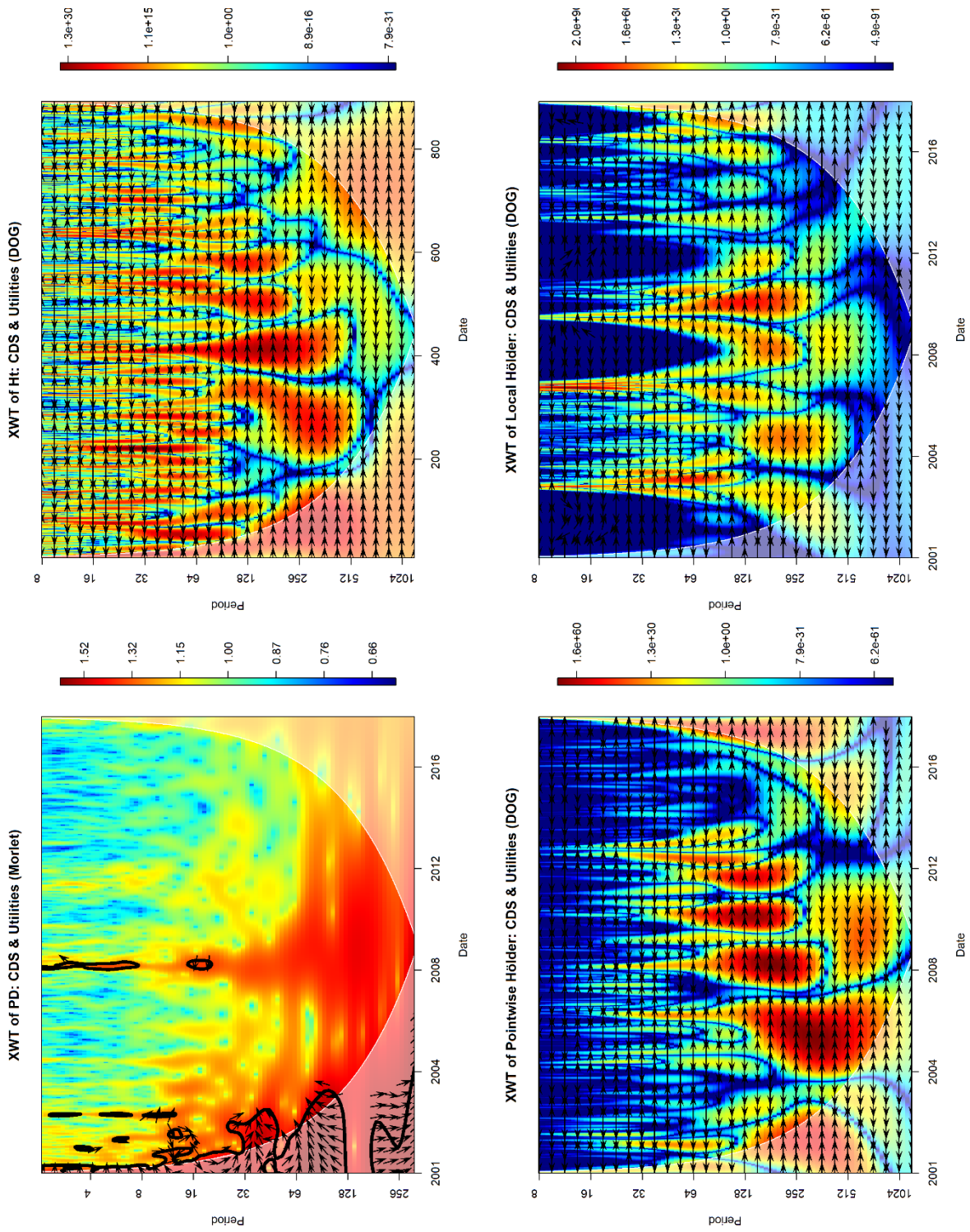
(c) XWT: CDS versus Basic Materials

Fig. 2-27. (Continued)



(d) XWT: CDS versus Consumer Non-Cyclicals

Fig. 2-27. (Continued)



(e) XWT: CDS versus Utilities

Fig. 2-27. (Continued)

3. Vector Wavelet Coherence for Multiple Time Series

Summary

This chapter introduces a new wavelet methodology to handle multivariate time series dynamic co-movements via extending multiple and quadruple wavelet coherence methodologies. The primary motivation of our works is to measure wavelet coherence analytically for the specific dimension. Thanks to the analytical solution, both smoothed complex wavelet coherence (C^d) and vector wavelet coherence (VR^2) can be calculated for any dimension. Two illustrative cases employ to explore the method. The first illustration designates that dynamic co-movement between VIX and stock indices over the period between January 2000 to November 2019. Vector wavelet coherence methodology is employed to examine the structure of dynamic relationships. Empirical results revealed that the relationships detected are not significant for most time-frequencies. The second application aims to approve existing multiple, quadruple, five, and six wavelet coherences. In order to validate, we generate synthetic sine curves and employ vector wavelet coherence for both multivariate ($y \sim x_1,x_2$), quadruple ($y \sim x_1,x_2,x_3$), five ($y \sim x_1,x_2,x_3,x_4$), and six ($y \sim x_1,x_2,x_3,x_4,x_5$) coherencies. The results of VMC only capture the relational frequencies and verify the existing methodologies.

3.1. Introduction

The wavelet analysis has progressively become a standard econophysics study for time-series analysis. Wavelet transforms can help us to enlarge time series into the time-frequency domain. Moreover, it can discover localized cyclic periodicities. There are two kinds of wavelet transforms; the continuous and its discrete equivalent. “The discrete wavelet transform is beneficial for noise reduction and data compression. On the other hand, the continuous one is more suitable for feature extraction.” [20]

In literature, many studies have proposed new techniques and tools for continuous wavelet analysis to feature extraction. For example, Torrence and Compo (1998) [19] provided a user-friendly toolkit for the wavelet transform. Maraun and Kurts (2004) [18] proposed a cross wavelet transform and developed a wavelet coherence (WTC). Wavelet coherence is an excellent method for considering the co-movement between two (or more)-time series. Contagion and spillover are also used in the literature in place of co-movement. Grinsted et al. (2004) [20] incorporated WTC into the package by adding to the toolkit of Torrence and Compo (1998). Mihanovic et al. (2009) [21] introduced two new techniques, which are partial wavelet coherence (PWC) and multiple wavelet coherence (MWC). Oygur and Unal (2017) [36] proposed quadruple wavelet coherence (QWC) and analyzed quadruplex structures in time series analysis. Eventually, in this study, we proposed the general explication for wavelet coherence. Thus, the WTC, MWC, and QWC have carried to the n-dimensional generalized form.

The chapter's content is structured as follows: Vector wavelet coherence (VWC) is proposed in Section 3.2. In Section 3.3, two separate applications are employed to demonstrate the proposed vector wavelet coherence. Conclusion and remarks are discussed in Section 3.4. Besides, we will provide links to the vector wavelet coherence R package and introduce core R functionality.

3.2. Methodology

3.2.1. Vector Wavelet Coherence

The squared n-dimensional vector wavelet coherency between series y and other series x_1, x_2, ..., x_n will be denoted by $VR^2_{y(x_1x_2,\dots,x_n)}$ (or $VR^2_{y(q)}$ and is given by the formula

$$VR^2_{y(q)} = VR^2_{1(23\dots n)} = 1 - \frac{M^d}{S_{11}M^d_{11}}, \tag{3-1}$$

where M ($n \times n$ Hermitian matrix) is the smoothed cross-wavelet spectra S_{ij} which is the smoothed version of W_{ij}

$$S_{ij} = S(W_{ij}), \tag{3-2}$$

where S is a certain smoothing operator.

$$M = \begin{bmatrix} S_{11} & S_{12} & S_{13} & \dots & S_{1n} \\ S_{21} & S_{22} & S_{23} & \dots & S_{2n} \\ S_{31} & S_{32} & S_{33} & \dots & S_{3n} \\ \dots & \dots & \dots & \dots & \dots \\ S_{n1} & S_{n2} & S_{n3} & \dots & S_{nn} \end{bmatrix}. \tag{3-3}$$

Remember, if the matrix M is a Hermitian matrix, we can express $M = M^*$, where $*$ is a conjugate transpose. Hence,

$$\begin{cases} \forall\, i \neq j, & SW_{ij} = SW^*_{ji} \\ \forall\, i, & SW_{ii} = S(|W_i|^2) \in \Re^+ \end{cases} \tag{3-4}$$

The cofactor of the (i, j) element in matrix M is named as:

$$M^d_{ij} = (-1)^{(i+j)}\det M^j_i, \tag{3-5}$$

where M^j_i shows the sub-matrix, which achieves from M via removing row i and column j. Additionally, $M^d = \det M$.

The matrix C represents the smoothed complex wavelet coherencies (ρ_{ij}) that are derived from the matrix M.

$$C = \begin{bmatrix} 1 & \rho_{12} & \rho_{13} & \dots & \rho_{1n} \\ \rho_{21} & 1 & \rho_{23} & \dots & \rho_{2n} \\ \rho_{31} & \rho_{32} & 1 & \dots & \rho_{3n} \\ \dots & \dots & \dots & \dots & \dots \\ \rho_{n1} & \rho_{n2} & \rho_{n3} & \dots & 1 \end{bmatrix}, \tag{3-6}$$

Note that $\rho_{jj} = \frac{S(W_{jj})}{\sqrt{S\left(|W_j|^2\right) S\left(|W_j|^2\right)}} = 1$ As M, the matrix C like the M matrix, reveals the Hermitian feature ($\rho_{ij} = \rho_{ji}^*$).

Then, we can define the n-dimensional vector coherence by the following formula:

$$VR_{1(q)}^2 = 1 - \frac{C^d}{C_{11}^d}. \tag{3-7}$$

3.3. Examples

In this chapter, two applications are employed to demonstrate the proposed vector wavelet coherence methodology's validity. In the first example, we examine the co-movements among the VIX and the stock indices and compare them with the wavelet correlation methodology ([53], [54]). The last example illustrates the multiple [22], quadruple [36], five [55], and six wavelet coherences with the data generated by the synthetic sine curves.

3.3.1. Co-movement of VIX and stock indices

This section demonstrates the vector wavelet coherence (VWC) practice with data from VIX and the nine stock indices by comparing vector wavelet coherence and wavelet multivariate global and local correlation toolbox [56]. Stock indices to be used for analysis are following: iBovespa (BVSP), Dow Jones Industrial Average (DJI), CAC 40 (FCHI), FTSE 100 (FTSE), S&P 500 (GSPC), Nasdaq Composite (IXIC), IPC Mexico (MXX), Nikkei 225 (N225), Russell 2000 (RUT). We used weekly data (closing prices) of analysis over the period from January 2000 to November 2019, consisting of 1035 observations. VIX and stock indices collect from the Bloomberg data services. All series transform into the continuously compounded (log-differences) returns. The continuously compounded returns calculate as

$R_t = 100 \times \ln(P_t/P_{t-1})$, where R_t is the return in percent, and P_t and P_{t-1} denote the closing price on time t and $t-1$, respectively.

Table 3-1. Stationarity tests

	ADF	PP	KPSS	PSR
BVSP	-10.22 [0.01]	-1216.71 [0.01]	0.076 [0.10]	95.098 [0.00]
DJI	-10.362 [0.01]	-1073.296 [0.01]	0.246 [0.10]	165.422 [0.00]
FCHI	-10.4 [0.01]	-1088.486 [0.01]	0.185 [0.10]	137.696 [0.00]
FTSE	-10.944 [0.01]	-1029.573 [0.01]	0.144 [0.10]	160.092 [0.00]
GSPC	-9.927 [0.01]	-1085.995 [0.01]	0.338 [0.10]	179.301 [0.00]
IXIC	-10.178 [0.01]	-1089.995 [0.01]	0.532 [0.10]	246.571 [0.00]
MXX	-10.419 [0.01]	-1099.012 [0.01]	0.239 [0.10]	186.468 [0.00]
N255	-9.579 [0.01]	-1056.013 [0.01]	0.295 [0.10]	66.737 [0.00]
RUT	-10.178 [0.01]	-1060.245 [0.01]	0.052 [0.10]	135.197 [0.00]
VIX	-12.318 [0.01]	-1095.87 [0.01]	0.013 [0.10]	69.536 [0.00]

Note. ADF denotes Augmented Dickey-Fuller, PP shows Phillips-Perron, and KPSS indicates Kwiatkowski–Phillips–Schmidt–Shin unit root tests. PSR shows Priestley-Subba Rao spectrum-based stationarity test. The test significance level is 95%, [.] indicates p-value.

Table 3-1 provides stationarity test results for VIX and stock indices. Unit root (ADF, PP, and KPSS) and spectrum-based (PSR) stationarity tests are employed. The results of the tests indicate that there is clear evidence to cannot reject stationarity. For this reason, a linear correlation can be meaningful. The paired correlation results of VIX against stock indices are examined in *Table 3-2*. Historical correlation results are statistically significant with respect to 99% confidence level even by parametric (Pearson) and non-parametric (Spearman, Kendall) models. Theoretically, stock indices and VIX index move in the opposite direction. As a natural consequence, all correlation results are negative. The highest correlation with VIX is the S&P 500 (GSPC) stock index. On the contrary, stock indices with the lowest linear correlation with VIX are iBovespa (Brazil), MXX (Mexico), and N225 (Japan).

Table 3-2. Correlation results of VIX against stock indices

	Pearson	Spearman	Kendall
BVSP	-0.436 [0.0000]	-0.438 [0.0000]	-0.302 [0.0000]
DJI	-0.692 [0.0000]	-0.717 [0.0000]	-0.529 [0.0000]
FCHI	-0.623 [0.0000]	-0.630 [0.0000]	-0.450 [0.0000]
FTSE	-0.617 [0.0000]	-0.619 [0.0000]	-0.442 [0.0000]
GSPC	-0.722 [0.0000]	-0.765 [0.0000]	-0.574 [0.0000]
IXIC	-0.638 [0.0000]	-0.698 [0.0000]	-0.507 [0.0000]
MXX	-0.519 [0.0000]	-0.532 [0.0000]	-0.371 [0.0000]
N255	-0.438 [0.0000]	-0.421 [0.0000]	-0.291 [0.0000]
RUT	-0.672 [0.0000]	-0.690 [0.0000]	-0.503 [0.0000]

Note. Pearson indicates Pearson's product-moment correlation, Kendall shows Kendall's rank correlation tau, and Spearman presents Spearman's rank correlation rho. [.] indicates p-value.

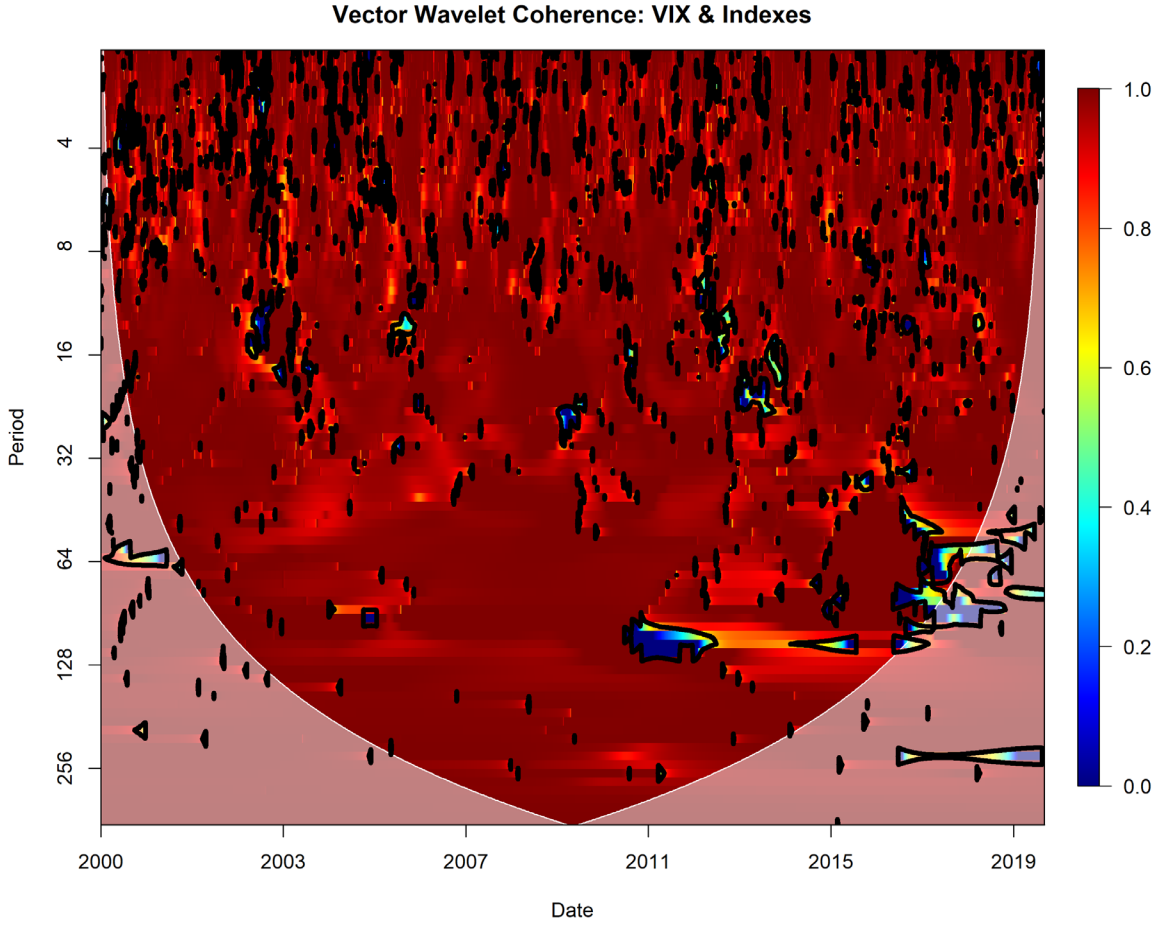


Figure 3-1. Vector wavelet coherence.

In order to discover the vector wavelet coherence, we take the Morlet wavelet of width to be 6. *Figure 3-1* presents the vector wavelet coherence results. VMC results show a high relationship between VIX and stock indices in almost all the time-frequency domains. However, the relationships detected are not significant for most time-frequency domains. Significant co-movement is observed, especially for high frequency after 2003, 2004, 2013, and 2015. For low frequency, there are weak connections in several regions after 2011.

3.3.2. Simulations

In this section, the vector wavelet coherence's accuracy has been tested on synthetically generated sine curves. Figure 3-2 represents the generated sine curves. The dependent variable defines in Eq. (3-10), and the variables x_1, x_2, x_3, x_4, and x_5 to be used as the explanatory variables given in Eqs. (3-11) to (3-15) have 4, 16, 64, 256, and 1024 frequency. We can define the synthetically generated sine curves by the following formulas:

$$y = \sin(2\pi t) + \sum_{i=1}^{5} \sin\left(\frac{\pi}{2^i} t\right) \tag{3-8}$$

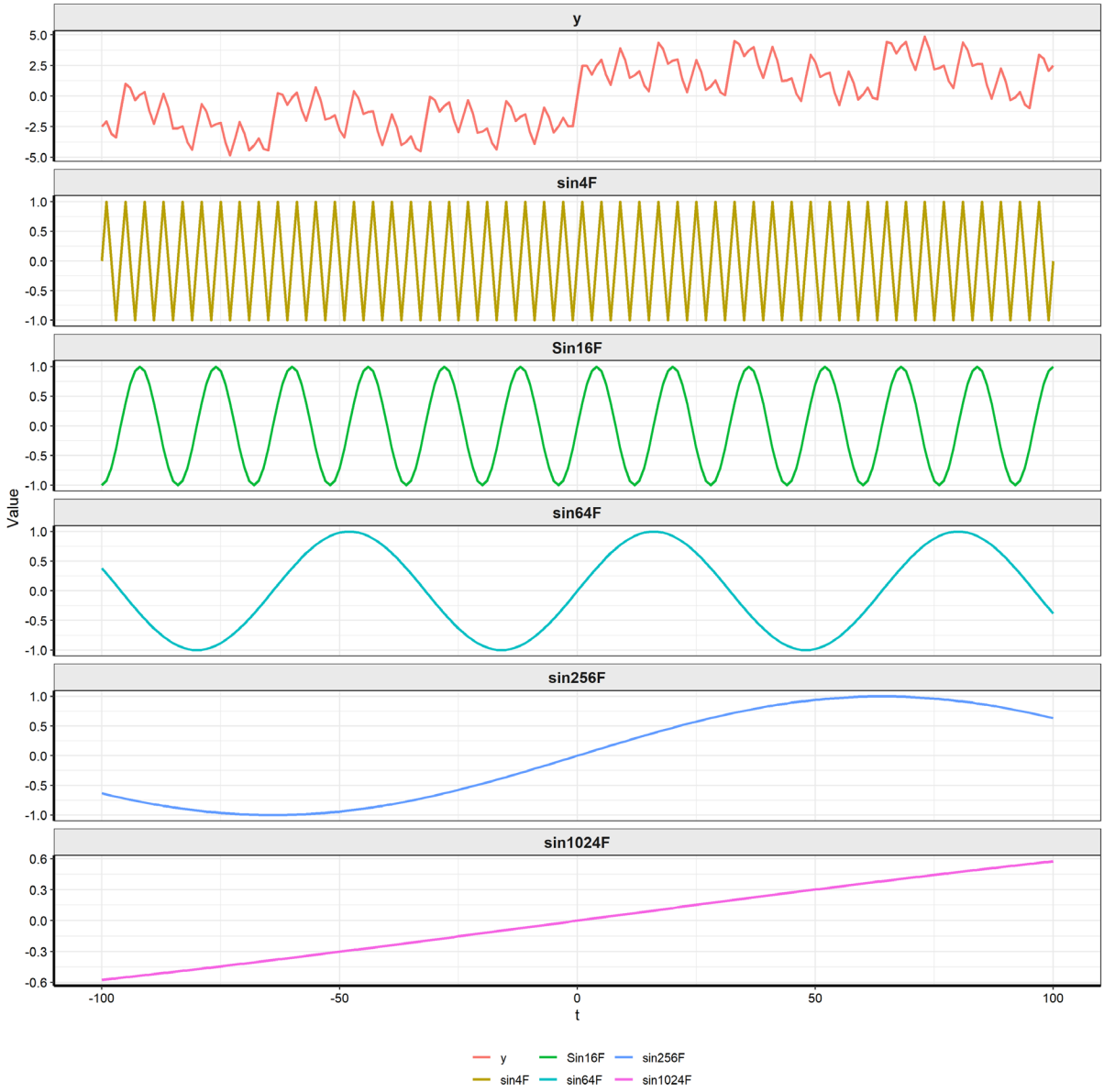
$$x_1 = \sin\left(\frac{\pi}{2} t\right) \tag{3-9}$$

$$x_2 = \sin\left(\frac{\pi}{8} t\right) \tag{3-10}$$

$$x_3 = \sin\left(\frac{\pi}{32} t\right) \tag{3-11}$$

$$x_4 = \sin\left(\frac{\pi}{512} t\right) \tag{3-12}$$

$$x_5 = \sin\left(\frac{\pi}{2028} t\right) \tag{3-13}$$



Note. y, x_1, x_2, x_3, x_4, and x_5 represent red, yellow, green, turquoise, blue, and purple curves, respectively.

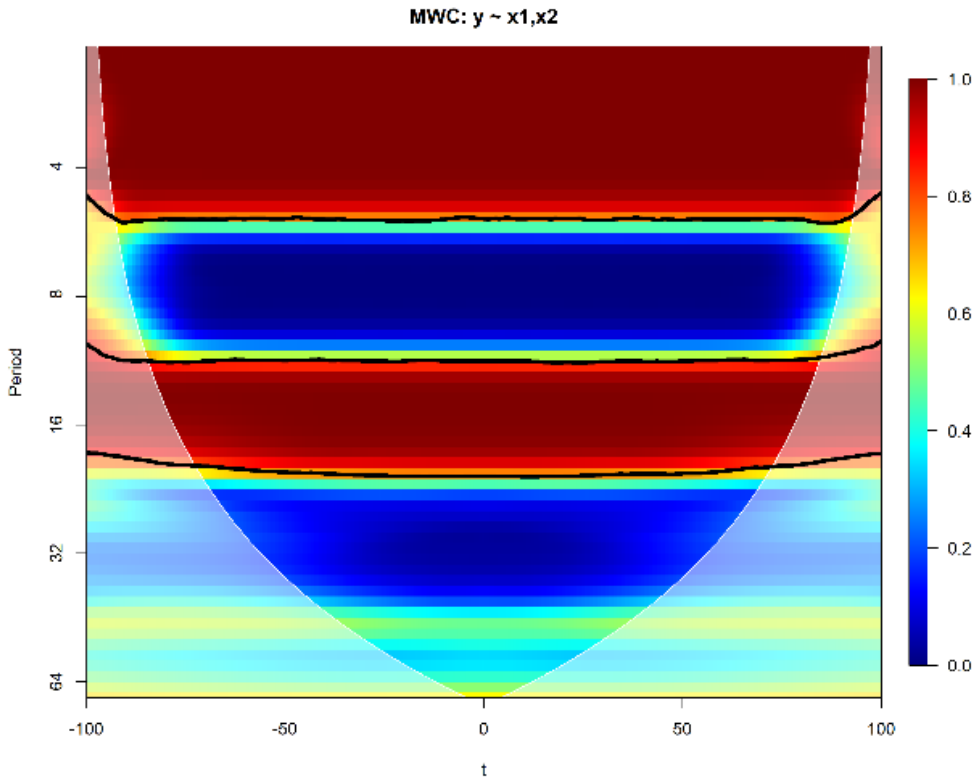
Figure 3-2. Simulations.

In *Figure 3-3*(a), the co-movements of the series y, x_1, and x_2 are examined by vector wavelet coherence. As expected, the relation between y and x_1 and x_2 curves is observed only in periods 4 and 16. It designates that the vector wavelet coherence results validate multiple wavelet coherence methodology.

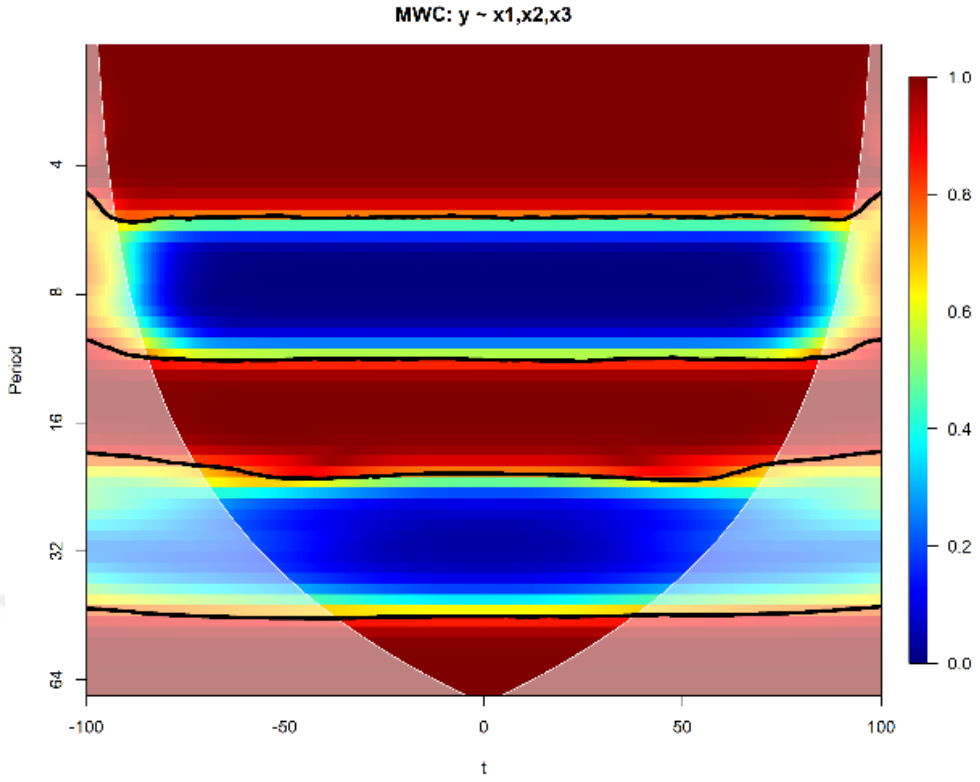
Figure 3-3(b) demonstrates quadruple wavelet coherence, which investigates the disclosure of y series by x_1, x_2, and x_3 series. The synthetic series (x_1, x_2, x_3) formed to have

a relationship with y series only in their periods. Duly, vector wavelet coherence only in the relevant periods (4, 16, and 64, respectively) has caught the relationship. Therefore, the generated synthetic sine curves verified the vector wavelet coherence results for both multiple wavelet coherence and quadruple wavelet coherence.

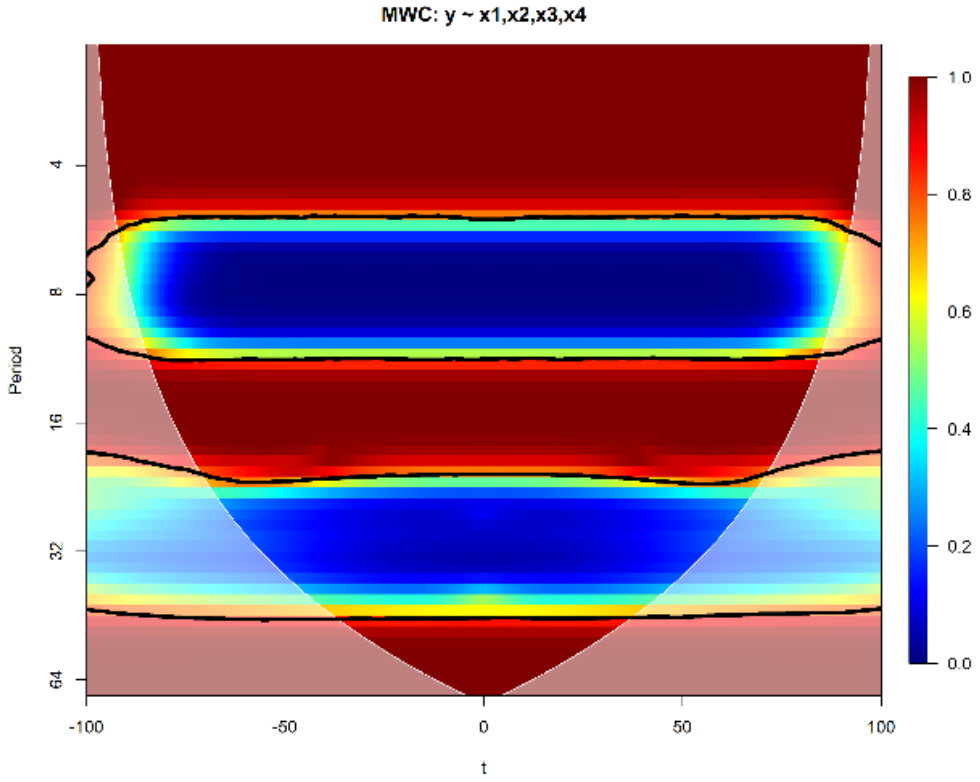
Figure 3-3 (c) and (d) indicate multiple wavelet coherence using five and six variables. The frequencies of x_1, x_2, x_3 sine curves include frequencies of x_4 and x_5 variables. Hence, the five and six multiple wavelet coherence results do not differ from the quadruple wavelet coherence results.



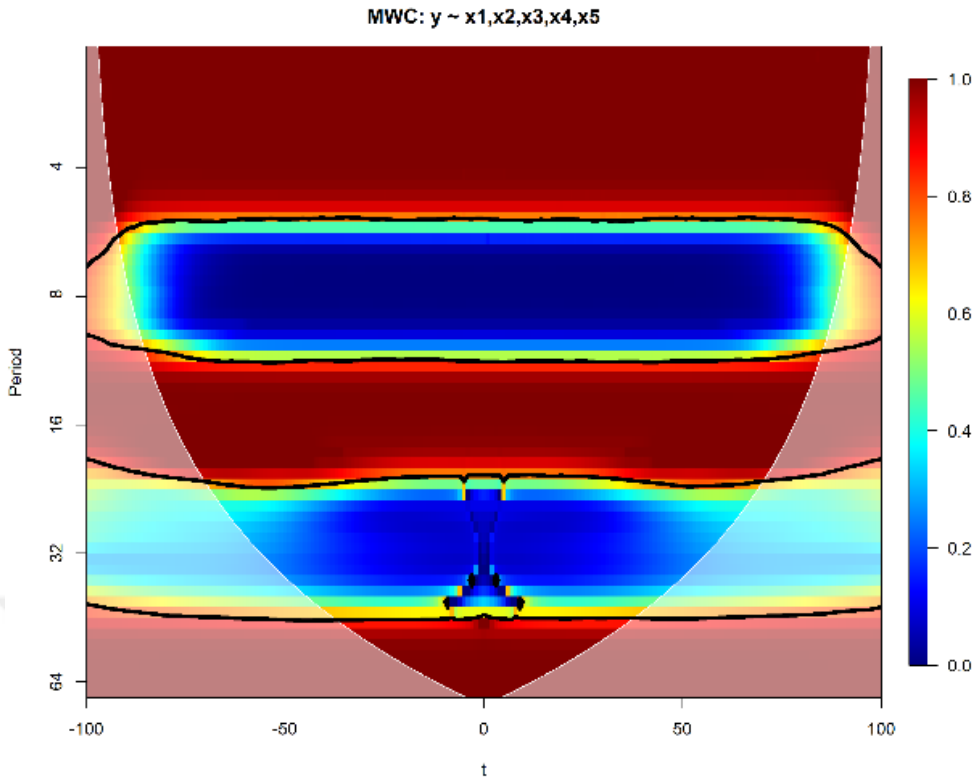
(a) $(y \sim x_1, x_2)$



(b) $(y \sim x_1, x_2, x_3)$



(c) $(y \sim x_1, x_2, x_3, x_4)$



(d) $(y \sim x_1, x_2, x_3, x_4, x_5)$

Figure 3-3. Multiple wavelet coherence.

3.4. Conclusion

This study suggests a new econophysics tool, the vector wavelet coherence, that may be useful in investigating dynamic co-movements of multivariate time series. The vector wavelet coherence is interpreted as the n-dimensional extension of multiple and quadruple wavelet coherences. Furthermore, in Section 3.3, we study two separate applications to illustrate the validity of the suggested VWC methodology. In the first example, we investigate the co-movement dynamics between VIX and stock indices. We design the synthetic sine curves to validate the second application's multiple wavelet coherence and quadruple wavelet coherence. We conclusively note that all these findings demonstrate this new tool's potential in the multivariate time series.

3.5. Supplemental material

Vectorwavelet [57] R computer packages facilities the computations of vector wavelet coherence.



vectorwavelet: Vector Wavelet Coherence for Multiple Time Series

New wavelet methodology (vector wavelet coherence) (Oygur, T., Unal, G, 2020 <doi:10.1007/s40435-020-00706-y>) to handle dynamic co-movements of multivariate time series via extending multiple and quadruple wavelet coherence methodologies. This package can be used to perform multiple wavelet coherence, quadruple wavelet coherence, and n-dimensional vector wavelet coherence analyses.

Version:	0.1.0
Depends:	biwavelet (≥ 0.20.19)
Imports:	iterators, spam, maps, fields, foreach, Rcpp
Suggests:	knitr, rmarkdown, devtools
Published:	2021-01-13
Author:	Tunc Oygur [aut, cre], Gazanfer Unal [aut], Tarik C. Gouhier [ctb], Aslak Grinsted [ctb], Viliam Simko [ctb]
Maintainer:	Tunc Oygur <info at tuncoygur.com.tr>
BugReports:	https://github.com/toygur/vectorwavelet/issues
License:	GPL-2 | GPL-3 [expanded from: GPL (≥ 2)]
URL:	https://github.com/toygur/vectorwavelet
NeedsCompilation:	no
CRAN checks:	vectorwavelet results

Downloads:

Reference manual:	vectorwavelet.pdf
Package source:	vectorwavelet_0.1.0.tar.gz
Windows binaries:	r-devel: vectorwavelet_0.1.0.zip, r-release: vectorwavelet_0.1.0.zip, r-oldrel: vectorwavelet_0.1.0.zip
macOS binaries:	r-release: vectorwavelet_0.1.0.tgz, r-oldrel: vectorwavelet_0.1.0.tgz

Linking:

Please use the canonical form https://CRAN.R-project.org/package=vectorwavelet to link to this page.

Figure 3-4. vectorwavelet R package.[5]

[5] "They can be obtained from The Comprehensive R Archive Network (CRAN) at https://cran.r-project.org/package=vectorwavelet."

4. References

[1] C. M. Reinhart and K. S. Rogoff, This time is different: eight centuries of financial folly, princeton university press, 2009.

[2] G. Katechos, "On the relationship between exchange rates and equity returns: A new approach," *Journal of International Financial Markets, Institutions and Money,* vol. 21, p. 550–559, 2011.

[3] C.-H. Lin, "The comovement between exchange rates and stock prices in the Asian emerging markets," *International Review of Economics & Finance,* vol. 22, p. 161–172, 2012.

[4] I.-C. Tsai, "The relationship between stock price index and exchange rate in Asian markets: A quantile regression approach," *Journal of International Financial Markets, Institutions and Money,* vol. 22, p. 609–621, 2012.

[5] C. Walid, A. Chaker, O. Masood and J. Fry, "Stock market volatility and exchange rates in emerging countries: A Markov-state switching approach," *Emerging Markets Review,* vol. 12, p. 272–292, 2011.

[6] P. F. Diamandis and A. A. Drakos, "Financial liberalization, exchange rates and stock prices: Exogenous shocks in four Latin America countries," *Journal of Policy Modeling,* vol. 33, p. 381–394, 2011.

[7] G. C. Nath and G. P. Samanta, "Relationship between Exchange Rate and Stock Prices in India-An Empirical Analysis," *Available at SSRN 475823,* 2003.

[8] K. Phylaktis and F. Ravazzolo, "Stock prices and exchange rate dynamics," *Journal of International Money and Finance,* vol. 24, p. 1031–1053, 2005.

[9] H. Zhao, "Dynamic relationship between exchange rate and stock price: Evidence from China," *Research in International Business and Finance,* vol. 24, p. 103–112, 2010.

[10] I. Choi and D. Park, "Causal relation between interest and exchange rates in the Asian currency crisis," *Japan and the World Economy,* vol. 20, p. 435–452, 2008.

[11] M. A. Ahmad, R. U. Ahmad and A. R. Rehman, "Do interest rate, exchange rates effect stock returns?," *A Pakistani Perspective, International Research Journal of Finance and Economics,* vol. 50, p. 146–150, 2010.

[12] M. Pirovano, "Monetary policy and stock prices in small open economies: Empirical evidence for the new EU member states," *Economic Systems,* vol. 36, p. 372–390, 2012.

[13] C. Ioannidis and A. Kontonikas, "The impact of monetary policy on stock prices," *Journal of Policy Modeling,* vol. 30, p. 33–53, 2008.

[14] Andries, Alin Marius; Ihnatov, Iulian; Tiwari, Aviral Kumar, "Analyzing time–frequency relationship between interest rate, stock price and exchange rate through continuous wavelet," *Economic Modelling,* vol. 41, p. 227–238, 2014.

[15] J. P. Gupta, A. Chevalier, F. Sayekt and others, "The Causality between interest rate, exchange rate and stock price in emerging markets: The case of the Jakarta Stock Exchange," *Fuzzy Sets in Management, Economics, and Marketing,* p. 145, 2001.

[16] M. E. Hamrita and A. Trifi, "The relationship between interest rate, exchange rate and stock price: A wavelet analysis," *International Journal of Economics and Financial Issues,* vol. 1, p. 220, 2011.

[17] H. M. K. Mok, "Causality of interest rate, exchange rate and stock prices at stock market open and close in Hong Kong," *Asia Pacific Journal of Management,* vol. 10, p. 123–143, 1993.

[18] D. Maraun and J. Kurths, "Cross wavelet analysis: significance testing and pitfalls," *Nonlinear Processes in Geophysics,* vol. 11, p. 505–514, 2004.

[19] Torrence, Christopher; Compo, Gilbert P., "A practical guide to wavelet analysis," *Bulletin of the American Meteorological society,* vol. 79, p. 61–78, 1998.

[20] A. Grinsted, J. C. Moore and S. Jevrejeva, "Application of the cross wavelet transform and wavelet coherence to geophysical time series," *Nonlinear processes in geophysics,* vol. 11, p. 561–566, 2004.

[21] H. Mihanović, M. Orlić and Z. Pasarić, "Diurnal thermocline oscillations driven by tidal flow around an island in the Middle Adriatic," *Journal of Marine Systems,* vol. 78, p. S157–S168, 2009.

[22] E. K. W. Ng and J. C. L. Chan, "Geophysical applications of partial wavelet coherence and multiple wavelet coherence," *Journal of Atmospheric and Oceanic Technology,* vol. 29, p. 1845–1853, 2012.

[23] Aguiar-Conraria, Luís; Soares, Maria Joana, "Oil and the macroeconomy: using wavelets to analyze old issues," *Empirical Economics,* vol. 40, p. 645–655, 2011.

[24] L. Aguiar-Conraria, N. Azevedo and M. J. Soares, "Using wavelets to decompose the time–frequency effects of monetary policy," *Physica A: Statistical mechanics and its Applications,* vol. 387, p. 2863–2878, 2008.

[25] C. Torrence and P. J. Webster, "Interdecadal changes in the ENSO-monsoon system," *Journal of Climate,* vol. 12, p. 2679–2690, 1999.

[26] R. S. Tsay, Multivariate time series analysis: with R and financial applications, John Wiley & Sons, 2013.

[27] H. Lütkepohl and D. S. Poskitt, "Specification of echelon-form VARMA models," *Journal of Business & Economic Statistics,* vol. 14, p. 69–79, 1996.

[28] M. Simionescu, "The accuracy assessment of macroeconomic forecasts based on econometric models for Romania," *Procedia Economics and Finance,* vol. 8, p. 671–677, 2014.

[29] E. Kahraman and G. Ünal, "Multiple Wavelet Coherency Analysis and Forecasting of Metal Prices," *arXiv preprint arXiv:1602.01960,* 2016.

[30] M. Gülerce and G. Ünal, "Using wavelet analysis to uncover the co-movement behavior of multiple energy commodity prices," *International Journal of Wavelets, Multiresolution and Information Processing,* vol. 14, p. 1650047, 2016.

[31] Asandului, Mircea; Lupu, Dan; Claudiu, Gabriel; Musetescu, Radu, "DYNAMIC RELATIONS BETWEEN CDS AND STOCK MARKETS IN EASTERN EUROPEAN COUNTRIES.," *Economic Computation & Economic Cybernetics Studies & Research,* vol. 49, p. 151–170, 2015.

[32] B. B. Mandelbrot, "The variation of certain speculative prices," in *Fractals and scaling in finance*, Springer, 1997, p. 371–418.

[33] Peters, Edgar E.; Peters, Donada, Fractal market analysis: applying chaos theory to investment and economics, vol. 24, John Wiley & Sons, 1994.

[34] Tang, Junjun; Wang, Jing; Huang, Cheng; Wang, Guolun; Wang, Xiong, "Subprime mortgage crisis detection in US foreign exchange rate market by multifractal analysis," in *Young Computer Scientists, 2008. ICYCS 2008. The 9th International Conference for*, 2008.

[35] Kuperin, Yu A.; Schastlivtsev, R. R., "Multifractal Analysis and Local Hoelder Exponents Approach to Detecting Stock Markets Crashes," 2008.

[36] Oygur, Tunc; Unal, Gazanfer, "Evidence of Large Fluctuations of Stock Return and Financial Crises from Turkey: Using Wavelet Coherency and Varma Modeling to Forecast Stock Return," *Fluctuation and Noise Letters,* vol. 16, p. 1750020, 2017.

[37] Bharath, Sreedhar T.; Shumway, Tyler, "Forecasting default with the KMV-Merton model," *This article is available in SSRN,* 2004.

[38] Kantelhardt, Jan W.; Zschiegner, Stephan A.; Koscielny-Bunde, Eva; Havlin, Shlomo; Bunde, Armin; Stanley, H. Eugene, "Multifractal detrended fluctuation analysis of nonstationary time series," *Physica A: Statistical Mechanics and its Applications,* vol. 316, p. 87–114, 2002.

[39] Zhou, Wei-Xing, "Multifractal detrended cross-correlation analysis for two nonstationary signals," *Phys. Rev. E,* vol. 77, no. 6, p. 066211, 6 2008.

[40] Jiang, Zhi-Qiang; Zhou, Wei-Xing, "Multifractal detrending moving-average cross-correlation analysis," *Phys. Rev. E,* vol. 84, no. 1, p. 016106, 7 2011.

[41] Arianos, Sergio; Carbone, Anna, "Detrending moving average algorithm: A closed-form approximation of the scaling law," *Physica A: Statistical Mechanics and its Applications,* vol. 382, pp. 9-15, 2007.

[42] Abry, Patrice; Goncalves, Paolo; Véhel, Jacques Lévy, Scaling, fractals and wavelets, John Wiley & Sons, 2013.

[43] Podobnik, Boris; Grosse, Ivo; Horvatić, Davor; Ilic, S.; Ivanov, P. Ch; Stanley, H. Eugene, "Quantifying cross-correlations using local and global detrending approaches," *The European Physical Journal B,* vol. 71, p. 243, 2009.

[44] E. A. F. Ihlen, "Introduction to multifractal detrended fluctuation analysis in Matlab," *Frontiers in physiology,* vol. 3, p. 141, 2012.

[45] Matia, Kaushik; Ashkenazy, Yosef; Stanley, H. Eugene, "Multifractal properties of price fluctuations of stocks and commodities," *EPL (Europhysics Letters),* vol. 61, p. 422, 2003.

[46] Cumhur, T. A. Ş.; Ünal, Gazanfer, "MULTIFRACTAL BEHAVIOUR IN NATURAL GAS PRICES BY USING MF-DFA AND WTMM METHODS," *International Journal of Economics and Finance Studies,* vol. 5, p. 44–55, 2013.

[47] Wang, Yudong; Wei, Yu; Wu, Chongfeng, "Cross-correlations between Chinese A-share and B-share markets," *Physica A: Statistical Mechanics and its Applications,* vol. 389, pp. 5468-5478, 2010.

[48] W. Zhang, P. Wang, X. Li and D. Shen, "Quantifying the cross-correlations between online searches and Bitcoin market," *Physica A: Statistical Mechanics and its Applications,* vol. 509, pp. 657-672, 2018.

[49] Y. A. Kuperin and M. M. Morozova, "Statistical and Multifractal Properties of the Time Series Generated by a Modified Minority Game," 2010.

[50] J. L. Véhel and P. Legrand, "Signal and Image processing with FracLab," in *Thinking in Patterns*, World Scientific, 2004, p. 321–322.

[51] Chung, Ching-Fan, "Calculating and analyzing impulse responses for the vector ARFIMA model," *Economics Letters,* vol. 71, p. 17–25, 2001.

[52] Hansen, Peter R.; Lunde, Asger; Nason, James M., "The Model Confidence Set," *Econometrica,* vol. 79, pp. 453-497, 2011.

[53] Fernández-Macho, Javier, "Wavelet multiple correlation and cross-correlation: A multiscale analysis of Eurozone stock markets," *Physica A: Statistical Mechanics and its Applications,* vol. 391, p. 1097–1104, 2012.

[54] Fernández-Macho, Javier, "Time-localized wavelet multiple regression and correlation," *Physica A: Statistical Mechanics and its Applications,* vol. 492, p. 1226–1238, 2018.

[55] Gülerce, Mustafa; Ünal, Gazanfer, "Electricity price forecasting using multiple wavelet coherence method: Comparison of ARMA versus VARMA," *International Journal of Financial Engineering,* vol. 5, p. 1850004, 2018.

[56] Fernández-Macho, Javier, "wavemulcor: Wavelet Routines for Global and Local Multiple Correlation," *R package,* 2018.

[57] Oygur, Tunc; Unal, Gazanfer, "Traces of the Multifractal Nature of the Financial Crises in Turkey: Co-Movement of the Hölder Exponents and Large-Scale Forecast," *Fluctuation and Noise Letters,* p. 2050029, 2020.

5. Appendix A: R programming codes for VWC

```
#' Compute n-dimensional vector wavelet coherence
#'
#' @param y time series y in matrix format (\code{m} rows x 2 columns).
#'   The first column should contain the time steps, and the second
#'   column should contain the values.
#' @param x multivariate time series x in a matrix format
#'   (\code{m} rows x n columns). The first column should
#'   contains the time steps, and the other  columns should
#'   contains the values.
#' @param pad pad the values will change with zeros to increase the speed
#'   of the transform. Default is TRUE.
#' @param dj spacing between successive scales. Default is 1/12.
#' @param s0 smallest scale of the wavelet. Default is \code{2*dt}.
#' @param J1 number of scales - 1.
#' @param max.scale maximum scale. Computed automatically
#'   if left unspecified.
#' @param mother type of mother wavelet function to use. Can be set to
#'   \code{morlet}, \code{dog}, or \code{paul}. Default is \code{morlet}.
#'   Significance testing is only available for \code{morlet} wavelet.
#' @param param nondimensional parameter specific to the wavelet function.
#' @param lag1 vector containing the AR(1) coefficient of each time series.
#' @param sig.level significance level. Default is \code{0.95}.
#' @param sig.test type of significance test. If set to 0, use a regular
#'   \eqn{\chi^2} test. If set to 1, then perform a time-average test.
#'   If set to 2, then do a scale-average test.
#' @param nrands number of Monte Carlo randomizations. Default is 300.
#' @param quiet Do not display a progress bar. Default is \code{FALSE}
#'
#' @return Return a \code{vectorwavelet} object containing:
#' \item{coi}{matrix containg cone of influence}
#' \item{rsq}{matrix of wavelet coherence}
#' \item{phase}{matrix of phases}
#' \item{period}{vector of periods}
#' \item{scale}{vector of scales}
#' \item{dt}{length of a time step}
#' \item{t}{vector of times}
#' \item{xaxis}{vector of values used to plot xaxis}
#' \item{s0}{smallest scale of the wavelet }
#' \item{dj}{spacing between successive scales}
#' \item{mother}{mother wavelet used}
#' \item{type}{type of \code{vectorwavelet} object created (\code{vwc})}
#' \item{signif}{matrix containg \code{sig.level} percentiles of wavelet
coherence based on the Monte Carlo AR(1) time series}
#'
vwc <- function (y, x, pad = TRUE, dj = 1/12, s0 = 2 * dt, J1 = NULL,
                 max.scale = NULL, mother = "morlet", param = -1,
                         lag1 = NULL, sig.level = 0.95, sig.test = 0,
                         nrands = 300, quiet = FALSE) {

  mother <- match.arg(tolower(mother), c("morlet", "paul", "dog"))

  # Check data format ########
  checked <- n.check.data(y = y, x = x)
  xaxis <- y[, 1]
  dt <- checked$y$dt

  t <- checked$y$t
  n <- checked$y$n.obs
```

```
  if (is.null(J1)) {
    if (is.null(max.scale)) {
      max.scale <- (n * 0.17) * 2 * dt
    }
    J1 <- round(log2(max.scale/s0)/dj)
  }

  # Get AR(1) coefficients ########
  if (is.null(lag1)) {
    y.ar1 <- ar1nv(y[, 2])$g
    x.ar1 <- as.numeric(apply(x[,-1], 2, function(x) {ar1nv(x)$g }))

    lag1 <- c(y.ar1, x.ar1)
  }

  # Standard deviation ########
  y.sigma <- sd(y[, 2], na.rm = TRUE)
  x.sigma <- sd(x[, 2], na.rm = TRUE)

  df <- cbind(y,x[,-1])
  colnames(df) <- c("t","y",paste0("x",1:(ncol(x)-1)))

  n_dim <- ncol(df)-1

  # Get CWT of each time series ########
  wt.res <- list()
  for(i in 2:ncol(df)) {
    xi <- df[,c(1,i)]
    temp.col <- colnames(df)[i]
    wt.res[[temp.col]] <- wt(d = xi,pad = pad, dj = dj, s0 = s0,
                                          J1 = J1, max.scale = max.scale,
                                          mother = mother, param = param,
                                          sig.level = sig.level,
                                          sig.test = sig.test,
                                          lag1 = lag1[i-1])
    rm(xi);rm(temp.col)
  }
  rm(i)

  s.inv <- 1/t(wt.res[["y"]]$scale)
  s.inv <- matrix(rep(s.inv, n), nrow = NROW(wt.res[["y"]]$wave))

  s.wt.res <- list()
  for(i in 2:ncol(df)) {
    temp.col <- colnames(df)[i]
      temp.wt.res <- wt.res[[temp.col]]$wave
    s.wt.res[[temp.col]] <- smooth.wavelet(s.inv*(abs(temp.wt.res)^2),
                                                                dt,
                                                                dj,

wt.res[[temp.col]]$scale)
    rm(temp.col, temp.wt.res)
  }
  rm(i)

  coi.res <- matrix(NA, nrow = n, ncol = (ncol(df)-1))
  for(i in 2:ncol(df)) {
    temp.col <- colnames(df)[i]
    coi.res[,(i-1)] <- wt.res[[temp.col]]$coi
    rm(temp.col)
  }
```

```
  rm(i)
  coi <- apply(coi.res, 1, function(x) min(x, na.rm = T))
  rm(coi.res)

  # Cross-wavelet computation ########
  cw <- list()
  smooth.cw <- list()
  rsq <- list()
  r <- list()
  for(i in 2:(ncol(df)-1)){
    for(j in (i+1):ncol(df)){
      temp.col.i <- colnames(df)[i]
      temp.col.j <- colnames(df)[j]
      temp.cw <- wt.res[[temp.col.i]]$wave *
                              Conj(wt.res[[temp.col.j]]$wave)
      temp.smooth.cw <- smooth.wavelet(s.inv*(temp.cw), dt, dj,
wt.res[["y"]]$scale)
      temp.rsq <- abs(temp.smooth.cw)^2/
                              (s.wt.res[[temp.col.i]] *
s.wt.res[[temp.col.j]])
      temp.r <- sqrt(temp.rsq)

      cw[[paste0(temp.col.i,"-",temp.col.j)]] <- temp.cw
      smooth.cw[[paste0(temp.col.i,"-",temp.col.j)]] <- temp.smooth.cw
      rsq[[paste0(temp.col.i,"-",temp.col.j)]] <- temp.rsq
      r[[paste0(temp.col.i,"-",temp.col.j)]] <- temp.r

      rm(temp.col.i);rm(temp.col.j);rm(temp.cw);
        rm(temp.smooth.cw);rm(temp.rsq);rm(temp.r)
    }
    rm(j)
  }
  rm(i)

  # Wavelet coherence ########
  r_tilde <- list()
  for(i in 1:(ncol(df)-1)) {
    for(j in 1:(ncol(df)-1)) {
      temp.col.i <- colnames(df)[i+1]
      temp.col.j <- colnames(df)[j+1]
      if(i==j) {
        r_tilde[[paste0(temp.col.i,"-",temp.col.j)]] <- 1
      } else if (j > i) {
        r_tilde[[paste0(temp.col.i,"-",temp.col.j)]] <-
r[[paste0(temp.col.i,"-",temp.col.j)]]
      } else {
        r_tilde[[paste0(temp.col.i,"-",temp.col.j)]] <-
Conj(r[[paste0(temp.col.j,"-",temp.col.i)]])
      }
    }
    rm(j)
  }
  rm(i)

  ##Cofactor function ########
  cofactor.wavelogy <- function(ii, jj, del_ii, del_jj, level, n_dim,order)
{

    order.sign <- if(order %% 2 == 1) 1 else -1
    temp.col.i <- colnames(df)[ii+1]
    temp.col.j <- colnames(df)[jj+1]
```

```
    res <- order.sign * r_tilde[[paste0(temp.col.i,"-",temp.col.j)]]

    ii_vec <- setdiff(c(1:n_dim),del_ii)
    jj_vec <- setdiff(c(1:n_dim),del_jj)

    if(n_dim-level != 2) {

      temp.res <- 0
      for(kk in 1:(n_dim-level)) {
        temp.res <- temp.res + cofactor.wavelogy(ii=min(ii_vec),

jj=jj_vec[kk],

del_ii=c(del_ii,min(ii_vec)),

del_jj=c(del_jj,jj_vec[kk]),

level=level+1,

n_dim, order=kk)
      }
      res <- res * temp.res
    } else {

      temp.col.i_1 <-  colnames(df)[ii_vec[1]+1]
      temp.col.j_1 <-  colnames(df)[jj_vec[1]+1]

      temp.col.i_2 <-  colnames(df)[ii_vec[2]+1]
      temp.col.j_2 <-  colnames(df)[jj_vec[2]+1]

      res <- res * (r_tilde[[paste0(temp.col.i_1,"-",temp.col.j_1)]]*
                                    r_tilde[[paste0(temp.col.i_2,"-
",temp.col.j_2)]] -
                                r_tilde[[paste0(temp.col.i_2,"-
",temp.col.j_1)]]*
                                    r_tilde[[paste0(temp.col.i_1,"-
",temp.col.j_2)]])
    }
    return(res)
  }

  ##Cxx ########
  Cxx <- 0
  for(k in 1:n_dim) {
    Cxx <- Cxx + cofactor.wavelogy(ii=1, jj=k, del_ii=1,
                                                  del_jj=k, level=1, n_dim,
order=k)
  }

  C11 <- cofactor.wavelogy(ii=1, jj=1, del_ii=1,
                                    del_jj=1, level=1, n_dim, order=1)

  ##Rsq ########
  rsq <- 1 - (Cxx / C11)

  # Phase difference ########
  phase <- atan2(Im(cw[["y-x1"]]), Re(cw[["y-x1"]]))

  if (nrands > 0) {
    signif <- wtc.sig(nrands = nrands, lag1 = c(y.ar1, x.ar1),
```

```
                      dt = dt, n, pad = pad, dj = dj, J1 = J1, s0 = s0,
                      max.scale = max.scale, mother = mother, sig.level =
sig.level,
                      quiet = quiet)
  }
  else {
    signif <- NA
  }

  results <- list(coi = coi,
                  rsq = rsq,
                  phase = phase,
                  period = wt.res[["y"]]$period,
                  scale = wt.res[["y"]]$scale,
                  dt = dt,
                  t = t,
                  xaxis = xaxis,
                  s0 = s0,
                  dj = dj,
                  mother = mother,
                  type = "vwc",
                  signif = signif)

  class(results) <- "vectorwavelet"
  return(results)
}
```